Title
POSITIVE MUONS IN CONDENSED MEDIA

Authors
Schenck, Alexander
Crowe, Kenneth M.

Publication Date
1973-04-01

To be published in the Proceedings
of the Zuoz School of Intermediate
Energy Physics, Zuoz, Switzerland,
April 13-14, 1973

LBL-2184
c.1

POSITIVE MUONS IN CONDENSED MEDIA

Alexander Schenck and Kenneth M. Crowe

April 1973

Prepared for the U. S. Atomic Energy Commission
under Contract W-7405-ENG-48

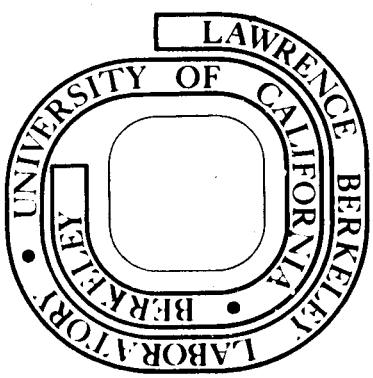

LBL-2184
c.1

DISCLAIMER

POSITIVE MUONS IN CONDENSED MEDIA

Alexander Schenck* and Kenneth M. Crowe

Lawrence Berkeley Laboratory, University of California
Berkeley, California 94720

ABSTRACT

This paper is an account of three lectures given at The Topical Meeting on Intermediate Energy Physics, April 1973, at Zuoz, Switzerland, in which a broad picture was presented of positive muons used as probes in condensed matter physics and chemistry. The relevant properties of μ^+ are given, the preparation of the polarized μ^+ beam is described, and there is a discussion of the experimental set-ups. The formation of muonium during the slowing down of μ^+ in matter is treated, and some related early measurements discussed. The quasi-free μ^+ precession and the possible depolarization affecting it in solid and liquid media are examined. Muonium, its quasi-free evolution, and its chemical reactions are covered, with emphasis on solid insulator and semiconductor environments. Finally, the use of μ^+ as a probe in matter is compared with other more conventional methods.

POSITIVE MUONS IN CONDENSED MEDIA

Alexander Schenck* and Kenneth M. Crowe
Lawrence Berkeley Laboratory, University of California
Berkeley, California 94720

I. INTRODUCTION

These lectures will be concerned with the application of positive muons as probes in condensed media physics and chemistry. In each experiment muons are brought to rest in a target containing solid or liquid substances. Positive muons are implanted in this way in whatever substance one likes. Due to the finite momentum distribution of a muon beam and to range straggling, muons will stop almost homogeneously over the target volume, even if the volume is as large as 1000 cm^3. Therefore the muons will be exposed to the real bulk properties of the target material.

By implanting muons we have joined the growing community of ion implanters; in fact, through muon implantation, one is very often studying the same properties that others study with heavier ions. We will see later what the muon can achieve compared with heavier ions, and what its shortcomings are. For future complementary research with both muons and heavier ions, it may be a lucky circumstance that meson factories and the new generation of heavy-ion accelerators are coming into operation almost at the same time.

In contrast to negative muons, the implanted positive muons are not captured into atomic or molecular orbits, and neither interact with nor are captured by nuclei. We may consider an implanted positive muon to be a light isotope of hydrogen; very often it suffices to think of the muon as a proton. When we ask ourselves "What happens to an implanted positive

*Present address: SIN, Villigen, Switzerland.

muon?" the first thing to do is find out what one knows about the fate of protons under the same conditions. Interestingly, as we will find out, knowledge concerning the proton under these conditions is generally scarce and hard to obtain. It is fortunate, therefore, that one can use the muon as a proton substitute to learn more about the proton's role in a condensed media environment

The point of interest, of course, is the magnetic interactions of the muon within the medium of the target. The muon sees with its magnetic moment all the internal magnetic field components that are present at the site of the implanted muon. These local fields may be created by nuclei, electrons, paramagnetic ions, and all kinds of hyperfine interactions. By measuring the interaction energy, one may expect to learn something about these internal fields and their origin. However, it is not only possible to study the static features of local fields, it is also possible to obtain information regarding the dynamic properties of internal fields. This is accomplished by studying the spin depolarization of muons which originally were implanted more or less polarized.

The causes of depolarization processes can be quite different in origin; and we may expect to encounter all the spin relaxation mechanisms that are dealt with in NMR and ESR studies, as well as in others. It will become evident that chemical kinetics, for instance, play an important role in depolarization phenomena.

II. BASIC MUON PROPERTIES

How do we measure magnetic interaction energies? How do we observe spin relaxation? Let us first deal with these questions by summarizing some of the muon properties that are important to us. Table I contains some basic information about the muon[1] which will be adequate for

our purposes in the context of this chapter. Except for its mass and its finite lifetime, the muon is in nearly every respect like an electron or positron.

In a magnetic field $\vec{H}$ the Zeeman splitting frequency is given as follows:

$$\omega = \frac{2\vec{\mu}_\mu \cdot \vec{H}}{\hbar} = \frac{g}{2} \frac{eH}{m_\mu c} \simeq 2\pi \frac{2.8}{207} H \left[\frac{\text{rad}}{\text{sec}}\right] \quad (1)$$

or

$$\frac{\nu}{H} = \frac{\omega}{2\pi} \frac{1}{H} \simeq 13.5 \frac{\text{k Hz}}{\text{gauss}} .$$

ω is also the Larmor precession frequency a muon would have in a transverse magnetic field of the same strength $(\vec{H} \perp \vec{S}_\mu)$.

The positive muon decays with the emission of an energetic electron:

$$\mu^+ \rightarrow e^+ + \nu_e + \bar{\nu}_\mu .$$

As will be shown in Section IV, the decay positron shows an asymmetric distribution with respect to the spin of the muon due to the violation of parity in weak interactions. This distribution is given by the expression:

$$P(\theta) \sim (1 + a(E_e) \cos\theta) \quad (2)$$

or

$$dN(\theta) \sim (1 + a(E_e) \cos\theta)\, d\Omega, \quad (3)$$

where $dN(\theta)$ is the decay rate into the solid angle $d\Omega$. The asymmetry parameter $a(E_e)$ is a function of the positron energy E_e. Figure 1 shows roughly the dependence of a on the positron energy. If positrons of all energies are observed, one obtains an average asymmetry of $\bar{a} = 1/3$. By observing only the higher energy positrons, one can increase somewhat the average experimentally observed asymmetry.

Figure 1 also displays the energy spectrum of the decay positrons. It is cut off at about 52.8 MeV. The average energy of the positrons is roughly 35 MeV. This is rather large compared with the energy of electrons emitted in β-decay of nuclei; therefore it is relatively easy to observe most of the electrons, even if the decaying muons are placed deep inside a target of convenient size.

In order to observe experimentally the asymmetric decay pattern, it is, of course, necessary that the spins of all muons be more or less parallel, or in other words, that the implanted muons be polarized. Once this is accomplished, the effective asymmetry of the positron distribution, including the muon polarization, can easily be measured. As a matter of fact, highly polarized muon beams can be readily obtained from pions decaying in flight by means of a proper momentum selection. This is, again, a consequence of parity violation in the weak decay of pions, which leads to a complete polarization of the decay muons in the rest frame of the pion.[1] The achieved beam polarization is generally of the order of 80%. Taking the polarization into account we rewrite Eq. (3) as follows

$$dN(\theta) \sim (1 + P\,\overline{a\,(E_e)}\cos\theta)\,d\Omega. \qquad (4)$$

III. EXPERIMENTAL METHODS

Now, what are the experimental methods for measuring $P\bar{a}$? It is obvious that a separate measurement of P and $\bar{a}$ is possible only if one of the two quantities is known beforehand. This is generally not the case (for exceptions, see later).

It is convenient to distinguish between two experimental arrangements:

1) The target in which the muons are to be stopped is placed in zero magnetic field or in a longitudinal field with respect to the spin-polarization vector $\vec{P}$. The arrangement is indicated in Fig. 2. By observing the positron rates in the two counter telescopes, we are measuring the forward decay rate and the backward decay rate, respectively, with respect to the polarization vector. Calling the forward rate N^+ and the backward rate N^-, one can form the ratio (from Eq. 4):

$$\frac{N^+ - N^-}{N^+ + N^-} = P\,\bar{a}\;\;\overline{\cos(\theta = 0°, 180°)}\,. \qquad (5)$$

This ratio is seen to be proportional to $P\,\bar{a}$ with a proportionality factor given by the average of $\cos\theta$ over the solid angle covered by the counters. This factor is of course < 1. [It is hereby assumed that $\overline{\cos(\theta = 0°)} = \overline{\cos(\theta = 180°)}$.] The experimentally observed asymmetry is thus smaller than $P\,\bar{a}$ due to finite solid-angle resolution. To give a number: in many experiments $P\,\bar{a}\;\overline{\cos\theta}$ is of the order of about 20%, if no other effects are present. Equation 5 is also correct if a time differential measurement is performed. P may then display a time dependence (see below).

2) The target is placed in a magnetic field whose direction is perpendicular to the muon polarization. The spinning muons will then start to precess with a frequency given by Eq. 1, the Larmor frequency; thus the asymmetric decay pattern will rotate. The situation is shown in Fig. 3. In order to make the precession visible, a time differential measurement has to be performed. The angle between muon spin and observable positron trajectory (fixed by the geometry

of the counter telescope) will vary in time as

$$\theta = \omega t .$$

The positron rate in the counter telescope as a function of muon lifetime in the target is then described by the following formula, starting from Eq. 4 and taking the experimental decay law into account:

$$dN(\theta,t) \sim \frac{1}{\tau_\mu} \exp(-t/\tau_\mu)\,[1 + P\ \bar{a}\ \cos(\omega t + \phi)]\,d\Omega\,dt. \qquad (6)$$

For an actual experimental set-up, taking finite time and solid angle resolution into account, which we shall describe by a factor $f < 1$, Eq. 6 becomes:

$$\Delta N(\theta,t) \sim \frac{1}{\tau_\mu} \exp(-t/\tau_\mu)\,[1 + P\ \bar{a}\ f \cos(\omega t + \phi)]\,. \qquad (7)$$

ϕ is the phase of the polarization for $t = 0$, and depends on the actual e^+ counter alignment with respect to the μ^+ beam. As will be discussed later, ϕ may also depend on the early fate of the muon in the target. $P\ \bar{a}\ f$ is the effective experimentally observable decay asymmetry; hence forth we will set $A = P\ \bar{a}\ f$.

The physical interpretation of Eq. 7 is as follows: When a muon decays, the probability of observing a decay positron will be a maximum at the moment when the muon spin points onto the positron telescope, and a minimum for the antiparallel case. The exponential decay curve, visible in a time differential measurement, will thus be cosine-modulated, as indicated in Fig. 4.

We have spoken about time differential measurements. How is this actually done and what is the experimental arrangement in practice?

Schematic diagrams of an actual experimental arrangement are shown in Figs. 5a and b. These diagrams are valid for the longitudinal field as well as the transverse field arrangement. The principal components of the necessary electronics are shown in the same figure.

A stopped muon is signaled by the logic combination $(B1+B2)\cdot M\cdot S1\cdot \overline{S2X}$. Likewise, a decay positron will be identified by the signal $S2X\cdot E\cdot S2\cdot S3\cdot \overline{(B1+S1+M)}$. The μ-stop signal will be used to start a clock and to create a gate signal of about 10 μsec length. The positron signal in coincidence with the gate signal will stop the clock. The gate signal thus defines the time interval after the muon stop during which one waits for the decay electron. In this way, for each observed muon decay, one measures the individual lifetime of the decayed muon. From these data one can form a histogram: positron rate versus elapsed lifetime, which should be described by one of the distribution formulas, Eq. 5 or Eq. 7, depending on the field arrangement. These formulas will then be fitted to the histograms, yielding the interesting parameters.

It is demanded, of course, that no second muon stop during the time one is waiting for the decay positron; otherwise, it becomes unclear from which muon the positron originated. This limits the actual stopping rate to about 10^4 μ^+/sec, a rate much less than it will be possible to achieve at SIN, for instance. Although this limitation is a very unfortunate feature of the time differential method, it is nevertheless the most versatile method and has to be used for most of the problems to be studied. However, the high muon fluxes at meson factories will be a great advantage because with them one can use extremely small targets. At SIN, an experimental set-up uses 0.5-cm^3 targets with a density of about 0.5 g/cm^2. (Conventional targets are much larger with densities of 8 to 20 g/cm^2 and cross sections

adapted to the μ-beam cross sections.) This will allow one to investigate particularly small single crystals and other rare substances.

IV. EXPERIMENTAL TYPES OF MUON DEPOLARIZATION PHENOMENA AND COMPLETE PHENOMENOLOGICAL RATE DISTRIBUTION FORMULAS

The first experimenters to check on parity invariance in muon decay were Garwin, Ledermann, and Weinrich.[2] Using a transverse field arrangement, they did indeed detect an asymmetry which in graphite, calcium, and polyethylene was close to the theoretically expected value of $\bar{a} = 1/3$. In nuclear emulsion, however, the asymmetry detected amounted to only about 1/6. This suggests the presence of some depolarization mechanism in nuclear emulsion that leads to a partial depolarization. Further, this partial depolarization must have happened in a very short time after the muon stopped because the residual polarization did not exhibit any time dependence; that is, $A(t) \equiv A$. This kind of depolarization can be described as being fast but incomplete; we will call this process a "fast" depolarization.

A different kind of depolarization process was detected by Swanson[3] in 1958 in boron carbide (B_4C), studying also muon precession. The result is shown in Fig. 6. Plotted is the positron rate versus elapsed lifetime. The distribution shows the expected cosine modulation; but the amplitude exhibits a decrease in time, which can be described with an exponential decay law. The time constant for this damping is about 1.5 μsec. We will call a depolarization with a directly observable time dependence a "slow" depolarization.

Taking these two phenomena into account, we will rewrite Eq. 3 and Eq. 7 as follows:

Longitudinal field

$$\Delta N(t) \sim \frac{1}{\tau_\mu} \exp(-t/\tau_\mu) \left[1 + \xi_{\parallel} F_{\parallel}(t) A \right] \qquad (8)$$

Transverse field

$$\Delta N(t) \sim \frac{1}{\tau_\mu} \exp(-t/\tau_\mu) \left[1 + \xi_{\perp} F_{\perp}(t) A \cos(\omega t + \phi) \right] \qquad (9)$$

$\xi_{\parallel}, \xi_{\perp} (\lesssim 1)$ = "fast" depolarization factors

$\xi_{\parallel} A, \xi_{\perp} A$ = effective residual asymmetry

$F_{\parallel}(t), F_{\perp}(t)$ = "slow" depolarization functions

ω = precession frequency of muon

ϕ = phase of residual polarization for t extrapolated to zero.

In many cases F(t) is given by an exponential decay law (see Swanson[3]). More on F(t) later.

We are now in the midst of our subject matter. We are talking about destruction of muon polarization, which means either that the spins of individual muons must flip over or that the coherence of the precession phases of a muon ensemble is somehow destroyed. No doubt this must be related to the magnetic interactions of the muon within the target environment.

As far as the fast depolarization is concerned, very strong internal magnetic fields must be present in which the muon spin can turn over in a very short time. In view of this, Friedman and Telegdi[4] in 1957 proposed to explain the fast depolarization as a consequence of the formation of the system $(\mu^+ e^-)$, which they called muonium.

V. MUONIUM (Mu)

Muonium is formed when a positive muon captures an electron and thus becomes neutralized.[5] It is like atomic hydrogen except that its mass is about 1/10 of the hydrogen mass. The smaller mass of the muon, however, has only a little effect on the reduced mass of the complete system which is very close to the reduced mass of hydrogen:

$$m^*_{Mu} \simeq 0.995\, m^*_H .$$

Therefore, the binding energy and the size of this atom are practically the same as for atomic hydrogen.

Muon spin and electron spin are coupled strongly by a hyperfine interaction of the Fermi contact type in the muonium ground state (refer to the lecture presented by V. L. Telegdi at this Conference). The Hamiltonian for the hyperfine interaction in an external magnetic field is given by the following well-known expression:[5]

$$\mathcal{H} = A\ \vec{S}_\mu \cdot \vec{J}_e + g_J \mu_0^e \vec{J}_e \cdot \vec{H} + g_\mu \mu_0^\mu \vec{S}_\mu \cdot \vec{H} \qquad (10)$$

with

$$A = \hbar\,\omega_0 = \frac{8\pi}{3} g_J \mu_0^e g_\mu \mu_0^\mu \left| \psi_S(0) \right|^2, \qquad (10a)$$

where $\hbar\,\omega_0$ = hyperfine splitting energy in zero field, $\vec{S}_\mu$ = muon spin, $\vec{J}_e$ = electron spin, g_J and g_μ are electron and muon g-values, μ_0^e and μ_0^μ are electron and muon Bohr magnetons, and $\left| \psi_S(0) \right|^2$ = electron density at the muon site. Energy eigenvalues can be calculated with the Breit-Rabi formula. Plotting the energy eigenvalues as a function of magnetic field strength, we obtain the Breit-Rabi diagram shown in Fig. 7.

At low fields, the total spin F is a good quantum number and the levels are labeled in terms of m_F. In a strong field the muon and electron

spin are more or less decoupled; and we have to label separately by the electron and muon magnetic quantum numbers. There is a crossover of the two upper states at about 160 kilogauss; at this point the external field is equal to the field produced by the electron at the muon site.

Zeeman eigenstates can easily be constructed as follows:

$$\psi_1 = |+1/2\rangle_e \; |+1/2\rangle_\mu \tag{11a}$$

$$\psi_2 = \alpha\,|+1/2\rangle_\mu\,|-1/2\rangle_e + \beta\,|-1/2\rangle_\mu\,|+1/2\rangle_e \tag{11b}$$

$$\psi_3 = |-1/2\rangle_e \; |-1/2\rangle_\mu \tag{11c}$$

$$\psi_4 = \beta\,|+1/2\rangle_\mu\,|-1/2\rangle_e - \alpha\,|-1/2\rangle_\mu\,|+1/2\rangle_e \tag{11d}$$

$$(\psi = |m\rangle_{e,\mu})$$

with

$$\alpha^2 + \beta^2 = 1$$

$$\alpha = \frac{1}{\sqrt{2}}\left(1 - \frac{X}{\sqrt{1+X^2}}\right)^{1/2}$$

$$\beta = \frac{1}{\sqrt{2}}\left(1 + \frac{X}{\sqrt{1+X^2}}\right)^{1/2}$$

$$X = \frac{(g_J \mu_0{}^e - g_\mu \mu_0{}^\mu) H}{\omega_0 \hbar} \simeq \frac{H}{1580}$$

where H is the external field in gauss. For large H, $\alpha \to 0$ and $\beta \to 1$, reflecting the decoupling of muon and electron spin.

When the muon captures an electron, the initial state may have either parallel spins or antiparallel spins; that is, $|+1/2\rangle_\mu\,|+1/2\rangle_e$ or $|+1/2\rangle_\mu\,|-1/2\rangle_e$, assuming that $|+1/2\rangle_\mu$ is the polarization of the stopped muons. Each initial state will be equally populated because there is normally an equal number of electrons with spin up and spin down in the target. An exception is to be expected in a ferromagnetic substance (see below).

The state with parallel spins, as is evident, is already an eigenstate of the Hamiltonian. This is not true for the antiparallel state, which will

develop in time to a mixed state consisting of a time-dependent superposition of ψ_1 and ψ_2, the two states with $m_F = 0$. That is, the mixed state is one in which the muon and the electron each precess—opposite to each other and with equal frequency—in the magnetic field set up by the other particle. The plane of precession contains the external magnetic field vector. We write:

$$|+1/2\rangle_\mu \; |-1/2\rangle_e \xrightarrow{t}$$

$$\psi(t) = A \exp(\frac{-iE_2t}{\hbar})\,\psi_2 + B \exp(\frac{-iE_4t}{\hbar})\,\psi_4 \qquad (12)$$

with $A^2 + B^2 = 1$.

Substituting ψ_2 and ψ_4 in this equation (using Eqs. 11b and 11d) we may rewrite Eq. 12 as follows

$$\psi(t) = P_+(t)\,|+1/2\rangle_\mu\,|-1/2\rangle_e + P_-(t)\,|-1/2\rangle_\mu\,|+1/2\rangle_e \qquad (13)$$

with

$$P_+(t) = \alpha \cdot A \exp(\frac{-iE_2t}{\hbar}) + \beta \cdot B \exp(\frac{-iE_4t}{\hbar})$$

$$P_-(t) = \beta \cdot A \exp(\frac{-iE_2t}{\hbar}) - \alpha \cdot B \exp(\frac{-iE_4t}{\hbar}).$$

$P_+^2(t)$ is then the probability of finding the muon in the state $|+1/2\rangle_\mu$; that is, $P_+^2(t)$ is the time-dependent polarization of the muon in the mixed state. After some arithmetic, taking into account that

$$\psi(t=0) = |+1/2\rangle_\mu \; |-1/2\rangle_e,$$

we obtain

$$P(t) = P_+^2(t) = 1 - 4\alpha^2\beta^2 + 4\alpha^2\beta^2 \cos \omega_0 t. \qquad (14)$$

As can be seen, the time dependence of the polarization is represented by a very fast modulation with frequency ω_0, the hyperfine splitting

frequency $[\omega_0 \cong 2\pi(4.46\times10^9)\frac{\text{rad}}{\text{sec}}]$ or the frequency with which the muon precesses in the magnetic hyperfine field. As this precession is very fast, it cannot be resolved experimentally and appears to be averaged out to zero. Hence, in a longitudinal field the net polarization in the mixed state, which can be measured, is given as follows:

$$\bar{P} = 1 - 4\alpha^2\beta^2 = \frac{X^2}{1+X^2} \tag{15}$$

and the total polarization, adding the polarization in the triplet state, is then:

$$\bar{P}_{tot} = \frac{1}{2} + \frac{1}{2}\,\frac{X^2}{1+X^2}. \tag{16}$$

Equation 16 is plotted in Fig. 8. The quenching of depolarization at high fields (Paschen-Bach region) reflects again the decoupling of muon and electron spin at high fields. Depolarization of muons in the free muonium state is thus a consequence of the limited time resolution of the experimental apparatus. In principle, no polarization is lost in an irreversible thermodynamic manner.

VI. EXPERIMENTAL OBSERVATIONS AND SPECULATIONS UP TO 1966

Many experiments in early times tried to observe the quenching of the fast depolarization by strong longitudinal magnetic fields. In fact, up to 1966 most experiments were concerned with this aspect.[6-12] One common observation was that apparently no depolarization occurred in metals. In all other cases depolarization of various degrees was visible. Some kind of quenching of the depolarization in the Paschen-Bach region was generally observed; however, in most cases Eq. 16 did not represent the data. In the following, some of the findings will be presented.

Figure 9 shows quenching curves for various temperatures, obtained by stopping muons in sulphur. This figure is taken from Eisenstein et al.[12] At room temperature even high magnetic fields (~4 kilogauss) cannot restore the polarization to better than 50% of the initial polarization. At liquid helium temperatures, complete quenching is already achieved at about 400 gauss.

Figure 10, taken from the work of the same authors, shows quenching curves at room temperature in LiF, MgO, and red phosphorous. Again the data do not follow the predicted behavior.

Figure 11 is taken from the work of Gorodetzky et al.[10] Shown are experimentally observed quenching curves in various materials. Again there is no agreement with the curve given by Eq. 16.

The above figures reveal a very small polarization in zero magnetic field. By increasing the field a little, a sharp increase in residual polarization occurs which quickly levels off to a much slower increase. This is one of the puzzles that has not yet been explained satisfactorily. (This effect may be due to randomly oriented magnetic fields from impurities.)

In view of these disagreements, it was repeatedly proposed that multiple muonium formation may be made responsible for the observed behavior. Multiple muonium formation was thought to happen during the slowing down process. Several authors designed formulas to take this into account.[7, 11, 13] In some cases[12] the new formulas lead to improved fits. In view of the addition of two or more additional parameters, this is not too surprising and it may not mean very much (see also Ref. 11). The principal question we have to ask ourselves is whether multiple muonium formation during the slowing down process has the power to produce any depolarization. Obviously this is a question of timescale, which we will treat in

the next chapter.

Up to 1966, very few experiments had been performed in a transverse field arrangement.[3,14,15] The most relevant one is the already mentioned one by Swanson.[3] The results are collected in a rough manner in Table II. Metals and semimetals show no depolarization, such as in the longitudinal field case. Other inorganic and organic substances show a fast depolarization of varying degree; but contradictory to the longitudinal field case, the residual polarization appeared to be independent of applied transverse field strength. No reasonable explanation of these findings was offered in Ref. 3.

The general absence of depolarization in metals was originally thought of as resulting from a very fast electron exchange process:

$$\mu^+ e^-_{\uparrow} + e^-_{\downarrow} \rightarrow \mu^+ e^-_{\downarrow} + e^-_{\uparrow}$$

resulting in a decoupling of muon and electron spin (see Iakovleva[16]). The muon would thus precess as if free but would still be bound to an electron. This view was later replaced by what is still believed to be the case: that Coulomb screening of the muons by conduction electrons will prevent muonium formation; if muonium is ever formed, it will donate its electron to the conduction band.

Finally, a measurement by Feher et al.,[17] who used silicon targets with different impurity concentrations, should be mentioned. The results obtained in zero magnetic field are shown in Fig. 12. At high n-type impurity concentration (the sample being effectively a conductor) no depolarization occurred; neither did it occur in a sample with high p-type impurity concentration. However, almost complete depolarization was achieved at a n-type impurity concentration corresponding to about 10^{14} free electrons/cm^3. The free electron concentration thus has a very important influence on depolar-

ization in semiconductors. In a later paper,[12] quenching curves obtained in doped silicon were interpreted in terms of the formation of shallow donor muonium, which is much less strongly bound muonium with a consequently smaller hyperfine interaction.

VII. THE SLOWING DOWN PROCESS AND THE STATUS OF THE MUON AFTERWARDS

The most important gross features of the slowing down process are displayed in the flow diagram shown in Fig. 13. The boxes contain information on the mechanisms involved and give relevant references. On the left side, time estimates for the different sections of the slowing down process are given, making use of Refs. 18-21. The cited papers (except Ref. 18) refer to the slowing down in gases. The estimates were obtained by scaling roughly, using the higher density of a condensed matter target, the numbers given in the references. The right side gives a list of depolarization processes (and estimates of their magnitude) that are supposed to occur during the different parts of the slowing down process. As can be seen, the time that passes between "stable" muonium formation and complete thermalization is too short to cause any appreciable rotation of the muon spin in the hyperfine field in the singlet state, even if multiple muonium formation were to occur during this time. The depolarization effect will be even smaller if less strongly bound muonium is formed. Also in the electron capture and loss region only a little depolarization can be expected to occur. Thus, the total depolarization during slowing down may safely be estimated to be $<4\%$. From proton neutralization measurements (see Fig. 14), it can be inferred that the neutralization of muons (that is, muonium formation) will occur with effectively 100% yield.[22]

Near the end of the energy range, say at about 20 eV, muonium is likely to participate in hot-atom reactions[18] by which it may be bound diamagnetically into a molecule, or it may become part of a chemical radical with an unpaired electron. As there is a lot of energy available in epithermal (hot) reactions, many reactions will become possible that are forbidden in the thermal region for lack of energy to overcome potential barriers (high activation energies).

The situation after slowing down is summarized as follows:

1. No appreciable depolarization has occurred;
2. Muons are in the state of thermalized muonium, or
3. Muons are part of hot-atom reaction products:
   a) Molecules with saturated bonds (μ^+ in a diamagnetic environment)
   b) Chemical radicals (μ^+ and unpaired electron are coupled by hyperfine interaction—similar system to Mu, but with smaller ω_0).

What is to be expected then?

1. Chemical reactions of thermalized muonium ($\equiv$ hydrogen) and of muon radicals.
2. Interactions of the (paramagnetic) impurity with its environment: μ^+e^- (in solids) $\rightarrow U_2$ center.
3. Modifications of the electronic structure of μ^+e^-; that is, muonium forms an impurity state in the host lattice.
4. Direct interactions of the muon with its environment, e.g. diffusion, etc.

VIII. MUON PRECESSION AT THE QUASI-FREE LARMOR FREQUENCY AND SLOW DEPOLARIZATION IN SOLIDS

In this and the following section we want to discuss phenomena that can be observed by looking at the fraction of muons that proceeded through the hot-atom channel and ended up in a molecule with saturated chemical bonds; that is, muons with no hyperfine interaction acting on them. We will consider only the transverse field case, by studying muon precession at the quasi-free Larmor frequency. This section will be devoted to precession phenomena in solids.

For a given field H the precession frequency is given by

$$\omega = \frac{e}{m_\mu c} H = \gamma_\mu \cdot H \qquad (17)$$

We will now consider the case in which H is a function of position.

a) Assume that H has only a limited number of discrete values over the target volume. We then have to replace the cosine in the rate distribution formula by a sum over cosines with different discrete frequencies ω_i:

$$\cos(\omega t+\phi) \rightarrow \sum_i P_i \cos(\omega_i t+\phi), \qquad (18)$$

where P_i is the fraction of muons that precess with ω_i. It is clear that this will result in a more or less complicated beat phenomenon in the precession pattern.

b) Next let us assume that there is a continuous distribution of field values over the target volume,

$$H = H(x, y, z).$$

We then have to replace the cosine in Eq. 7 by an integral:

$$\cos(\omega t+\phi) \rightarrow \int_{\text{target vol.}} \cos[\,\omega(x,y,z)\,t+\phi]\,dx\,dy\,dz. \qquad (18')$$

It is assumed also that the muon stopping rate is constant over the target volume. This integral can be rewritten as follows

$$\int_{\text{target vol.}} \Longrightarrow \int_0^\infty e^{i(\omega t+\phi)}\, f(\omega)\, d\omega,$$

which now implies only an integration over ω. $f(\omega)$ is a distribution function of the probability density for finding muons precessing with frequency ω; that is, it is the frequency spectrum.

The frequency spectrum $f(\omega)$ can be observed directly in NMR experiments in solids, and is nothing more than the NMR line shape. Thus, the muon precession pattern is the Fourier transform of the corresponding NMR line shape that would be measured in a NMR experiment with stopped muons.[23] Such an experiment is possible, and has been performed for a magnetic moment determination.[24]

The above integral can often be expressed as:

$$\int_0^\infty e^{-i(\omega t+\phi)}\, f(\omega)\, d\omega \cong F(t)\, \cos(\omega^* t+\phi), \qquad (19)$$

where ω^* is the average frequency and $F(t)$ can be approximated by a Gaussian or exponential decay function with relaxation time T_2. $F(t)$ thus describes a slow relaxation and can be identified with the $F_\perp(t)$ introduced into Eq. 9.

For complicated field distributions, such as in a superconductor of Type II, the precession pattern will, of course, be much more complex. It may however, be used to determine such field distributions, being the spatial Fourier transform thereof (see for example, Ref. 25).

c) Suppose now that the muon could diffuse easily in the crystal. Then the internal field distribution would appear somewhat washed out, and we would have a condition which in NMR is known as motional narrowing.[23] The NMR line will become smaller, a splitting will disappear, and the Fourier transform will show a damping with a much longer relaxation time T_2. This effect should be visible, particularly in metals, with T_2 displaying a marked temperature dependence.

2. What magnetic field is really determined by measuring the precession frequency ω, assuming now a constant ω over the target volume? Of course, it is the local field seen by the muon at its site. This local field is not necessarily identical with the applied external field. Generally, the local field at some position in a crystal will be given by[26]

$$\vec{H}_{loc} = \vec{H}_{ext} + \vec{H}_{dm} - \vec{H}_{L} + \vec{H}_{int} \qquad (20)$$

$\vec{H}_{ext}$ = external field

$\vec{H}_{dm}$ = demagnetization field, depending on the geometry of the sample

$\vec{H}_{L}$ = Lorentz cavity field, the field at the center (probe site) of a spherical cavity cut (as a mathematical fiction) out of the specimen. The field is produced by the magnetization density on the surface of the cavity.

$\vec{H}_{int}$ = internal magnetic field produced by magnetic sources inside the cavity ($= \Sigma \vec{h}_i$).

By expressing the local field according to Eq. 20 one has taken into account the discontinuous structure of a crystal.

a) In a diamagnetic crystal $\vec{H}_{dm} + \vec{H}_L$ are vanishingly small. In an insulator, contributions to $\vec{H}_{int}$ arise only from nuclear moments (see the example below). In a paramagnetic crystal $\vec{H}_{dm} + \vec{H}_L$ are still very small and may in many cases just be neglected. $\vec{H}_{int}$ will consist of contributions from the various paramagnetic ions inside the cavity. For a crystal with cubic symmetry or for isotropic media $\vec{H}_{int}$ will be zero. For more details see Ref. 27.

b) In a metal there will be a very special internal field originating from the polarization of conduction electrons in an external magnetic field. In NMR experiments this field causes the famous Knight shift.[23, 27] The field is given by the expression

$$\vec{H}_{int} = \frac{8}{3}\pi \left| u(0) \right|^2 \chi_s \vec{H}_{ext} \qquad (21)$$

with

χ_s = Pauli spin susceptibility

$= \frac{1}{2} \gamma_e \hbar^2 N(\epsilon_F)$

$|u(0)|^2$ = density of conduction electrons at the muon site

$N(\epsilon_F)$ = density of states at the Fermi level

$= (2\pi m^*/\hbar^2) \cdot (3n V^2/\pi n')^2$

m^* = effective mass of conduction electrons, depends on the actual band structure.

Conventional measurements of the Knight shift require the performance of NMR with a metal probe. Due to the skin effect, the hf-field will penetrate only into a thin surface region, and it may sometimes be questionable whether one measures the bulk Knight shift

of the probe material or some surface properties. With the help of the muon one would measure real bulk Knight shifts.[14]

c) In ferromagnetic and antiferromagnetic substances the measurement of H_{int} may shed light on some of the properties of these magnetic materials which are still not understood and which are still the subject of a lively controversy. A first example of a measurement in Ni (M. L. G. Foy et al.)[28] has been described by Kossler at this conference.

3. Examples

We will now describe a measurement which provides a good illustration of the possible phenomena discussed in paragraphs 1a, 1b, and 2a of this section. This experiment was performed with a single crystal of gypsum ($CaSO_4 \cdot 2H_2O$).[29] The basic assumption is that muons are placed by hot reactions of muonium into the site of a proton in one of the two water molecules that are present in the unit cell of this crystal. The next neighbor proton will create a magnetic dipole field at the site of the muon, given by this expression

$$\delta H_\mu = \pm \frac{\mu_p}{r^3} (3 \cos^2 \theta - 1), \qquad (22)$$

where μ_p = magnetic moment of proton, θ = angle between the magnetic moment vector of the proton and the muon-proton radius vector, and r = the muon-proton distance.

Depending on whether the proton spin is parallel or antiparallel to an external field, the dipole field will either add to or subtract from the external field. As we have two differently oriented H_2O molecules in the unit cell we will expect up to four different muon

precession frequencies, as is evident from Fig. 15. ω_2 and ω_3 belong to the first pair; ω_1 and ω_2 belong to the second pair. In addition, the muon will feel the field components due to protons (and perhaps to magnetic impurities) farther away, which will lead to a frequency distribution around each ω_i. From NMR measurement one can infer that the distribution is of Gaussian shape.

Taking the Fourier transform of this complete pattern, one obtains for F(t) the following expression:

$$F(t) = \exp\left(\frac{-t^2}{T_2^2}\right) \cos\left(\tfrac{1}{2}\Delta\omega_1 t\right) \cos\left(\tfrac{1}{2}\Delta\omega_2 t\right); \qquad (23)$$

with $\Delta\omega_1 = \omega_2 - \omega_1 = \omega_4 - \omega_3$

$\Delta\omega_2 = \frac{1}{2}(\omega_4 - \omega_1) + \frac{1}{2}(\omega_3 - \omega_2)$

$T_2 = \frac{4}{\Delta\omega}$.

There are actually two beat frequencies, $\Delta\omega_1$ and $\Delta\omega_2$, and a damping function of Gaussian form with a relaxation time T_2 related to the field distribution width $\Delta\omega$. The actual numbers for the beat frequencies $\Delta\omega_1$ and $\Delta\omega_2$ depend on the crystal orientation in the external field and can be calculated without difficulty.

Figures 16a and b show data for F(t) for two different crystal orientations. The solid lines are calculated ones, not fits. Clearly visible is the beat behavior as well as the damping. The agreement between data and calculated curve in Fig. 16b does not look too good; however, in this case the crystal orientation in the external field was not accurately known.

IX. SLOW DEPOLARIZATION IN PARAMAGNETIC LIQUIDS

The NMR line shape in liquids is generally described by a Lorentzian curve. The Fourier transform of this is an exponential decay function describing the relaxation of the transverse (with respect to the external magnetic field) spin components. Slow muon depolarization in transverse fields is thus expected to obey an exponential decay law:

$$F_{\perp}(t) = e^{-t/T_2} \qquad (24)$$

where T_2 is the transverse or spin-spin relaxation time. Relaxation in this case means the loss of phase coherence among the spins of the precessing muons. Slow depolarization in a longitudinal field arrangement is also described by an exponential decay law:

$$F_{\parallel}(t) = e^{-t/T_1} \qquad (25)$$

with T_1 = the longitudinal or spin-lattice relaxation time. Relaxation in this case consists of transitions between the Zeeman states of the muons caused by interactions with the lattice, the lattice providing or absorbing the energy quanta involved. No longitudinal slow depolarization has yet been measured in paramagnetic solutions.

The muons that are observed at the free muon Larmor precession frequency must be, as emphasized before, in a diamagnetic position, either placed there by hot-atom reactions or by thermal reactions of muonium. From results on hot-tritium chemistry in aqueous solutions one knows that preferentially the molecule THO is formed.[30] It can be assumed that the same will happen in hot-atom reactions of muonium, yielding the molecule MuHO. As the residual polarization in pure water is about 0.5, we conclude that about 50% of all muons go through the hot-atom channel, by replacing

a proton in a water molecule.

The muon now has the same place as a proton, and it can be assumed that the muon spin will be subject to relaxation processes in the same way as the proton spin. Proton spin relaxation phenomena in aqueous solutions have been investigated quite intensively by the method of NMR.[23]

Particularly suitable for studying slow relaxation phenomena with muons are paramagnetic aqueous solutions, where T_2 can be expected to be small enough to be detected over the muon lifetime.[31] From the theory of relaxation[23] it follows that

$$\frac{1}{T_2} \approx (\mu)^2 \tag{26}$$

where μ = magnetic moment of the particle involved. By comparing proton and muon relaxation times in the same solution under the same conditions, one thus expects the ratio:

$$\frac{T_2(p)}{T_2(\mu)} = \frac{\mu_\mu^2}{\mu_p^2} \approx 10. \tag{27}$$

Figure 17 shows T_2 data for muons obtained in paramagnetic Fe^{3+} solutions.[32] Plotted is T_2 versus paramagnetic ion concentration. The lower data points, connected by a solid straight line, were obtained from a solution of $Fe(NO_3)_3$. The upper solid line represents proton NMR results in the same solution. The ratio between the muon and proton data is indeed about 10. For lack of NMR data, the results obtained in $FeCl_3$ and $Fe(ClO_4)_3$ could not be analyzed in the same way. The deviation between the data from $Fe(NO_3)_3$ solutions and data from $Fe(ClO_4)_3$ and $FeCl_3$ solutions is not fully understood and needs further investigation.

There is one important point. NMR measurements were generally done in solutions with concentrations not exceeding 10^{21} paramagnetic ions/cm^3, for reasons related to problems regarding line width, signal strength, rf power, and others. This limits proton-NMR measurements to cases with relaxation times above microseconds. It is, however, easy to measure much shorter relaxation times with muons in much stronger concentrated solutions. In principle, transverse and also longitudinal relaxation times can be measured down to, say, 10^{-8} sec.

In strongly concentrated solutions, not suitable for study by NMR, new effects may show up. This is demonstrated by measurements performed with $MnCl_2$ solutions of up to 5 moles/l Mn^{2+} concentration ($\approx 3\times10^{21}$ ions/cm^3).[33] The analysis also gives a good example of what kind of effects are involved and what information may be extracted from experimental results. At lower concentrations, $MnCl_2$ solutions have been extensively studied with proton-NMR by many authors, particularly by Bloembergen et al.[34]

The model used in the analysis is that the paramagnetic Mn^{2+} ions are surrounded by six water molecules forming a hydration sphere. Protons (or muons) in this hydration sphere are subject to two time-dependent magnetic interactions: dipole-dipole interaction between paramagnetic ion and proton (or muon), and a scalar coupling or spin-exchange interaction caused by the nonvanishing wavefunction of the ion at the site of the proton (or muon) in the hydration sphere. These interactions lead to the following expressions for the transverse relaxation time T_2:[34, 35]

$$\frac{1}{T_2} = \frac{4}{60}\frac{1}{r^6} S(S+1)\gamma_{p(\mu)}^2 \gamma_{ion}^2 h^2 [7\tau_c + 13\tau_c(1+\omega_s^2\tau_c^2)^{-1}] + \frac{1}{3} S(S+1) A_{p(\mu)}^2 h^{-2} [\tau_e + \tau_e(1+\omega_s^2\tau_e^2)^{-1}] P. \quad (28)$$

The first term on the right-hand side of Eq. 28 is due to the dipole-dipole interaction, and the second term is caused by the spin-exchange interaction. The symbols are defined as follows: S = ion spin (5/2); r = internuclear distance between ion and proton (muon); γ_p or γ_μ and γ_{ion} = the respective gyromagnetic ratios; $A_\mu = 3.18\ A_p$, the coupling constant for exchange interaction; ω_s = Larmor precession frequency of the ion; P = probability of finding a proton (or a muon) in the hydration sphere; and τ_c and τ_e are the respective correlation times, which are a measure of the time dependence of the involved interactions.

The time dependence of the dipole-dipole interaction may be caused by rotational diffusion of the Mn^{2+} complex, by chemical exchange of the H_2O (MuHO) molecules, and by spin relaxation of the paramagnetic ion, each measured by correlation times τ_r, τ_h, and τ_s. Thus

$$\frac{1}{\tau_c} = \frac{1}{\tau_r} + \frac{1}{\tau_h} + \frac{1}{\tau_s} \tag{29}$$

and correspondingly,

$$\frac{1}{\tau_e} = \frac{1}{\tau_h} + \frac{1}{\tau_s} \tag{30}$$

(The scalar coupling is not influenced by rotational diffusion.)

The temperature dependence of the correlation times τ_r, τ_h is described by a type of Arrhenius law

$$\tau = \tau_o\ e^{V/RT} \tag{31}$$

where V is the activation energy for rotational diffusion or chemical exchange. The temperature dependence of τ_s is more complicated and involves the mechanisms leading to the electronic relaxation.[34]

Equations 28, 29, 30, and 31 represent in a typical way the amount of information obtainable from relaxation studies in paramagnetic solutions.

Figure 18a shows the dipole-dipole term (top dashed curve) and the T spin-exchange term (lower dashed curve) which are obtained using reasonable values for the respective correlation times and correcting for the larger magnetic moment of the muon. For concentrations below 10^{20} $MnCl_2^{++}/cm^3$ there is a good agreement between the scaled predictions for muons. Note that the data break sharply and there seems to be a quenching of the relaxation mechanism. A reasonable approach toward understanding these deviations from Eq. 28 is to assume that some of the correlation times become concentration-dependent at higher concentrations due to intermolecular interactions of Mn^{2+} complexes. In particular, spin-spin interactions among Mn^{2+} ions might lead to concentration-dependent correlation times. Indeed, ESR measurements by Garstens and Liebson and Hinckley and Morgan[36] show a concentration-dependent line width in concentrated Mn^{2+} solutions. The data can be approximated by

$$\tau_s^* = \frac{1.24\times10^{-9}}{N^2} + 1.27\times10^{-11} \text{ sec},$$

where τ_s^* is now used as an additional effective correlation time in the proton(muon)-ion interactions.[37] N = ion concentration in moles/liter. The temperature dependence of τ_s^* can also be obtained from Ref. 36. For a 3 M solution, one finds

$$\frac{1}{\tau_s^*} = 1.76\times10^{7}\left[\,710 - 2.8\times10^{3}\exp\left(-\frac{1.26\times10^{3}}{RT}\right)\right]. \qquad (32)$$

The total correlation time τ_e for the spin-exchange interaction is now given by

$$\frac{1}{\tau_e} = \frac{1}{\tau_s} + \frac{1}{\tau_s^*} + \frac{1}{\tau_h}, \tag{33}$$

where τ_s is the usual electron spin relaxation time and τ_h is the mean time for the muon to remain in the hydration sphere. The total correlation time τ_c for the dipole-dipole interaction is given by

$$\frac{1}{\tau_c} = \frac{1}{\tau_r} + \frac{1}{\tau_h} + \frac{1}{\tau_s} + \frac{1}{\tau_s^*} \tag{34}$$

where τ_r is the rotational correlation time. At room temperature $\tau_s \approx 3\times10^{-9}$, $\tau_h \approx 2\times10^{-8}$, $\tau_r \approx 3\times10^{-11}$ sec.[34]

In Fig. 19a we again present our data from Fig. 18; however, the concentration (P) dependence is now divided out. If the correlation times were concentration-independent, $1/T_2P$ would be constant. If we insert the total correlation times τ_e and τ_c (Eqs. 33 and 34) into the general expression Eq. 28 with the other parameters taken from Ref. 35, we get the solid line in Fig. 19a, which fits our data excellently. The dashed lines in Fig. 19a represent spin-exchange and dipole-dipole contributions separately.

If we use, however, Eq. 28 together with Eqs. 32 and 33 and the temperature dependence for τ_r and τ_h from Ref. 34, we obtain the dotted curve in Fig. 19b for 11 kG, which—as is clearly evident—does not adequately describe the measured T_2-versus-temperature data in a 3 M solution.

By assuming that Eq. 33 correctly describes the temperature dependence of τ_s^* and by not considering an abnormal τ_h behavior, we are forced to adopt parameters different from the ones in Ref. 34 in the expression

$$\tau_r = \tau_r^0 \exp(V_r/RT), \tag{35}$$

where V_r is the activation energy of the rotational motion of the Mn^{2+} complex. Using $V_r = 8.5$ kcal/mole-liter and $\tau_r^0 = 1.73 \times 10^{-17}$ sec, we obtain for $1/T_2P$ versus temperature the lower solid curve at 11 kG and the upper one at 4.5 kG external field strength.[38]

The large value for the activation energy at 3 $\underline{M}$ concentration as compared with $V_r = 4.5$ kcal/mole-liter at low concentrations seems to be reasonable in view of the strongly increased viscosity of a 3 $\underline{M}$ $MnCl_2$ solution [η (3 $\underline{M}$) $\approx$ 3.2 centipoises]. It would be of great interest to establish some firm experimental relationships here with respect to the dynamics of this liquid.[38]

We now discuss some questionable assumptions in our analysis.

1) The results of Ref. 36 for ESR line width were obtained in an external field of 3 kG. In our analysis we neglected possible field dependence of the ESR line widths and assumed the same values in fields of 4.5 and 11 kG. This is justified only if the relevant correlation time τ obeys the inequality $\tau\,\omega_s(11\text{ kG}) < 1$ or $\tau < 5 \times 10^{-12}$ sec.

2) The results of Ref. 36 were obtained in $Mn(ClO_4)_2$ solutions, whereas we used $MnCl_2$ solutions.

3) Although we had to change V_r and τ_r^0 in order to fit the temperature dependence of a 3 $\underline{M}$ solution, we had to assume that τ_r remains relatively independent of concentration at 295°K in order to obtain the fit in Fig. 19a.

4) In view of the quality of the fit, as shown in Fig. 19a, τ_h has been assumed to be concentration-independent. This assumption needs, of course, further justification. In particular, a concentration-dependent activation energy for chemical exchange might reduce the value of V_r to less than 8.5 kcal/mole-liter.

5) The whole analysis was performed on the basic assumption that $Mn(H_2O)_6^{2+}$ formation continues almost unchanged up to the strongest concentrations.

These assumptions emphasize how further use of muon-depolarization studies might also contribute to our knowledge about structure and dynamics of fluids. In order to accomplish this program in Mn^{2+} solutions, measurements of relaxation times have to be performed in transverse as well as in longitudinal fields, as a function of varying field strengths, as a function of temperature in various concentrations, and finally in solution with different anions.

X. QUASI-FREE MUONIUM EVOLUTION

In view of the possibility that muonium reacts chemically and that the muonium-electron spin may relax, a more refined treatment of muon depolarization becomes necessary. Such a refined treatment was given by the Russian physicists Ivanter and Smilga[39, 40] starting from some older work by Iakovleva and Nosov.[41] In the following two sections we will try to give a brief description of their treatment and the results.

We begin with the usual muonium Hamiltonian but introduce, in addition, a term $\hat{F}$ representing the electron-lattice interaction and a term $\hat{W}$ representing a lattice-lattice interaction; both terms are time dependent.[42] The latter makes sure that polarization transferred from the electron to the muonium lattice environment is dissipated throughout the lattice.

$$\mathcal{H} = A\,\vec{S}_\mu \cdot \vec{J}_e + g_J\,\mu_0^e\,\vec{J}_e \cdot \vec{H} + g_\mu \mu_0^\mu \vec{S}_\mu \cdot \vec{H} + \hat{F} + \hat{W}. \qquad (36)$$

We define a spin density matrix for muonium in terms of the Pauli spin matrices σ_i:

$$\rho = \frac{1}{2}\left[1 + \vec{P}_\mu \vec{\sigma}_\mu + \vec{P}_e \vec{\sigma}_e + \sum_{i,j=1} \rho_{ij}\, \sigma_u{}^i\, \sigma_e{}^j\right] \tag{37}$$

$\vec{P}_\mu$ is the muon polarization vector with components ρ_{10}, ρ_{20}, ρ_{30} (x, y, z); and $\vec{P}_e$ is the electron polarization vector with components ρ_{01}, ρ_{02}, ρ_{03}. We are interested in the time evolution of $\vec{P}_\mu$. The time derivative of ρ is given by the usual formula

$$\frac{d\rho}{dt} = -\frac{i}{\hbar}\left[\mathcal{H}, \rho\right]. \tag{38}$$

Generally this will lead to equations known as the Wangsness-Bloch equations.

Let us first neglect $\hat{F} + \hat{W}$; that is, we are interested only in the free evolution of the muon polarization in the muonium state. Inserting Eqs. 36 and 37 into Eq. 38 and using the commutator relations of the σ, we obtain the following system of differential equations:

$$\begin{aligned}
\frac{d\rho_{il}}{dt} &= \frac{\omega_0}{2}\left(\rho_{j0}\,\epsilon_{ilj} - \rho_{0k}\,\epsilon_{ilk}\right) + \omega_j^{\,e}\,\rho_{ik}\,\epsilon_{ljk}\,\omega_j^{\,\mu}\,\rho_{kl}\,\epsilon_{ijk} \\
\frac{d\rho_{10}}{dt} &= -\frac{\omega_0}{2}\,\rho_{jk}\,\epsilon_{ljk} - \omega_i^{\,\mu}\,\rho_{k0}\,\epsilon_{lik} \\
\frac{d\rho_{01}}{dt} &= \frac{\omega_0}{2}\,\rho_{jk}\,\epsilon_{ljk} + \omega_i^{\,e}\,\rho_{0k}\,\epsilon_{lik}\,.
\end{aligned} \tag{39}$$

Without specifying the time-dependent terms $\hat{F}$ and $\hat{W}$, we know from the very beginning that the effect of $\hat{F} + \hat{W}$ must result in a damping of the pure and mixed electron components because of the random time structure of $\hat{F}$ and $\hat{W}$. Introducing a common relaxation rate 2ν for all pure and mixed electron components, we simply have to complete the system (Eqs. 39) as follows:

$$\dot{\rho}_{i1} = \frac{\omega_0}{2}(\rho_{j0}\epsilon_{i1j} - \rho_{0k}\epsilon_{i1k}) + \omega_j^e \rho_{ik}\epsilon_{1jk} - \omega_j^\mu \rho_{kl}\epsilon_{ijk} - 2\nu\rho_{il}$$

$$\dot{\rho}_{10} = -\frac{\omega_0}{2}\rho_{ik}\epsilon_{1jk} - \omega_i^\mu \rho_{k0}\epsilon_{1ik} \qquad (40)$$

$$\dot{\rho}_{01} = \frac{\omega_0}{2}\rho_{jk}\epsilon_{1jk} + \omega_i^e \rho_{0k}\epsilon_{1ik} - 2\nu\rho_{01} .$$

It now turns out that this system splits naturally into two irreducible parts, one involving only the longitudinal components of $\vec{P}_\mu$ and $\vec{P}_e$, the other only the transverse components with respect to $\vec{H}$. Schematically we write:

$$\dot{\rho} = \left(\begin{array}{c|c} \text{long.} & \\ \hline & \text{trans.} \end{array}\right) \rho ,$$

with ρ expressed as a column matrix. The matrix is then a 16×16 matrix. We now want to treat the subsystem referring to the transverse components in somewhat more detail. The magnetic field is directed along Z, and the initial polarization along X. Following Ref. 39 we introduce the following complex combinations

$$\rho_\mu = \rho_{10} + i\rho_{20} , \quad \rho_e = \rho_{01} + i\rho_{02} ,$$
$$\rho_\mu' = \rho_{31} + i\rho_{32} , \quad \rho_e' = \rho_{13} + i\rho_{23} . \qquad (41)$$

ρ_μ, for instance, represents the muon polarization projected on the (x, y) plane ($\perp \vec{H}$). We further introduce

$$\tilde{\rho} = \begin{pmatrix} \rho_\mu \\ \rho_e \\ \rho_\mu' \\ \rho_e' \end{pmatrix} . \qquad (42)$$

The subsystem under consideration can then be written as

$$\frac{d\tilde{\rho}}{dt} = A \cdot \tilde{\rho} \tag{43}$$

with

$$A = \frac{\omega_0}{2} \begin{pmatrix} 2i\zeta x & 0 & -i & i \\ 0 & -(\frac{4\nu}{\omega_0} + 2ix) & i & -i \\ -i & i & -(\frac{4\nu}{\omega_0} - 2i\zeta x) & 0 \\ i & -i & 0 & -(\frac{4\nu}{\omega_0} + 2ix) \end{pmatrix}. \tag{44}$$

Solutions

(a) We first set $\nu = 0$ (no electron relaxation). We ask for the time dependence of the muon polarization in, e.g., the x-direction, the direction of the positron telescope. As a solution of Eq. 43 we obtain[43]

$$P_x(t) = \frac{1}{4}\left\{(1 + \frac{\omega_+}{Q}) \cos \omega_{12} t + (1 - \frac{\omega_+}{Q}) \cos \omega_{23} t + (1 - \frac{\omega_+}{Q}) \cos \omega_{14} t + (1 + \frac{\omega_+}{Q}) \cos \omega_{34} t\right\} \tag{45}$$

with

$$\omega_\pm = \frac{eH}{m_e c} (1 \pm \zeta) \tag{46}$$

$$Q = (\frac{1}{4}\omega_0^2 + \omega_+^2)^{1/2} \tag{47}$$

$$\zeta = \frac{m_e}{m_\mu}.$$

The ω_{ij} are Zeeman transition frequencies (see Fig. 7) with the following selection criteria (weak field notation):

$$\omega_{12} : \Delta F = 0, \Delta m_F = 1$$

$$\omega_{23} : \Delta F = 0, \Delta m_F = -1$$

$$\omega_{14} : \Delta F = 1, \Delta m_F = 1$$

$$\omega_{34} : \Delta F = 1, \Delta m_F = -1$$

For $H \to \infty$ the components with ω_{23} and ω_{14} will disappear, which again is a result of the decoupling of the muon and electron spins in the Paschen-Back region.

For very small magnetic fields, the above formula simplifies to the following expression

$$P_x(t) = \cos \frac{\omega_{14} - \omega_{34}}{2} t \,(1 + \cos \frac{\omega_{14} + \omega_{34}}{2} t). \qquad (48)$$

Figure 20 shows a plot of $P_x(t)$ versus t. Because $\frac{\omega_{14} + \omega_{34}}{2} = \omega_0$ the experimentally observable polarization will be only

$$P_{x(exp)}(t) = \cos \frac{\omega_{14} - \omega_{34}}{2} t = \cos \omega_{12} t.$$

Thus, one can observe the precession of the muon with the triplet Larmor frequency of muonium, which is 1/2 the free electron precession rate.

Either Fig. 20 or Eq. 48 can be constructed by direct physical consideration for the very weak field condition: muons in the triplet state will precess relatively slowly, while muons in the mixed state will precess relatively fast in the (x, y) plane. The evolution in time of the total polarization is shown in Fig. 21. Projection of the time evolution of the rosette in this figure on the x-axis will result in the curve shown in Fig. 20.

For somewhat larger fields (~100 gauss) one obtains an expression for $P_x(t)$ as follows:

$$P_x(t) = \cos \frac{\omega_{12} - \omega_{23}}{2} t \quad \cos \frac{\omega_{12} + \omega_{23}}{2} t \,(1 + \cos \omega_0 t)$$

$$\Omega = \frac{\omega_{12} - \omega_{23}}{2} \quad , \quad \omega_e = \frac{\omega_{12} + \omega_{23}}{2} \, . \tag{49}$$

There appears a beating factor with a frequency Ω which is just half of the difference between ω_{12} and ω_{23}. The beat frequency thus occurs in a region where the $|F = 1, m_F = 0\rangle$ term starts to be field dependent.

Figure 22 shows the result of a measurement by Gurevich et al.,[43] who observed muonium precession at 95 gauss in quartz. And indeed, as can be seen, the precession pattern shows a very nice beating behavior. From the beat frequency and the precession frequency ω_e one can calculate the hyperfine frequency ω_0:

$$\omega_0 = \frac{\omega_e^2}{\Omega} \, . \tag{50}$$

(b) Now assume that $\nu \neq 0$. For completeness we shall also list the solution of Eq. 43 for this case, with the x-axis of observation.[43]

$$P_x(t) = \frac{1}{2} e^{-t/\tau_1} \times \left(\left\{ \cos \Omega^* t + \frac{\sin \Omega^* t}{3\tau_1 \Omega [1 - (3\tau_1 \Omega)^{-2}]} \right\} \cos \omega_- t \right.$$

$$\left. + \frac{2\omega_+}{\omega_0 [1 - (3\tau_1 \Omega)^{-2}]} \sin \Omega^* t \sin \omega_- t \right) \, . \tag{51}$$

There appears an exponential damping factor, with a time constant τ_1 related to ν:

$$\tau_1 = \frac{2}{3\nu} \, . \tag{52}$$

There is also a beat frequency Ω^*, which turns out to be also dependent on τ_1

$$\Omega^* = \Omega [1 - (3\tau_1 \Omega)^{-2}]^{1/2} , \qquad (53)$$

where $\omega_\pm$ and Ω are defined as before. Thus, the electronic relaxation will lead to a damping of muon polarization as well as to a shift in the beat frequency. If chemical reactions of muonium were to occur, there would also be a damping, but no shift in the beat frequency. In principle, a shift in the beat frequency could be used to distinguish between these two possibilities, although in practice the shifts are very small and are mostly beyond experimental determination.

Anyhow, electronic relaxation may play an important role in muon depolarization in the muonium state. Figure 23 shows the results of a measurement by Myasishcheva et al.[44] They observed muonium precession at very small fields in fused quartz. As can be seen, the precession pattern displays a marked damping, depending on temperature. Interestingly, the damping is faster at lower temperature than at higher temperature. Future measurements will show whether we observe muonium chemistry in solids or are dealing with real relaxation phenomena. Both aspects are very interesting.

XI. CHEMICAL REACTIONS OF MUONIUM

Following the treatment of Ivanter and Smilga,[39] we assume that chemical reactions of muonium will lead to compounds in which the muon is in a diamagnetic position. That is, the muon spin is no longer subject to a hyperfine interaction and the muon will precess in a transverse magnetic field as though free. The above assumption does not necessarily reflect

the spectrum of the chemical reaction channels that may be present, as will be discussed later.[45] We are asking: What is the remaining polarization of these muons which have evolved from muonium?

The disappearance of muonium by chemical reactions can be described by an exponential decay law:

$$[\,\mathrm{Mu}\,] = [\mathrm{Mu}]_0\, e^{-t/\tau_{ch}} \tag{54}$$

with τ_{ch} = average chemical lifetime and $[\,\mathrm{Mu}\,]_0 = 1$. The fractions of Mu's that react and disappear at time t in an interval dt is then given by

$$d n_\mu = -\frac{1}{\tau_{ch}}\, e^{-t/\tau_{ch}}\, dt.$$

This fraction of the quasi-free muons will start to precess with the muon Larmor frequency ω_μ and will possess a polarization as in the muonium state at time t:

$$\rho_\mu(t) = \rho_x{}^{\mu}(t) + i\,\rho_y{}^{\mu}(t), \tag{55}$$

using the complex notation as in Eqs. 39-43.

The total polarization at time t_0 is then given by a superposition of all these fractions precessing with frequency ω_μ up to the time t_0, plus a term describing the polarization of the muons still in the muonium state:

$$\tilde{P}_\perp(t_0) = \int_0^{t_0} \rho_\mu(t)\, e^{i\omega_\mu(t-t_0)} \cdot e^{-t/\tau_{ch}}\, \frac{dt}{\tau_{ch}} + \rho_\mu(t_0)\, e^{-t/\tau_{ch}}. \tag{56}$$

For t_0 going to infinity or, in practice, to values much larger than τ_{ch}, we will obtain the residual polarization, that left over after muonium has long ceased to exist.

Fortunately, $\tilde{P}_\perp(t_0 \to \infty)$ can be identified with the Laplace transform of the system

$$\dot{\tilde{\rho}} = A\tilde{\rho} .$$

It is then possible to obtain an algebraic expression for $\tilde{P}_\perp(\infty)$ by standard methods without the need to solve the system of differential equations explicitly. Similarly, the residual polarization in a longitudinal field can be derived. Table III contains the explicit expressions for the residual polarizations. Note that $P_\perp(\infty)$ is a complex expression with

$$P_x = \mathrm{Re}[\tilde{P}_\perp(\infty)], \; P_y = \mathrm{Im}[\tilde{P}_\perp(\infty)] . \tag{57}$$

The phase ϕ of the residual polarization is then obtained from

$$\tan\phi = \frac{P_y}{P_x} . \tag{58}$$

In the presence of a hot-reaction channel, the formulas will have to be supplemented. If h is the fraction of muons that proceeded through the hot-atom channel, the total residual polarization may be expressed as follows:

Transverse component

$$P_{tot,\perp} = h\,\vec{x} + (1 - h)(P_x\,\vec{x} + P_y\,\vec{y}) . \tag{59}$$

Longitudinal component

$$P_{z,\,tot} = h + (1 - h)\,P_z . \tag{60}$$

As stated earlier, the fraction h of muons has conserved its full polarization; and the phase of this polarization is identical to that of the μ-beam polarization, which is $\phi_h = \pi$ for the experimental set up shown in Fig. 2.

From Eq. 57 or Eq. 59 we calculate a $P_{x,\,tot}$ and a phase ϕ which are to be identified with $\xi_\perp$ and ϕ of the positron distribution ($\phi_0 = \phi_h = \pi$); see Eq. 9. Likewise $\xi_\parallel = P_{z,\,tot}$. Equation 59 and Eq. 60 will be referred to as the Ivanter and Smilga equations.

Figure 24 shows schematically the dependence of $P_x = \xi_\perp$ and ϕ on the average chemical lifetime in a small field as given by the Ivanter and Smilga equations, assuming $\nu \equiv 0$ and $\phi_0 = 0$. The dashed curves refer to the case with no hot-atom reactions, the solid ones to the case including these. At very short chemical lifetimes ($< 1/\omega_0$) all muons will evolve from muonium with effectively the same spin phase. Consequently the superposition will lead to no depolarization, and the phase of the residual polarization is given by the phase of the initial polarization. With increasing chemical lifetime, an increasingly random distribution of muon spin phases will be established, resulting in a decreasing residual polarization. From Fig. 24 it is evident that the phase of the residual polarization will first get slightly positive and then negative due to the different signs of the magnetic moment of the electron and the muons.

An irreversible depolarization in a transverse field is thus brought about by the more or less partial randomization of the phases of the free muon precession, which is caused by chemical reactions of muonium at random times. Let us turn now to the question of how one can verify these mechanisms of muon depolarization by muonium formation and subsequent chemical reactions. Concerning chemical reactions, it would be desirable to change the muonium lifetime in some systematic way. This can be done in a solution, where it is possible to dissolve a substance with which muonium can react in any range of concentrations that one likes. Let us call the substance X. The solute is assumed to be chemically inert. We may have

a reaction equation of the form

$$Mu + X \rightarrow MuX$$

The equation governing the reaction rate for such a simple reaction is

$$\frac{d[Mu]}{dt} = -k[Mu][X] \tag{61}$$

with the already introduced solution

$$[Mu] = [Mu]_0 \, e^{-t/\tau_{ch}},$$

where k is the specific reaction constant and

$$\tau_{ch} = \frac{1}{k[N]} . \tag{62}$$

Thus, there is a simple relation between the chemical lifetime and the concentration of some substance with which muonium can react.

Example

It is well known that iodine molecules dissolved, for instance, in methyl alcohol will rapidly capture atomic hydrogen. The same may be expected for muonium. An experiment designed to measure the residual polarization of muons in this solution as a function of I_2 concentration was carried out by the Berkeley group.[46, 47] Figure 25 shows the results obtained in a transverse field of about 100 gauss.

At zero iodine concentration, the residual polarization is about 50% of the initial polarization. This residual polarization is explained as due to muons which proceeded through the hot channel. At medium I_2 concentration, we recognize the predicted saddle point; and at high concentrations, depolarization seems to disappear altogether. We also see that the phase behaves in just the predicted manner. Figures 26 and 27 show data from the same

solution obtained, however, in fields of 1 kG and 4.5 kG. As expected for strong fields, the saddle point has disappeared and the curve is much steeper due to a speed-up of the muonium precession. We now can fit the Ivanter and Smilga formulas for the residual polarization and the phase to these data, from which fit we obtain the absolute value for the specific reaction constant*; in this case it turned out to be

$$k = 1.4 \pm 0.2 \times 10^{11}\ \text{l/sec.mole}$$

The reaction that takes place is

$$I_2 + Mu \rightarrow Mu\,I + I.$$

This is a very large specific reaction constant, which is typical for a region where only diffusion limits the speed of reaction events. Each collision between two reaction partners leads to a reaction.

The activation energy for such processes must consequently be zero or negative. Absolute reaction constants may be measured in this way down to about 5×10^8 l/mole·sec. Smaller reaction constants may be measured from direct observation of muonium precession damping.

It is now of interest to compare muonium reaction rates with those for atomic hydrogen, provided atomic hydrogen reaction rates are known. From gas kinetic considerations, the absolute reaction constant is given by the following expression[48]

$$k = \frac{Z}{\substack{[X][Mu] \\ [H]}} = (r_X + \tau_{\substack{Mu \\ H}})^2 \left[8\pi k T \left(\frac{1}{m_{\substack{Mu \\ H}}} + \frac{1}{m_X}\right)\right]^{1/2} \qquad (63)$$

where Z is the collision number, [X] and [Mu] the relevant concentrations,

*It is assumed that $\nu = 0$, which can safely be done if $\nu << 1/\tau_{ch}$.

r_X and r_{Mu} are the atomic radii, and m_{Mu} and m_X are the masses of the atoms. For atomic hydrogen, we would have to insert an r_H and an m_H. In general, the mass of muonium and of hydrogen is much smaller than the mass of the substance X; so we may neglect $1/m_X$, beside $1/m_{Mu}$ or $1/m_H$. The ratio of k_{Mu}/k_H is then

$$\frac{k_{Mu}}{k_H} \simeq \left(\frac{m_H}{m_{Mu}}\right)^{1/2} \simeq 3. \tag{64}$$

If we adopt a more realistic approach to reaction kinetics in solutions, we will think in terms of diffusion. The specific reaction constant is then given by[48]

$$k = \frac{kT}{\eta_{Mu}} \frac{(r_X + r_{Mu})^2}{r_X r_{Mu}}, \tag{65}$$

with η the viscosity,

$$\eta \approx \sqrt{m_{\substack{Mu \\ H}}}\, e^{E/kT}, \tag{66}$$

where E is a diffusional activation energy. Assuming the same activation energy for the diffusion of atomic hydrogen and muonium, we find for the ratio k_{Mu}/k_H the same value as above.

The reaction constant for the reaction

$$H + I_2 \rightarrow HI + I_2$$

has been measured.[49] Adopting this value, we obtain

$$\left(\frac{k_{Mu}}{k_H}\right)_{exp} \simeq 3.2,$$

which is in close agreement with the predicted value.

The assumption of equal diffusion activation energy for Mu and H is questionable. Due to the lighter mass of the Mu, muonium will also have a larger zero point vibration energy, which may lead to a smaller activation energy for jumping from one site to the other. In addition, tunneling may become possible for muonium, also because of its lighter mass. The same considerations are, of course, applicable with respect to chemical activation energies. Thus, a muonium reaction may proceed much faster than just by a factor of three (for examples, see below).

So far, we have assumed that chemical reactions of muonium will place the muon into a diagmagnetic environment. But it may also happen that the result is a chemical radical with an unpaired electron. The muon is then still subject to a hyperfine interaction, although a weaker one. The radical itself may subsequently react. Thus, there will be an ongoing depolarization until the muon finally ends up in some diamagnetic environment. Phenomenological formalisms treating this more complicated situation have been worked out by Brewer et al.[50] and by W. Fischer.[51] For details see these references.

We want to mention one interesting difference in the approaches of Brewer et al. and Fischer. The formalism of Brewer assumes tacitly that the muon-electron spin correlation will not change during the transition from muonium to radical. This may be explained by assuming that the muonium electron becomes the unpaired electron. The formalism of Fischer assumes that the unpaired electron spin has no correlation with the muon spin at the instant the radical is formed. This may be explained by assuming that the unpaired electron is one belonging to the original molecule with which muonium reacted. Actually, both formalisms have the power to describe both cases. Only future measurements will show how it really is. Anyhow,

there is the possibility of learning something about the rate of certain electrons in chemical reactions. It should also be mentioned that by fitting the Brewer formulas to data points, one can crudely determine the hyperfine frequency in the radicals. As the hyperfine frequency is related to the spin density of the unpaired electron at the muon site, this will give important information on the electronic structure of the radical.

So far, we have shown the results for iodine dissolved in methyl alcohol as the typical example. However, there are a number of more complicated cases which have recently been studied experimentally. The general mechanism is summarized by Fig. 28. The case of I_2 in methyl alcohol is represented by a combination of the left-hand path for the hot reaction (~ 50%) and the extreme right-hand path for the remaining thermalized portion.

Figure 29 shows the case where Br_2 is dissolved in benzene at 200 gauss. The dotted lines are the fit obtained with the same model as used for iodine (Fig. 25), with an obviously poor fit. To correct this discrepancy the inner paths in Fig. 28 are introduced, and the parameters are varied for a good fit. The solid line is the best fit obtained. Similarly, H_2O_2 in water was studied (Fig. 30). Results for HNO_3 in water are shown in Fig. 31; and finally, Fig. 32 shows results for $Fe(ClO_4)_3$ in water. In comparing these rate constants with the corresponding rates for analogous radicals in which the muon is replaced by a proton, the difference in masses of Mu and H should affect only the "dynamics" of the processes. Even MuO$^{\cdot}$, the lightest muonic radical envisioned, should diffuse through liquids at the same rate as its protonic analog, HO$^{\cdot}$; the "kinetics" are virtually indistinguishable. Comparisons of reaction rates of muonic and protonic versions of these radicals should therefore admit of straight-

forward interpretation in terms of the dynamics of the activated complex.

The most serious difficulty with this interpretation is the uncertainty as to which radical is actually being produced. In the cases of HNO_3 and $Fe(ClO_4)_3$ solutions, for instance, we do not attempt to identify the radical species. The fitted value for ω_r/ω_0, while imprecise, does provide a hint as to likely candidates, suggesting $MuO^{\cdot}$ in the case of $Fe(ClO_4)_3$. However, this cannot be regarded as conclusive evidence, and the products of the reactions

$$Mu + NO_3^- \xrightarrow{(k_{mxr})} R \text{ (unidentified)} \quad \text{and}$$

$$Mu + ClO_4^- \xrightarrow{(k_{mxr})} \text{(muonium-containing radical)}$$

must be regarded as unknown. It would be possible to determine the hyperfine coupling in the radicals to higher precision using a longitudinal field technique, but this has not yet been undertaken.

In some cases it is possible to deduce the identity of the radical, if there is only one species of "reagent" and the products of its reaction with H are well known. In hydrogen peroxide solutions, for instance, there seems little doubt that reactions

$$Mu + H_2O_2 \xrightarrow{(k_{mxd})} HO^{\cdot} + MuHO \quad \text{and}$$

$$Mu + H_2O_2 \xrightarrow{(k_{mxr})} MuO^{\cdot} + H_2O$$

must dominate.[52] Therefore the radical species is most probably $MuO^{\cdot}$. Our value for the rate constant for reaction of $MuO^{\cdot}$ with H_2O_2 is $k_{rxd} = (1.4 \pm 0.2) \times 10^9$ liter/mole sec. The corresponding rate for $HO^{\cdot} + H_2O_2$ is about $(3 \pm 2) \times 10^7$ liter/mole sec, a factor of 50 slower.[49] This difference is almost certainly due to dynamic isotope effects, and deserves serious theoretical consideration.

The addition of H to benzene to form cyclohexadienyl is also a well-established reaction,[53] a fact which lends credence to the assumption that $C_6H_6Mu^{\cdot}$ is the radical involved in reactions

$$Mu + C_6H_6 \xrightarrow{(k_{msr})} C_6H_6Mu^{\cdot} \qquad \text{and}$$

$$C_6H_6Mu^{\cdot} + Br_2 \xrightarrow{(k_{rxd})} D \text{ (unidentified)}.$$

We are unaware of any measurement of the reaction rates for $C_6H_7^{\cdot}$ with Br_2 or I_2; our measurements of $k(C_6H_7Mu^{\cdot} + Br_2) = (3.6 \pm 1.0) \times 10^9$ liter/mole sec and $k(C_6H_6Mu^{\cdot} + I_2) = (2 \pm 1) \times 10^9$ liter/mole sec may represent the only information available on these reactions. In view of the large size of the $C_6H_6Mu^{\cdot}$ molecule and the similarity of the rates with Br_2 and I_2, the reaction is probably diffusion controlled in liquids.

In summary, one sees that there is much more to be learned by extending this type of measurement; we are seeing only the beginning of an extensive program of interesting chemical studies.

XII. MUONIUM IN SOLID INSULATORS

The evolution of muonium in an insulator is basically described by the formalism in section X. If muonium has a sufficiently long lifetime (no chemical reactions), direct muonium precession should be observable—as has been seen in ice, quartz,[44, 51, 54] and frozen CO_2.[44] The observed damping, as already mentioned, is probably the result of relaxation of the muonium electron spin. If chemical reactions between muonium and the solid take place rapidly, the Ivanter and Smilga equations may be applicable in describing the residual polarization.

As conjectured in section VII, muonium in a solid will form an impurity state. This may lower the electronic wavefunction density at the muon

site; consequently, the hyperfine interaction energy

$$A = \hbar\omega_0 = \frac{8\pi}{3} g_J \mu_0^e g_\mu \mu_0^\mu \left|\psi_S(0)\right|^2$$

is expected to be lower than in free muonium. Because $\left|\psi_S(0)\right|^2 = \frac{1}{\pi r_0^3}$, one may speak of an increase of the size of muonium in the crystal lattice.

Although muonium in ice, quartz, and solid CO_2 is well represented within the experimental accuracy by the Hamiltonian of Eq. 10, with ω_0 equal to the ω_0 of free muonium, results obtained in semiconductors (see next section) do indicate a change of size.

If we view muonium in a crystal as a paramagnetic impurity, by analogy with ESR results on paramagnetic impurities it is no longer obvious that the Hamiltonian of Eq. 10 provides a good description of a muonium center in a crystal under all circumstances. Instead, one is led to a Hamiltonian which is common in ESR work on paramagnetic impurities and which is known as the effective spin Hamiltonian:[55]

$$\mathcal{H} = \vec{J}_e \cdot \underset{\sim}{A} \cdot \vec{S}_\mu + \mu_0^e \vec{H} \cdot g_e \cdot \vec{J}_c + \mu_0^\mu \vec{H} \cdot g_\mu \cdot \vec{S}_\mu , \qquad (67)$$

where $\underset{\sim}{A}$, $\underset{\sim}{g}_e$ and $\underset{\sim}{g}_\mu$ are now tensors and $\vec{J}$, $\vec{S}$ are effective spins, not real spins. This phenomenological Hamiltonian thus becomes anisotropic. Values of J, S, $\underset{\sim}{g}$, and $\underset{\sim}{A}$ may be quite different from the true ones; and the relation between the effective entities and the real ones is often quite complicated. Anyway, by adopting such an effective spin Hamiltonian, one is able to describe quite complicated ESR patterns and their dependence on spatial orientation of the ESR probe. The next section will give an example in which this Hamiltonian is also appropriate for muonium in a semiconductor.

We now want to discuss a measurement of the longitudinal residual polarization in a single crystal of KCl by Ivanter et al.[56] Figure 33 shows

the results in dependence on the magnetic field strength. The Ivanter and Smilga formula Eq. 60 was fitted to these data, yielding

$$H_0 = \frac{H}{X} = \frac{\hbar\omega_0}{g_J\mu_0^e - g_\mu\mu_0^\mu} = 1540\pm60 \text{ G}$$

and the product $\nu\tau_{ch} = 1.81 \pm 0.10$ The fit is indicted by the solid line in Fig. 33. As can be seen, the low-field data are by no means reproduced by the fit. Apparently there are different mechanisms governing the low-field behavior. ω_0 appears to coincide within its error bars, which are quite large, with the vacuum value. Unfortunately, it is not possible to obtain separate values for ν and τ from the fit. This would be possible, however, if one could somehow fix the value for ω_0.

From ESR measurments on U_2 centers in KCl, the hydrogen analogue to muonium in a crystal, one obtains a hyperfine splitting frequency for the hydrogen ground state which is 3% smaller than the vacuum value.[57] Using for muonium in this crystal a 3% smaller value of ω_0, one arrives at the following numbers for ν and τ:

$$\nu = 3.5\times10^9 \text{ sec}^{-1}$$

$$\tau = 6.4\times10^{-10} \text{ sec}.$$

The lifetime appears rather short, which may be reasonable as the measurements were performed at room temperature. However, ν, which is the inverse of the spin-lattice relaxation time of the muonium electron, appears to be surprisingly large. If muonium were in a pure s-state no coupling of the electron spin to the diamagnetic lattice should occur; that is, there would be no coupling to phonons and, consequently, no relaxation should be visible. A spin-lattice interaction becomes possible if the spin is coupled to some orbital angular momentum (LS coupling), which in turn is sensitive to the electric crystal field. The crystal field is time modulated by phonon modes. Hence, the ground state of muonium in this crystal must contain some admixtures of excited muonium states, for instance, the 2p state. This

admixture has to be facilitated by the static part of the electric crystal field. An indication for this mechanism in the case of KCl is the 3% smaller hyperfine frequency of U_2 centers.

It is evident that a careful analysis of muon depolarization data involves a lot of crystal properties, and one might even hope to learn something about crystal properties by this procedure.

In the original work of Ivanter and Smilga, ν is always tacitly assumed to be field independent. This assumption is by no means obvious. Table IV lists formulas for the relaxation times of paramagnetic impurities in ionic crystals[58] as derived for different phonon processes: 1) the direct process, a one-phonon process; 2) the Raman process, involving two phonons; and 3) the Orbach process, which involves an excited electronic level. Only the Orbach process is field independent. Future muon depolarization measurements promise to shed some light on the phenomena actually ocurring. These processes are not, as is evident, a particular feature of the muon, but are of relevance in many other solid state phenomena.

So far, we have only considered muonium in a nonmagnetic insulator. Some particularly nice effects may be expected for muonium in a ferromagnetic insulator.[59] The muonium electron will be coupled by an exchange interaction to the ferromagnetically ordered spins of the sample—not so, however, the muon. The relevant Hamiltonian would thus be of the form:

$$\mathcal{H} = A \vec{S}_\mu \cdot \vec{S}_e + \left(g_e \mu_0^e \vec{H}_{loc} + \sum_i J_i \vec{S}_i \right) \vec{S}_e + g_\mu \mu_0^\mu \vec{H}_{loc} \cdot \vec{S}_\mu , \qquad (68)$$

with J_i being an exchange integral of the muonium electron with a neighbor electron, labeled i, whose spin is S_i. Thus, the electron will see an effective magnetic field which may be different by many orders of magnitude from the field that acts on the muon. There will also be an interesting

possibility for the muonium electron relaxation in ferromagnetic insulators, namely, the absorption or emission of magnons, the quanta of ferromagnetic spin waves. The measurement of relaxation times in these substances may lead, for instance, to a determination of magnon scattering cross sections with muonium.[59] Further, the presence of a majority spin on a ferromagnet leads to an unequal population of the $^1S_0$ and $^3S_1$ states of muonium.

XIII. MUONIUM IN SEMICONDUCTORS

The behavior of muons in semiconductors which form muonium can be studied by using the beating technique described in Section X. Gurevich et al.[43] observed that the hyperfine splitting deviated from the vacuum value

$$\nu_{Ge}/\nu_0 = 0.56 \pm 0.01.$$

Brewer et al.[60] have repeated these measurements in silicon and germanium using a slightly more sensitive technique. The extraction of frequencies in the muon polarization spectra is made by using a Fourier analysis of the entire elapsed time distribution; the computer program subtracts the background, corrects for natural decay, and obtains the frequency distribution over a wide range. For each strong component one can obtain a rough mean life for the damping. Figure 34 shows the results of such an analysis for p-type silicon at 70°K. Quartz is shown for comparison; the line separation varies with $1/\omega$:

$$\nu_{Si}/\nu_0 = 0.45 \pm 0.02.$$

This result would seem to contradict the earlier study of Feher et al.[17] where the "shallow donor" proposal was put forth; apparently, a large change in the electron wavefunction is not occurring. Wang and Kittel[61] have shown

that a "deep donor" model, in which the muonium is trapped within an interstitial site leading to a slight swelling of the wave function, must be responsible for this reduction in ν_0.

In their study, Wang and Kittel looked at several models. Briefly, the potential function for the bound electron is cut off at large radii due to screening by the valence band electrons of the neighboring silicon atoms. By invoking other data on the properties of the semiconductors, they are able to explain the magnitude of the reduction of ν_0, as well as the small difference between silicon and germanium. Other searches for atomic hydrogen in semiconductors have never yielded any results although it is well known that hydrogen diffuses freely in Ge and Si. Their conclusion is that we know more about muonium in Ge and Si than about H or H_2 in these crystals upon which rests most of modern solid state electronics technology.

In our cold p-type silicon spectra, we see not only the two familiar muonium peaks but also two others of similar amplitude, which we have called "anomalous muon precession" for lack of a positive identification of their source. Figure 34 shows a comparison between Fourier spectra for silicon and fused quartz in the same field, demonstrating the absence of anomalous precession in quartz. Whereas the muonium frequencies rise approximately linearly with field up to a few hundred gauss, and are independent of the orientation of the crystal in the field, the anomalous frequencies have the field dependence shown in Fig. 35, and are slightly anisotropic, as indicated. Both anomalous precession and muonium precession have a lifetime on the order of 300 nsec. Neither of these signals has been detected in n-type Si at 77°K or in any silicon sample at room temperature.

The anomalous frequencies are much higher than the free muon precession frequencies in weak magnetic fields. The muon must therefore be

coupled to a particle or system with a larger magnetic moment than its own, as in muonium, where it is coupled to an electron by the contact interaction. The field dependence of the data can in fact be fitted to frequences ν_{12} and ν_{34} of a modified Breit-Rabi formula (see Fig. 7), if the different crystal orientations are treated as separate cases. However, it is necessary to allow both the hyperfine coupling strength and the g-factor of the electron to vary in order to obtain a fit. For the case of the [111] crystal axis parallel to the field, the best value for ν_0/ν_0 (vac) is 0.0198 ± 0.0002; for [100] parallel to the field, the best value is ν_0/ν_0 (vac) $= 0.0205 \pm 0.0003$. In both cases the best value for g_J is 13 ± 3. Clearly, the spin g-factor of an electron cannot be much different from 2, nor can a pure contact interaction be anisotropic; this modified Breit-Rabi description is meant only as a phenomenological characterization of the data.

These results can be interpreted in terms of a number of physical models. Perhaps the simplest is shallow-donor muonium. Here the electron wavefunction is spread over many lattice sites, whereas the entire deep-donor muonium atom fits into one interstitial site. An s-state cannot produce the observed behavior, due to the relatively invariable spin g-factor of the electron. However, in the 2p state the orbital g-factor can be large and anisotropic: the electron wavefunction for a shallow donor must be a superposition of conduction band states, which may have small anisotropic effective masses. If the spin-orbit coupling for the electron is large, j_e becomes a good quantum number, and $\vec{J}_e'$ formally replaces $\vec{J}_e = \vec{S}_e$ in the Breit-Rabi Hamiltonian. A possible objection to this model is the requirement of a minimum lifetime of ~300 nsec for the 2p excited state. Hindrance of the normally fast radiative E1 transition $2p \rightarrow 1s$ can be explained by the small overlap between electron wavefunctions in the shallow-donor 2p state

and the deep-donor 1s state.

A second physical model is suggested by the large variety of ESR centers which have been observed in radiation-damaged silicon.[62] The muon may create a paramagnetic lattice defect (e.g., a broken bond) at the end of its range, combining with it to form a muon-defect bound state. Such a center can also be described by a modified Breit-Rabi Hamiltonian.

The possibility that the anomalous precession is due to formation of a bound state of a muon with an impurity atom is considered remote. The fractional concentration of impurity atoms in our sample is $\sim 10^{-8}$ or less; muons can be expected to slow from ~100 eV to thermal velocities within $\sim 10^3$ collisions.[63] Thus the probability of a muon passing within several lattice sites of an impurity atom at subionizing velocity is negligible. Furthermore, the time for deep-donor muonium atoms to diffuse to impurity atoms with muon affinities must be longer than ~300 nsec, the observed relaxation time for muonium precession.

However, in stopping, the muon must generate a high density of free electrons and holes, with which it may subsequently combine. If we regard the μ^+ as a positive impurity ion in an interstitial position, observations of impurity-exciton bound states in silicon[64] provide a precedent for two models involving excitons. The first model is the neutral muonium-exciton molecule ($\mu^+ e^- e^- h^+$), in which the two electrons are assumed to have paired spins, in analogy with ground-state H_2. The μ^+ is thus coupled to the hole by a dipole-dipole interaction. Orientational effects are predicted by this model if the molecule is "pinned" by being wedged into an oblong interstitial site in the unit cell.[65] A second model of this type is the ionized muonium-exciton molecule ($\mu^+ e^- h^+$), in which all three particles are coupled via contact interactions. These models draw support from the fact

that measured free exciton lifetimes in silicon at 80°K are about 400 nsec.[66]

None of the above physical models for anomalous muon precession can be eliminated on the basis of existing data; however, we feel that shallow-donor 2p muonium is the most probable explanation. In an earlier study at Columbia,[17,11] the "quenching" of μ^+ depolarization in silicon by a magnetic field applied parallel to the muon polarization was interpreted in terms of transitory muonium formation. Their results in p-type silicon at $\leq$ 77°K suggested the existence of two species of muonium with different hyperfine couplings. However, their prediction that muonium in silicon would only form a short-lived shallow-donor state is contradicted by our observation of long-lived deep-donor 1s muonium. If the anomalous precession is in fact due to shallow-donor 2p muonium (albeit long-lived), their conclusions will be at least partially vindicated. In any event, it is clear that positive muons can provide a great deal of new information about the behavior of hydrogen-like impurities in silicon.

XIV. COMPARISON WITH OTHER METHODS

It may be appropriate to list some of the advantages and disadvantages in measuring certain parameters with the help of the muon as compared with other methods, e.g. to U_2 centers. With regard to relaxation times, Fig. 36 summarizes the situation. The figure has been taken from Ref. 67 and has been supplemented by the range of relaxation times measurable by the muon and muonium, respectively.

The electronic relaxation times are generally measured by the method of ESR (electron spin resonance). The shortest relaxation times that can be measured are of the order of 10^{-9} sec. At least 10^{12} electron spins are needed to obtain a sufficient signal-to-noise ratio. ESR is normally not

applicable in zero external field. With the help of the muon, electronic relaxation times can be measured down to 10^{-11} sec. Only about 10^6 decay events need to be observed. The main disadvantage is that the longest relaxation times that can be measured are only of the order of several μsec. And, of course, implantation of muonium may not lead to the occupation of a site that is wanted for investigation.

The situation is similar with respect to nuclear T_1 and T_2 times. NMR, the most common method for measuring nuclear relaxation times, will not reach below 10^{-6} sec, whereas the muon can be used to measure relaxation times down to $\sim 10^{-8}$ sec. In zero local magnetic field, NMR becomes inapplicable; in metals, as argued before, NMR is a difficult-to-perform technique. However, with NMR one can measure very long relaxation times—minutes—whereas the upper limit in the muon technique is about 500 μsec. With respect to measurements of hyperfine frequencies, g_J factors, Zeeman splitting frequencies (Larmor frequencies), etc., ESR and NMR have the huge advantage of being very accurate. Application of the muon resonance technique is limited because of the muon's finite lifetime, which introduces a minimum line width.

Finally, there are a number of methods for measuring local fields in, for instance, metals and ferromagnetics: e.g., γγ-PAC, Mössbauer effect, oriented nuclei, NMR, and others. Many of these apply also to implanted ions. Besides the fact that many of these methods are restricted to certain substances, the main trouble with these methods is that the electron core of the probes causes a number of disturbing effects, such as core polarization, that mask or even change the weaker local fields to be measured. Also, many of the nuclei used as probes have a nuclear electric quadrupole moment which participates in all kinds of disturbing interactions, making it difficult

to obtain the desired information on internal local magnetic fields. But the muon is, so to speak, a bare particle carrying only a magnetic moment. Its feedback effects on the local field properties may be small and calculable. This is just what one requires from an ideal probe for exploring bulk properties.

XV. CONCLUDING REMARKS

We have mentioned some of the still persisting puzzles, and how their investigation may cast light on solid state properties, on diffusion mechanisms in a solution, on the chemical kinetics of the hydrogenlike muonium, and on interesting isotope effects. There are other puzzles that may have something to do with solid state chemistry or radical physics in a solid which have not been mentioned: such as, the very short T_2 times of about 30 to 50 nsec which one has measured in sulphur [68] solid $Fe(NO_3)_3$, and $Gd(NO_3)_3$.[69]

As far as chemistry is concerned, the situation looks most promising as the Ivanter and Smilga formulas and the refined theories of Brewer and Fischer provide a sound basis on which to analyze data and to extract meaningful parameters. In many acid organic and inorganic solutions, atomic hydrogen reaction rates are known,[70, 71] making it possible to study isotope effects. In neutral solutions many fewer studies have been performed; and in alkaline solutions practically nothing is known due to a competitive interference from OH^- ions which prohibits use of conventional methods. Here, muonium would be the ideal substitute for atomic hydrogen. Interestingly, the temperature dependence of atomic hydrogen reaction rates, as well as the dependence on the kind of solvent, have practically never been explored.

With regard to solid state physics, the application of muons has resulted in a number of interesting phenomena, and the future prospects are

most encouraging. A meaningful application, however, requires that researchers continue with some effort to learn how to ask meaningful questions that can be answered with the help of the muon, and that do not center on the muon's part of the problem under investigation.

ACKNOWLEDGMENTS

The authors would like to express their appreciation to F. N. Gygax, J. H. Brewer, B. D. Patterson, R. F. Johnson, and D. G. Fleming for their generous contributions and helpful criticism, and to Corrine Sergent and Yvonne Howell for assistance in preparing the manuscript.

This work was performed under the auspices of the U. S. Atomic Energy Commission.

REFERENCES AND NOTES

1. For more details see e.g., A. O. Weissenberg, Muons (North Holland, 1967).
2. R. L. Garwin, L. M. Ledermann, and M. Weinrich, Phys. Rev. 105, 1415 (1957).
3. R. A. Swanson, Phys. Rev. 112, 580 (1958).
4. J. I. Friedmann and V. L. Telegdi, Phys. Rev. 105, 1681 (1957); Phys. Rev. 106, 1290 (1957).
5. V. W. Hughes, Ann. Rev. Nucl. Sci. 16, 445 (1966).
6. J. Orear, G. Harris, and E. Bierman, Phys. Rev. 107, 322 (1957).
7. J. C. Sens, R. A. Swanson, V. L. Telegdi, D. D. Yovanovitch, Phys. Rev. 107, 1465 (1957).
8. A. O. Weissenberg and V. A. Smirnit-Skii, Sov. Phys. JETP 12, 175 (1960).
9. G. Charpak, F. J. M. Forley, R. L. Garwin, T. Muller, J. C. Sens, V. L. Telegdi, C. M. York, and A. Zichichi, Nuovo Cimento 22, 199 (1961).
10. S. Gorodetzky, Th. Muller, M. Port, A. Zichichi, Phys. Lett. 2, 133 (1962).
11. A. Buhler, T. Massam, Th. Muller, M. Schneegans, and A. Zichichi, Nuovo Cimento 29, 812 (1965).
12. B. Eisenstein, R. Prepost, and A. M. Sachs, Phys. Rev. 142, 217 (1966).
13. R. A. Ferrell, Y. C. Lee, and K. M. Pal, Phys. Rev. 118, 317 (1960).
14. D. P. Hutchinson, J. Menes, G. Shapiro, and A. M. Patlach, Phys. Rev. 131, 1351 (1963).

15. A. Buhler et al., Nuovo Cimento 29, 824 (1965).

16. I. V. Iakovleva, Sov. Phys. JETP 35, 676 (1959).

17. G. Feher, R. Prepost, and A. M. Sachs, Phys. Rev. Lett. 5, 515 (1960).

18. K. M. Crowe, J. F. Hague, J. E. Rothberg, A. Schenck, D. L. Williams, R. W. Williams, and K. K. Young, Phys. Rev. D5, 2145 (1972).

19. S. K. Allison, Rev. Mod. Phys. 30, 1137 (1958).

20. E. Fermi and E. E. Teller, Phys. Rev. 72, 399 (1947).

21. R. M. Mobley, thesis (Yale University, 1967), unpublished.

22. S. K. Allison and M. Garcia-Munoz, in Atomic and Molecular Processes, D. R. Bates, Ed. (Academic Press, New York, 1962), Ch. 19.

23. A. Abragam, The Principles of Nuclear Magnetism (Clarendon Press, Oxford, 1970).

24. T. Coffin, R. C. Garwin, S. Penman, L. M. Lederman, and A. M. Sachs, Phys. Rev. 109, 973 (1958).

25. J. Alonso and L. Grodzins, in Hyperfine Structure and Nuclear Radiations, E. Matthias and D. A. Shirley, Eds. (North Holland, Amsterdam, 1968), p. 549.

26. See e.g., K. H. Hellwege, Einführung in die Festkörperphysik II, (Springer Verlag, Berlin, 1970), Ch. 22.1.

27. See e.g., A. Narath, in Hyperfine Interactions, A. J. Freeman, K. B. Frankel, Eds. (Academic Press, New York, 1967), p. 287.

28. M. L. G. Foy, N. Heiman, W. J. Kossler, and C. E. Stronach, Phys. Rev. Lett. 30, 1064 (1973).

29. A. Schenck and K. M. Crowe, Phys. Rev. Lett. 26, 57 (1971).

30. R. Wolfgang, Progr. Reaction Kinetics 3, 99 (1965).

31. For a compilation see e.g., N. J. Poulis and W. P. A. Hass, Landolt-Bornstein, Zahlenwerte und Funktionen, Vol. II, Part 9, "Magnetic Properties I" (Springer Verlag, Berlin, 1962).

32. A. Schenck, Phys. Lett. 32A, 19 (1970) and unpublished results.

33. A. Schenck, D. L. Williams, J. H. Brewer, K. M. Crowe, and R.F. Johnson, Chem. Phys. Lett. 12, 544 (1972).

34. N. Bloembergen and L. O. Morgan, J. Chem. Phys. 34, 842 (1961).

35. R. A. Bernheim, T. H. Brown, H. S. Gutowsky, and D. E. Woessner, J. Chem. Phys. 30, 950 (1959).

36. C. C. Hinckley and L. O. Morgan, J. Chem. Phys. 44, 898 (1966).

37. A. W. Nolle and L. O. Morgan, J. Chem. Phys. 36, 378 (1962).

38. B. B. Garrett and L. Morgan, J. Chem. Phys. 44, 890 (1966).

39. I. G. Ivanter and V. P. Smilga, Sov. Phys. JETP 27, 301 (1968).

40. I. G. Ivanter and V. O. Smilga, Sov. Phys. JETP 28, 796 (1969).

41. V. G. Nosov and I. V. Iakovleva, Sov. Phys. JETP 16, 1236 (1963); and Nucl. Phys. 68, 609 (1965).

42. R. K. Wangsness and F. Bloch, Phys. Rev. 89, 728 (1953).

43. I. I. Gurevich, I. G. Ivanter, E. A. Meleshko, B. A. Nikal' skii, V. S. Roganov, V. I. Selivanov, V. P. Smilga, B. V. Sokolov, and V. D. Shestakov, Sov. Phys. JETP 33, 253 (1971).

44. G. G. Myasishcheva, Yu. V. Obukhov, V. S. Roganov, and V. G. Firsov, Sov. Phys. JETP 26, 298 (1968).

45. V. G. Firsov and V. M. Byakov, Sov. Phys. JETP 20, 719 (1965); A. I. Babaev, M. Ya. Balats, G. G. Myasishcheva, Yu. V. Obukhov,

V. S. Roganov, and V. G. Firsov, Sov. Phys. JETP 23, 583 (1966).

46. J. H. Brewer, K. M. Crowe, R. F. Johnson, A. Schenck, and R. W. Williams, Phys. Rev. Lett. 27, 297 (1971).

47. J. H. Brewer, K. M. Crowe, F. N. Gygax, R. F. Johnson, D. G. Fleming, and A. Schenck, to be published in Phys. Rev. A.

48. See e.g., E. A. Moelwyn-Hughes, Physical Chemistry, 2nd ed. (Pergamon Press 1965).

49. M. Anbar and P. Neta, Int. J. Appl. Rad. and Isotopes 18, 493 (1967).

50. J. H. Brewer, F. N. Gygax, and D. G. Fleming, Phys. Rev. A8, 77 (1973).

51. W. E. Fischer, SIN-preprint (1973).

52. J. P. Sweet and J. K. Thomas, J. Phys. Chem. 68, 1363 (1964).

53. B. D. Michael and J. Hart, J. Phys. Chem. 74, 2878 (1970).

54. I. I. Gurevich et al., Phys. Lett. 29B, 387 (1969).

55. See e.g., B. Bleany, in Hyperfine Interactions, A. J. Freeman, R. B. Frankel, Eds.(Academic Press, New York, 1967), Ch. I.

56. I. G. Ivanter, E. V. Minaichev, G. G. Myasishcheva, Yu. V. Obukhov, V. S. Roganov, G. I. Savel'ev, V. P. Smilga, and V. G. Firsov, Sov. Phys. JETP 35, 9 (1972).

57. J.-M. Spaeth, Z. Phys. 192, 107 (1966).

58. See e.g., A. A. Manenkov and R. Orbach, Eds. Spin-Lattice Relaxation in Ionic Solids (Harper and Row, New York, 1966).

59. H. C. Siegmann, S. Strässler, and P. Wachter, Proceedings of the Meeting on Muons in Solid State Physics (Bürgenstock, Switzerland, 1971), 2. Teil, p. 91.

60. J. H. Brewer, K. M. Crowe, F. N. Gygax, R. F. Johnson, B. D. Patterson, D. G. Fleming, and A. Schenck, Phys. Rev. Lett. 31, 143 (1973).

61. J. Shy-Yih Wang and C. Kittel, Phys. Rev. B7, 713 (1973).

62. G. Lancaster, ESR in Semiconductors (Plenum Press, New York, 1967).

63. This estimate is obtained by considering the mean energy loss in elastic collisions with stationary quasi-free silicon atoms.

64. J. R. Haymes, Phys. Rev. Lett. 4, 361 (1960).

65. V. M. Samoilov, Sov. Phys. JETP 31, 1189 (1970).

66. V. S. Vavilov and E. L. Nolle, Sov. Phys. Semicond. 2, 616 (1968).

67. H. H. Wickman, in Hyperfine Structure and Nuclear Radiations, E. Matthias and D. A. Shirley, Eds. (North Holland, Amsterdam, 1968).

68. I. I. Gurevich, L. A. Makar'ina, E. A. Meleshko, B. A. Nikol'skii, V. S. Roganov, V. I. Selivanov, and B. V. Sokolov, Sov. Phys. JETP 27, 235 (1968)

69. Unpublished data of Berkeley group.

70. P. Neta, Chemical Reviews 72, 533 (1972).

71. P. Neta, private communication (1973).

72. See e.g., E. Segre, Nuclei and Particles (Benjamin, New York, 1965), Ch. II.

73. G. W. Ford and C. J. Mullin, Phys. Rev. 108, 477 (1958).

74. G. Wentzel, Phys. Rev. 75, 1810 (1949).

75. H. S. W. Massey and E. H. S. Burhop, Electronic and Ionic Impact Phenomena (Clarendon Press, Oxford, 1952), p. 441.

Table I. Muon properties.

Spin ($\vec{S}_\mu$)	1/2
Mass (m_μ)	$206.7\ m_e = 105.6$ MeV
Magnetic moment ($\vec{\mu}_\mu$)	$\frac{g_\mu e\hbar}{2m_\mu c}\ \vec{S}_\mu\ (\approx 3.18\mu_p)$
Lifetime (τ_μ)	2.2 μsec

g_μ = anomalous Landé factor.

Table II. Results of the Swanson experiment.[3]

Target substance	Residual polarization
Metals (Al, Be, Li, Mg)	No depolarization visible
Semimetals (Si, graphite)	No depolarization visible
SiC, B_4C	No depolarization visible
P, S	0.05 - 0.1%
CsI, NaCl	0.12 - 0.17%
H_2O	0.5%
Organic substances (liquid, solid)	0.2 - 0.8%

Table III. Expressions for residual polarizations

$$\tilde{P}_{\parallel}(\infty) = 1 - (\omega_o\tau)^2\left(\frac{1}{2} + \nu_{\perp}\tau\right)\left\{(1 + 2\nu_{\perp}\tau)^2 + (\omega_o\tau)^2\left[\frac{(1+2\nu_{\perp}\tau)(1+\nu_{\parallel}\tau)}{(1+2\nu_{\parallel}\tau)} + x^2(1+\zeta)^2\right]\right\}^{-1},$$

where ω_o is the hyperfine frequency

τ is the chemical lifetime

$\nu_{\perp}$ is the electron spin relaxation parameter perpendicular to the field.

$\nu_{\parallel}$ is the electron spin relaxation parameter along the field.

$x = H/H_o$, the dimensionless magnetic field

$\zeta = m_e/m_u$

$$P_{\perp}(\infty) = -\frac{1}{\tilde{\tau}}\left\{\gamma_{\parallel} + i\,\frac{\left[A_o^2B_o^2 - (A_o+B_o)^2\right]}{\left[A_o B_o^2 - (A_o+B_o)\right]}\right\}^{-1}$$

where $\gamma_{\parallel} = 4\nu_{\parallel}/\omega_o$

$$A_o = i\left(\frac{1}{\tilde{\tau}} + \gamma_{\parallel}\right) + 2x\left(\zeta - \frac{\tilde{\omega}_{\mu}}{2x}\right)$$

$$B_o = i\left(\frac{1}{\tilde{\tau}} + \gamma_{\perp}\right) - 2x\left(1 + \frac{\tilde{\omega}_{\mu}}{2x}\right)$$

$$\tilde{\tau} = \frac{\tau\omega_o}{2}$$

$$\tilde{\omega}_{\mu} = \frac{2\omega_{\mu}}{\omega_o}$$

Table IV. Formulas for relaxation times of paramagnetic impurity spins in ionic crystals due to phonon process (H = magnetic field strength; T = temperature).

Process	Relaxation rate
Direct process: one-phonon exchange	$\frac{1}{T_1} \approx A \quad H^4 T$
Raman process: two-phonon exchange	$\frac{1}{T_1} \approx B_1 T^9 + B_2 H^2 T^7$
Orbach process	$\frac{1}{T_1} \approx C \exp\left(-\frac{\Delta_c}{kT}\right)$

FIGURE CAPTIONS

Fig. 1. Muon decay spectrum. Top curve: unpolarized spectrum. Bottom curve: asymmetry contribution.

Fig. 2. Typical beam setup. Top and side views of stopping target, counter arrangement, and magnet coils. (Not to scale.)

Fig. 3. Rotation of the asymmetric decay pattern of stopped positive muons in a transverse magnetic field $\vec{H}$.

Fig. 4. Typical experimental histogram. Carton tetrachloride at 100 gauss. The data are binned into 10-nsec bins for clarity; for fitting, 0.5-nsec bins were used. The mean muon lifetime τ_μ = 2.20 sec is indicated.

Fig. 5. (a) Fast logic for muon experiments. (b) Block diagram of logic network.

Fig. 6. Muon precession in boron carbide after decay and background correction. (From Ref. 3.)

Fig. 7. Hyperfine structure of muonium as a function of external magnetic field.

Fig. 8. Time averaged muon polarization for muonium in a longitudinal magnetic field X.

Fig. 9. Quenching of the depolarization in sulfur at three temperatures. (From Ref. 12.)

Fig. 10. Quenching of the depolarization in LiF, MgO, and red P at room temperature. (From Ref. 12.)

Fig. 11. Polarization vs. externally applied magnetic field for various targets: (a) carbon, (b) sulfur, (c) plastic scintillator, (d) water. (From Ref. 10.)

Fig. 12. Experimental values of the asymmetry parameter, a, for decay positrons from stopped muons: (a) versus free electron concentration in n-type silicon and free hole concentration in p-type silicon; (b) in one sample of n-type germanium (phosphorus-doped) at room temperature and liquid nitrogen temperature; and (c) in a graphite sample for which the maximum value of $a = 0.33$ is assumed to correspond to full muon polarization. The abscissas for n-type and p-type silicon have been joined at the value of the intrinsic concentration for room temperature ($\sim 10^{10}$ cm^{-3}). Since the product of the numbers of free holes and electrons in thermal equilibrium with the lattice is constant at a given temperature (i.e. $\sim 10^{20}$ for silicon at room temperature), the entire abscissa represents an increasing free electron concentration to the right (or an increasing hole concentration to the left). (From Ref. 17.)

Fig. 13. The slowing-down process.

Fig. 14. Evidence that protons approach the end of their range as H atoms. The critical velocity is $\alpha c = 2.2 \times 10^6$ m /sec. (From Ref. 18.)

Fig. 15. NMR spectrum analyzed using a simple dipole-dipole model for the two water molecules.

Fig. 16. (a) The obseved asymmetry, AF(t), for the gypsum crystal orientation having two NMR lines. The asymmetry is calculated for 0.5-μsec intervals versus muon lifetime. The constant background is approximately 2% at t = 0. The solid curve shows the theoretical AF(t).

(b) For a second crystal position, the four lines are seen to interfere at about 4 μsec; and the asymmetry reverses sign between 5 and 8 μsec before the statistics and background obscure the signal. The solid curve for AF(t) was calculated. The detailed agreement is marginal, suggesting that the actual crystal orientation was slightly different from the angles used. These angles were uncertain to ~10°. (From Ref. 29.)

Fig. 17. Concentration dependence of the transverse relaxation time in a $Fe(NO_3)_3$ solution for proton NMR and for μ^+ depolarization.

Fig. 18. (a) Transverse muon relxation times in $MnCl_2$ solutions. The dashed lines represent the spin-exchange and dipole-dipole terms. The solid line is the combined result. (b) Plot of τ_s^* vs. Mn^{2+} concentration at 295° K. Solid line was obtained from Ref. 36.

Fig. 19. (a) Plot of $1/T_2P$ vs. Mn^{2+} concentration. The solid curve is obtained by combining NMR and ESR results. The dashed curves show separately the contributions from spin-exchange and dipole-dipole interactions. (b) Plot of $1/T_2P$ vs. temperature. Dotted curve is the fit obtained without modifications. Solid curves result from our analysis at 4.5 and 11 kG. Dashed curves represent the spin-exchange and dipole-dipole contributions of our analysis separately to 11 kG.

Fig. 20. Evolution of muon polarization in free muonium in 100-G transverse field. P_x^{μ} = projection of μ^+ polarization along original polarization direction.

Fig. 21. Evolution of muonium in 100 gauss: Locus traced out by the tip of the muon polarization vector in the plane perpendicular to the magnetic field.

Fig. 22. Modulated precession of the μ^+-meson in fused quartz. The time analyzer channel width was t = 1.0 nsec. The smooth curve represents the theoretical law with best fit parameters selected using the minimum square method. The theoretical and experimental N(t) data are corrected for the decay exponential exp(-t/T). The magnetic field is $H_{\perp} = 95$ G. (From Ref. 54.)

Fig. 23. Muonium precession curve in crystalline quartz. Horizontal axis—number of channel (10.1 nsec wide); vertical axis—counts corrected for exponential decay of meson. (From Ref. 44.)

Fig. 24. Proper muonium mechanism in 100-G transverse field. Dependence of magnitude and phase of residual polarization upon chemical lifetime τ of free muonium. Positive phase is defined as being in the direction of μ^+ precession. Dashed curves: no hot chemistry. Solid curves: hot fraction h = 0.5.

Fig. 25. Results for iodine dissolved in methanol.

Fig. 26. I_2 in CH_3OH at 1000 gauss: proper muonium mechanism.

Fig. 27. I_2 in CH_3OH at 4500 gauss: proper muonium mechanism.

Fig. 28. Flow chart model of depolarization mechanism in liquids.

Fig. 29. Bromine in benzene at 200 gauss.

Fig. 30. Hydrogen peroxide in water at 100 gauss.

Fig. 31. Nitric acid in water at 100 gauss.

Fig. 32. Ferric perchlorate in water at 100 gauss.

Fig. 33. μ^+ polarization in single crystals of potassium chloride as a function of longitudinal magnetic field strength. (From Ref. 56.)

Fig. 34. Frequency spectra of muons in fused quartz at room temperature and in p-type silicon at 77° K. In both cases the applied field is 100 G. The vertical axis is the square of the Fourier amplitude, in arbitrary but consistent units. In the lower graph the vertical scale is expanded by a factor of 10 to the right of the dashed line. The prominent peaks (from left to right) are: the free muon precession signal at 1.36 MHz; a characteristic background signal at 19.2 MHz, due to rf structure in the cyclotron beam; the two anomalous frequencies at 43.6 ± 2.9 MHz (silicon only); and the two 1s muonium peaks centered about 139 MHz. The wider splitting of the two 1s muonium lines in silicon is due to the weaker hyperfine coupling. These spectra were produced by Fourier-analyzing the first 750 nsec of the experimental histograms. For comparison, the muon asymmetries obtained by maximum-likelihood fits to the first 5 μsec of data were 3.81% ± 0.35% for quartz and 5.05% ± 0.63% for p-type Si at 77° K.

Fig. 35. Dependence of anomalous frequencies in silicon upon field strength and crystal orientation. Round points and solid lines are data and best fit for [111] crystal axis along the field; triangular points and dashed lines are data and best for [100] axis along the field. Free muon, 1s muonium, and cyclotron background signals are not shown. A number of peaks appear in the spectra in addition to the fitted "proper" anomalous frequencies; these are unexplained. They are indicated by square points (for prominent peaks) and horizontal bars (for weak or questionable peaks). The higher of the "proper" anomalous frequencies is missing at several fields. This is because the spectra showed no statistically significant peaks at those positions.

Fig. 36. Approximate nuclear relaxation rates and their detection by standard techniques.

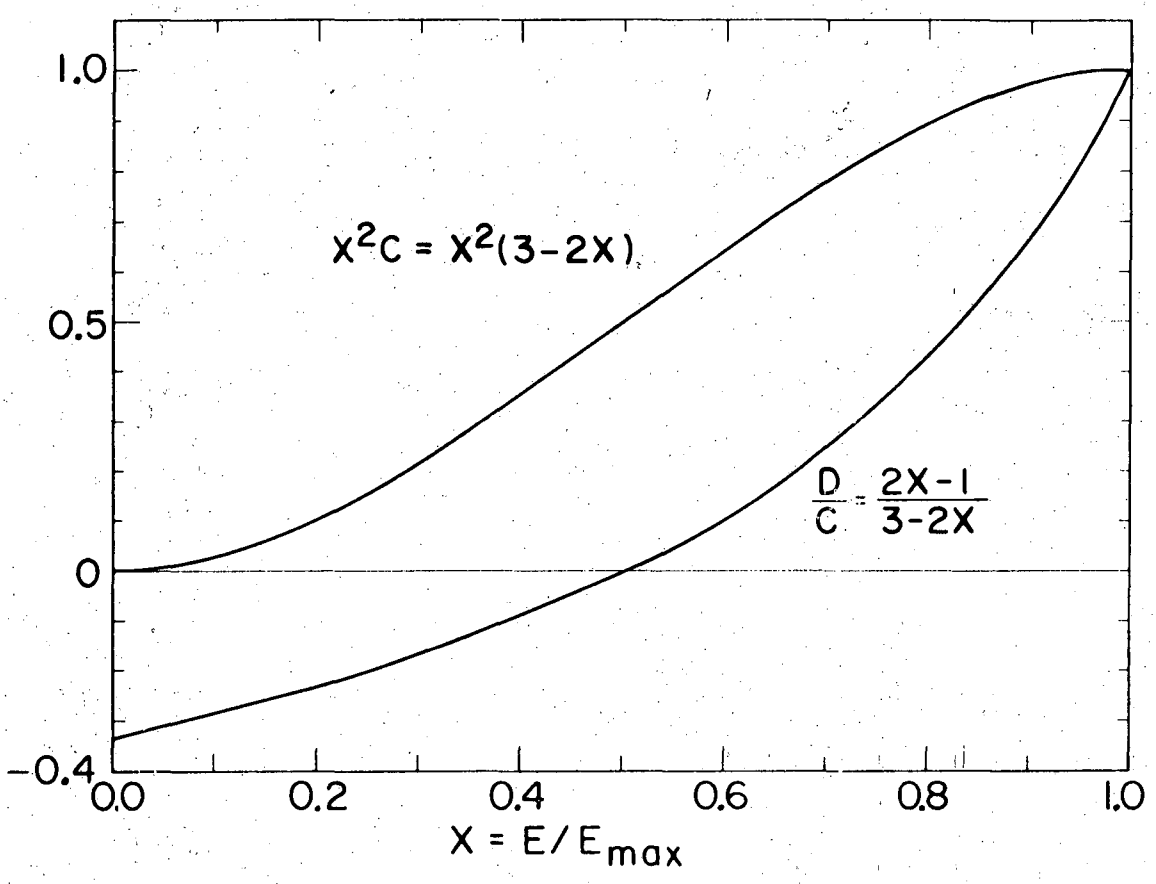

Fig. 1.

XBL7310-4240

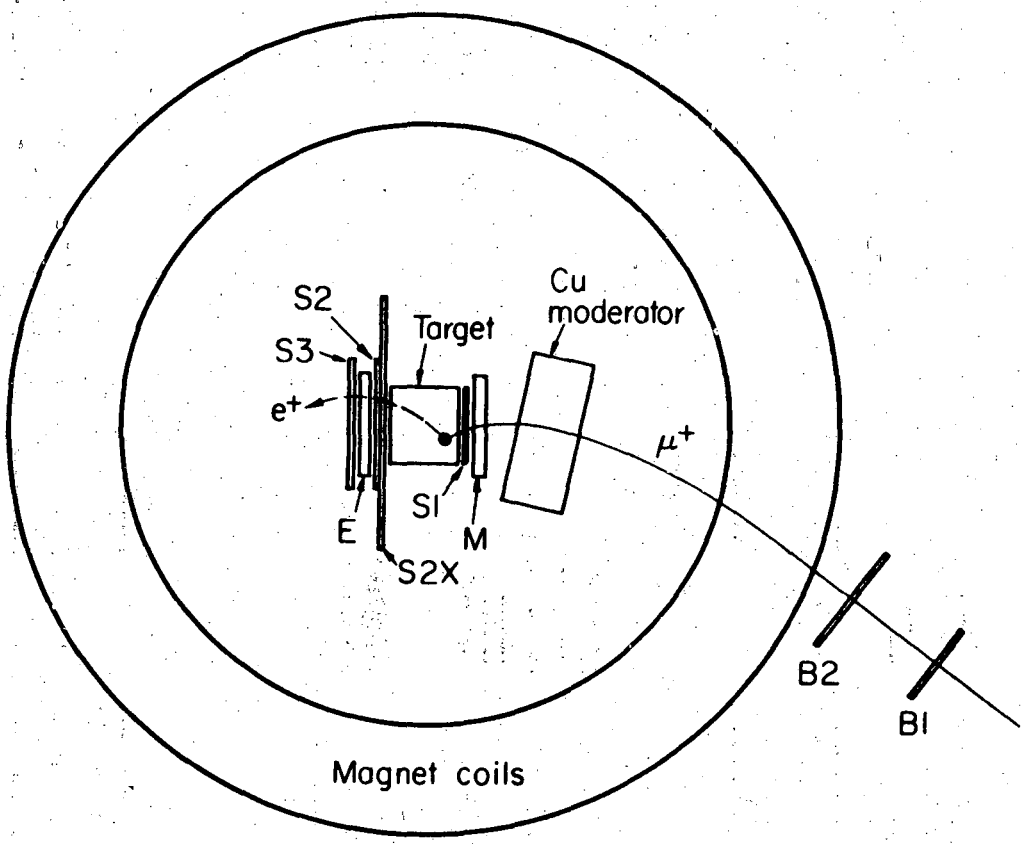

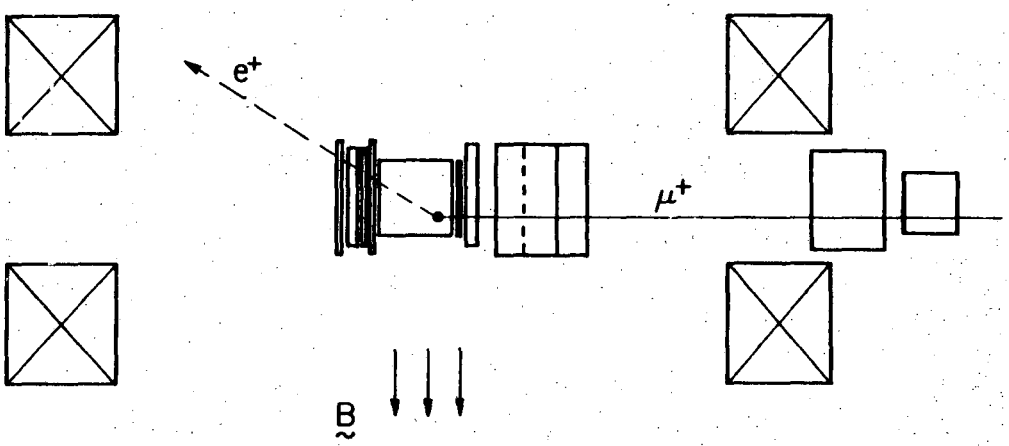

Fig. 2.

XBL735-2916

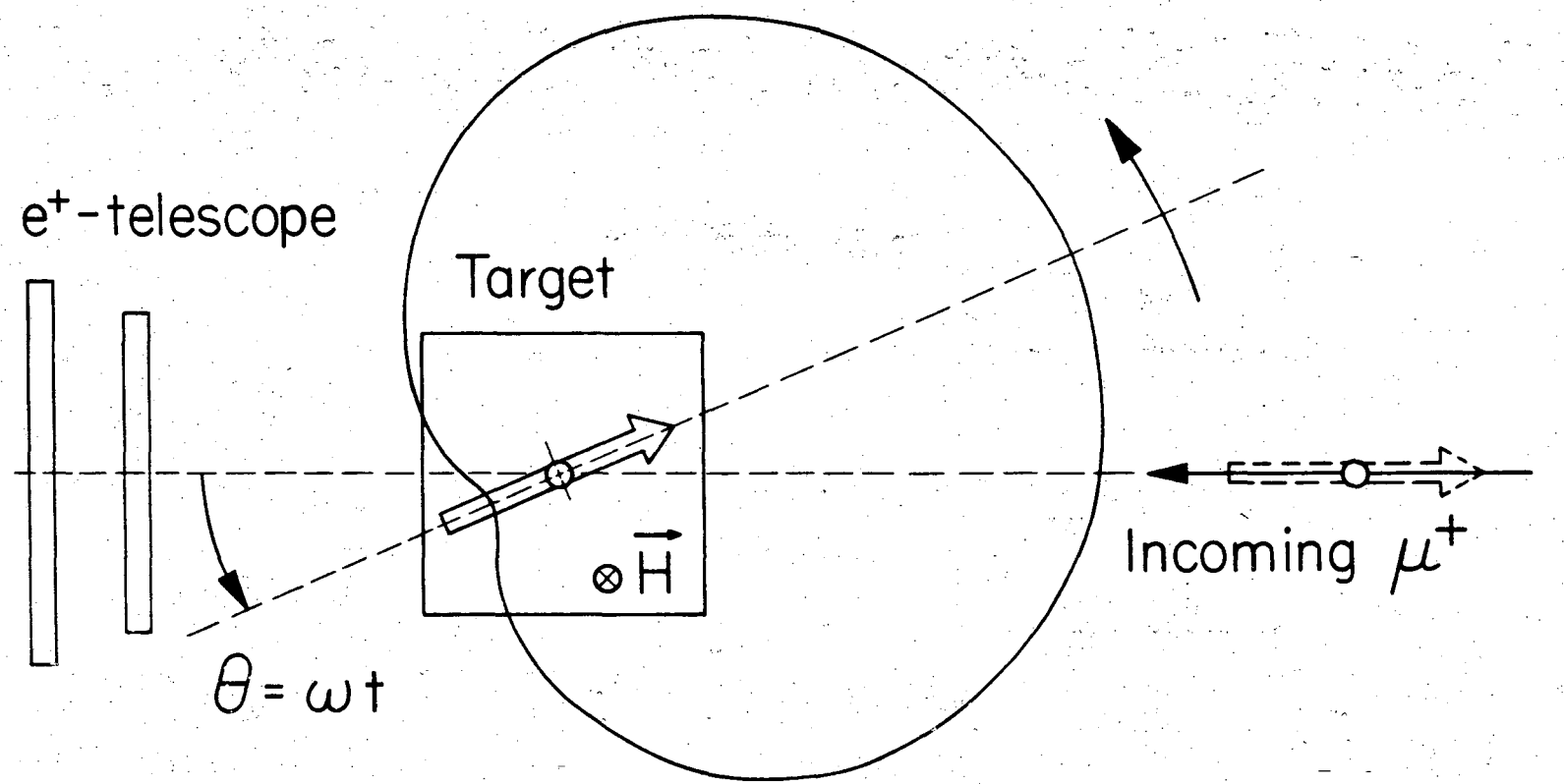

Fig. 3.

XBL7310-4191

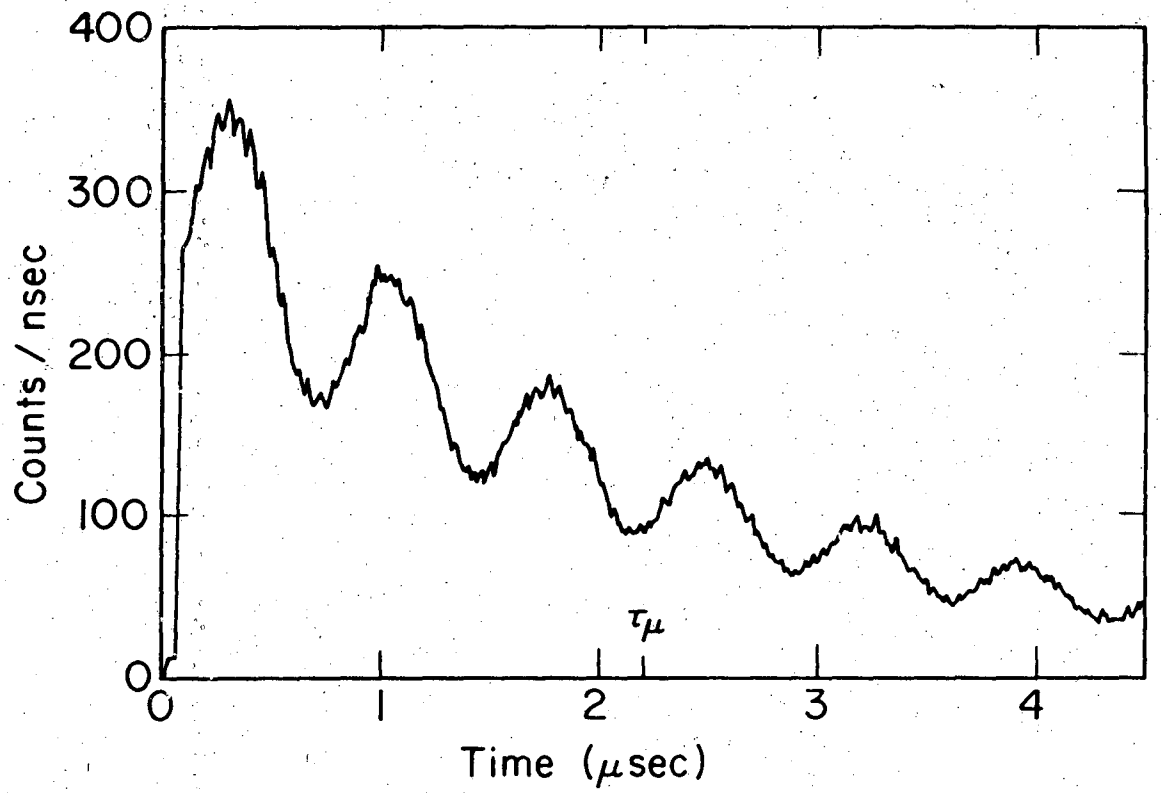

Fig. 4.

XBL735-2917

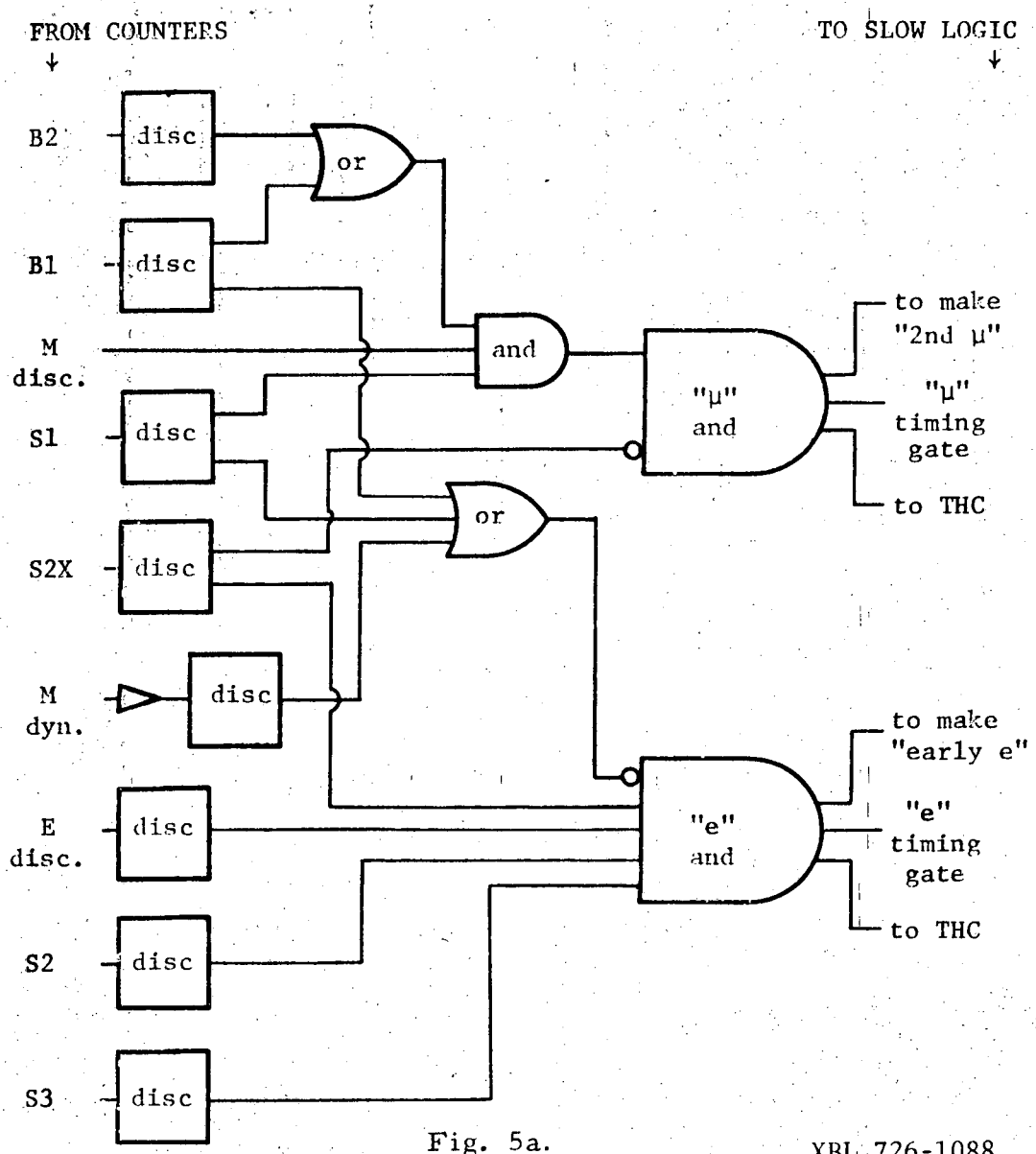

Fig. 5a.

XBL 726-1088

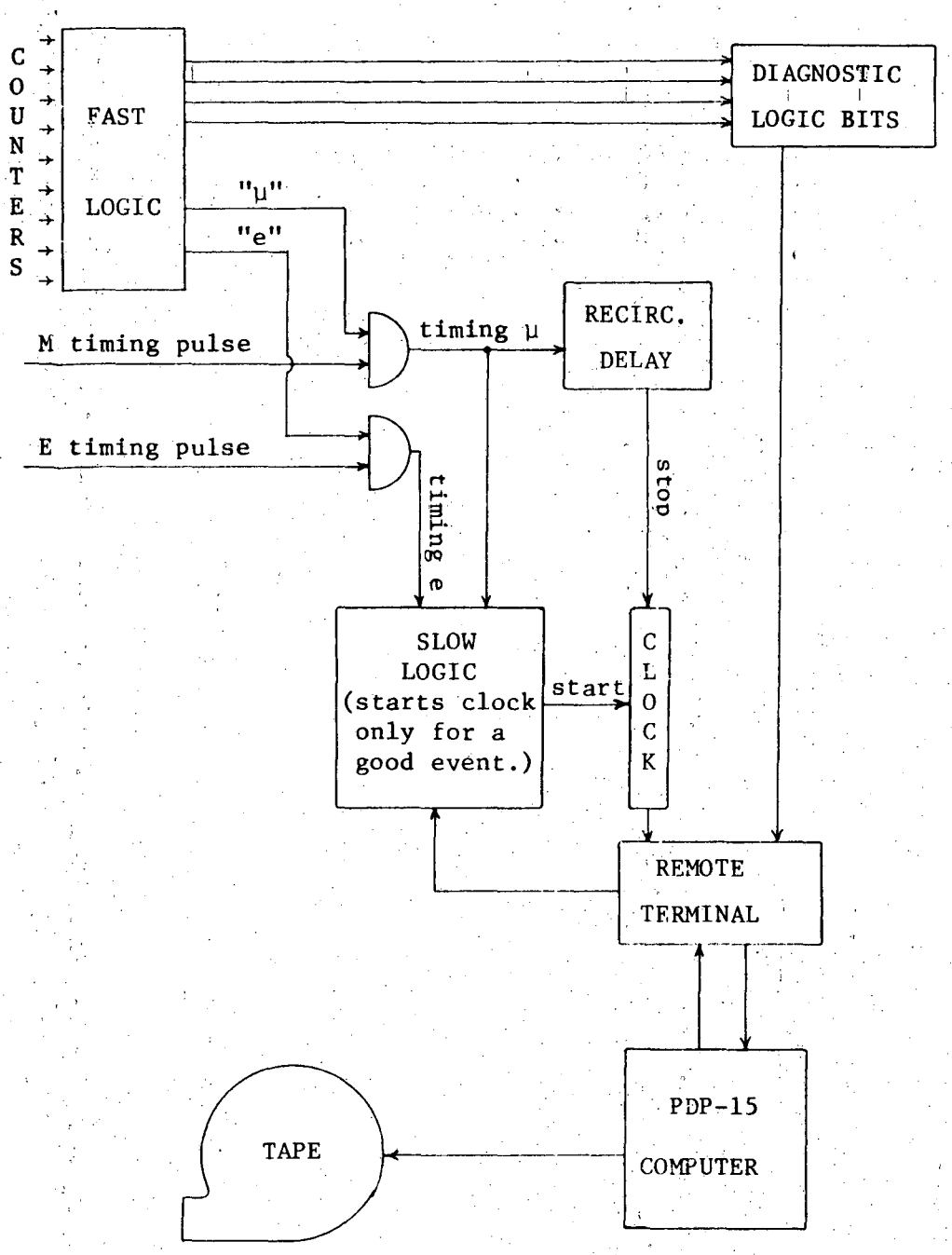

Fig. 5b. XBL 726-1094

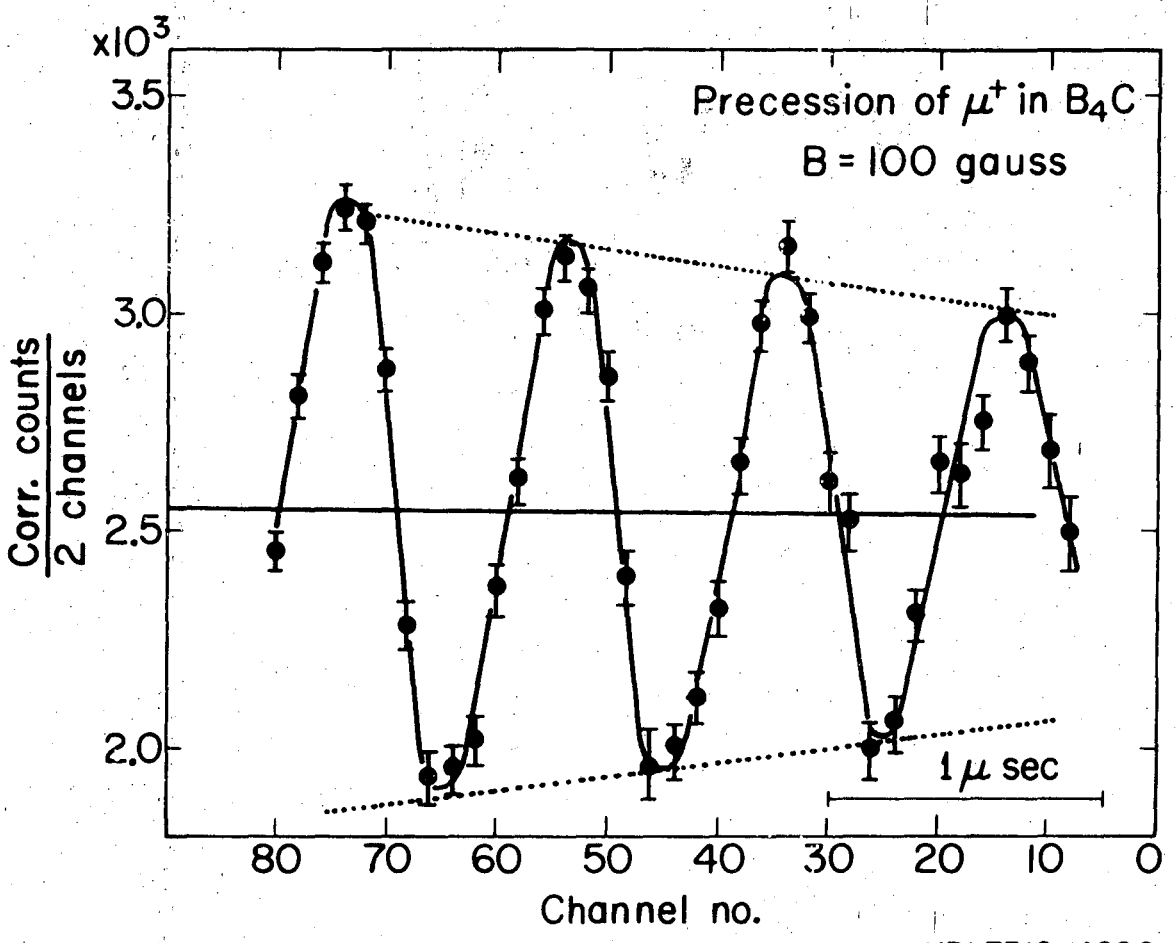
x10³
3.5
3.0
2.5
2.0
Corr. counts / 2 channels
Precession of μ⁺ in B₄C
B = 100 gauss
1 μ sec
80
70
60
50
40
30
20
10
0
Channel no.
XBL7310-4200

Fig. 6.

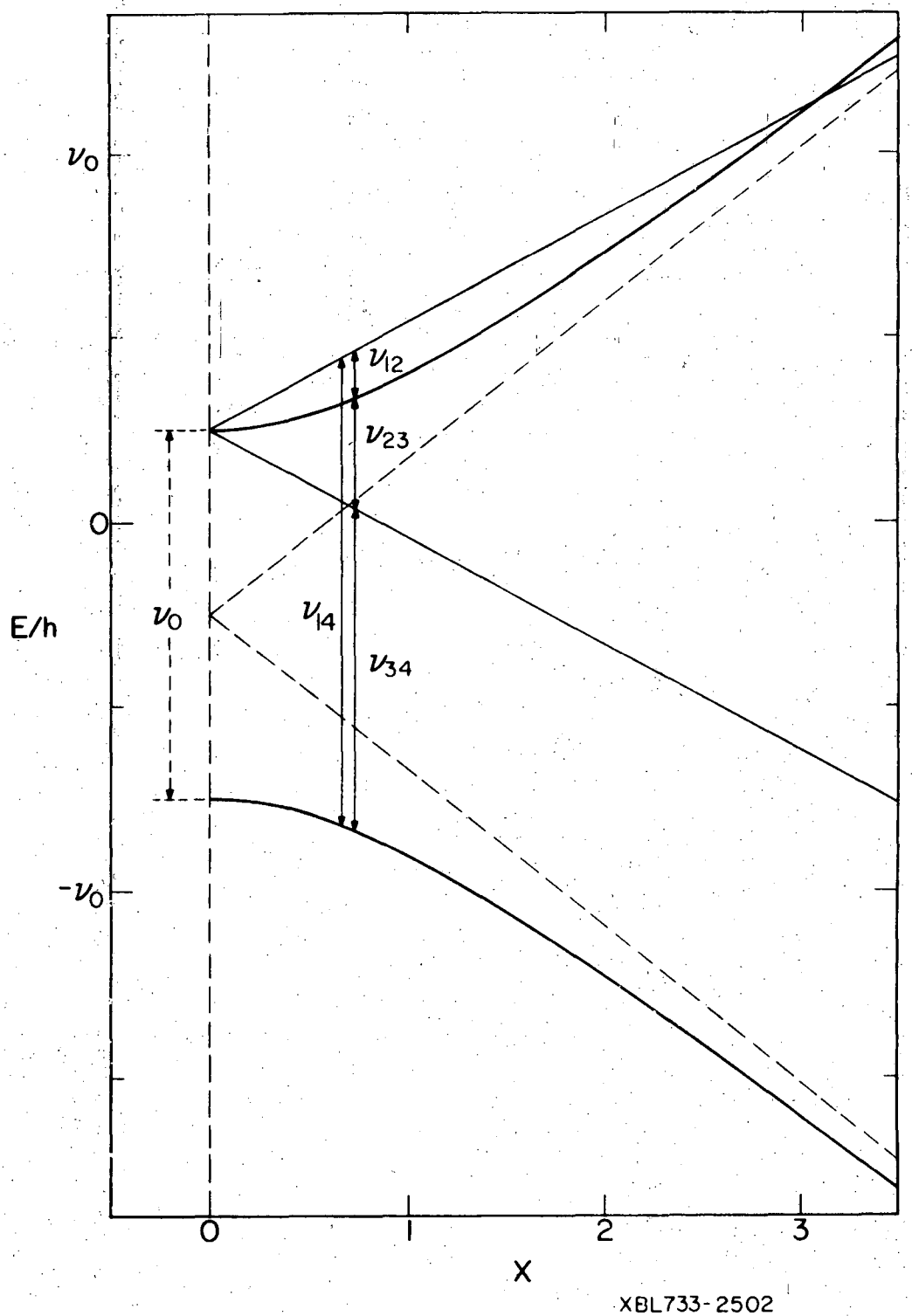

XBL733-2502

Fig. 7.

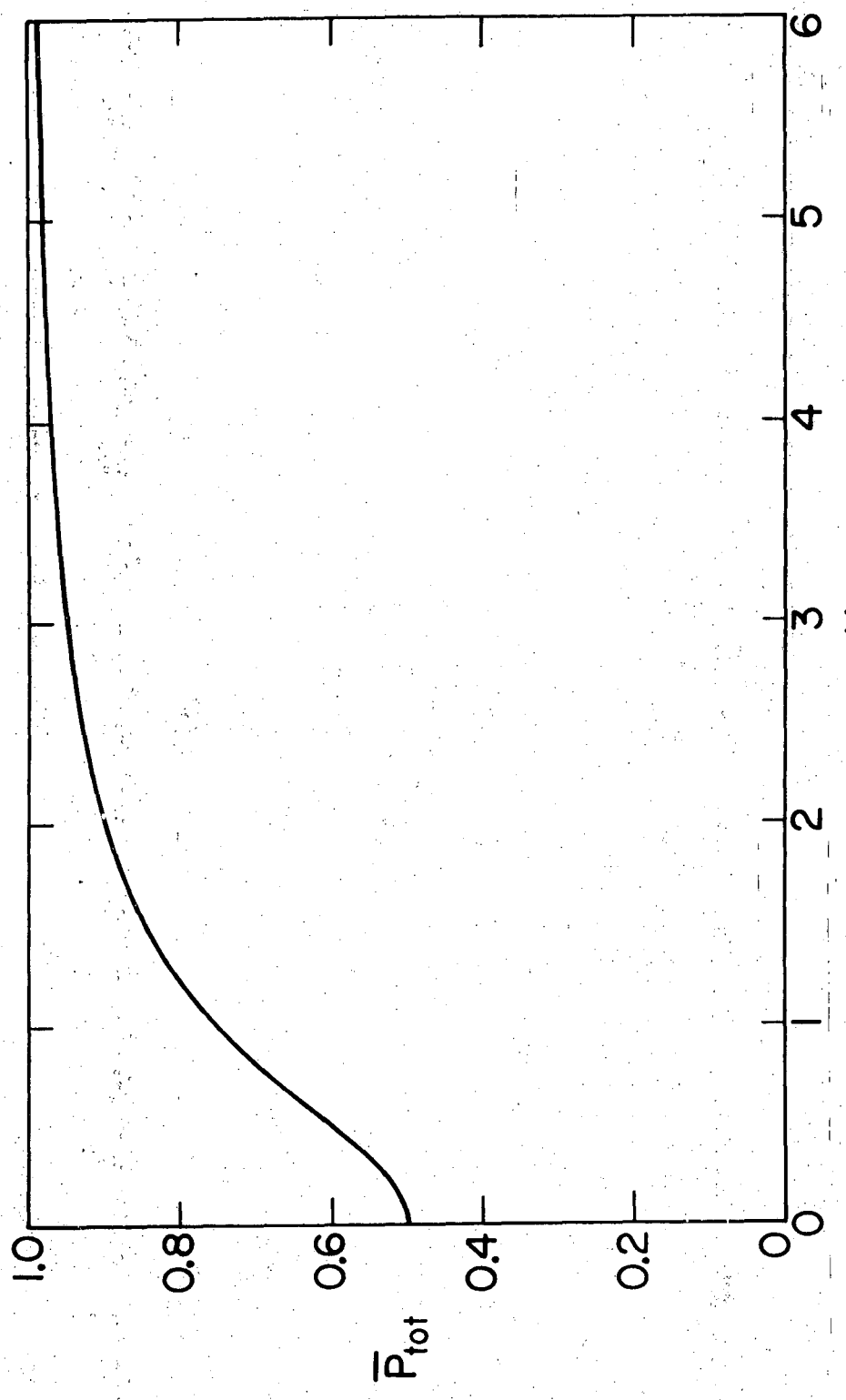

XBL7310-4189

Fig. 8.

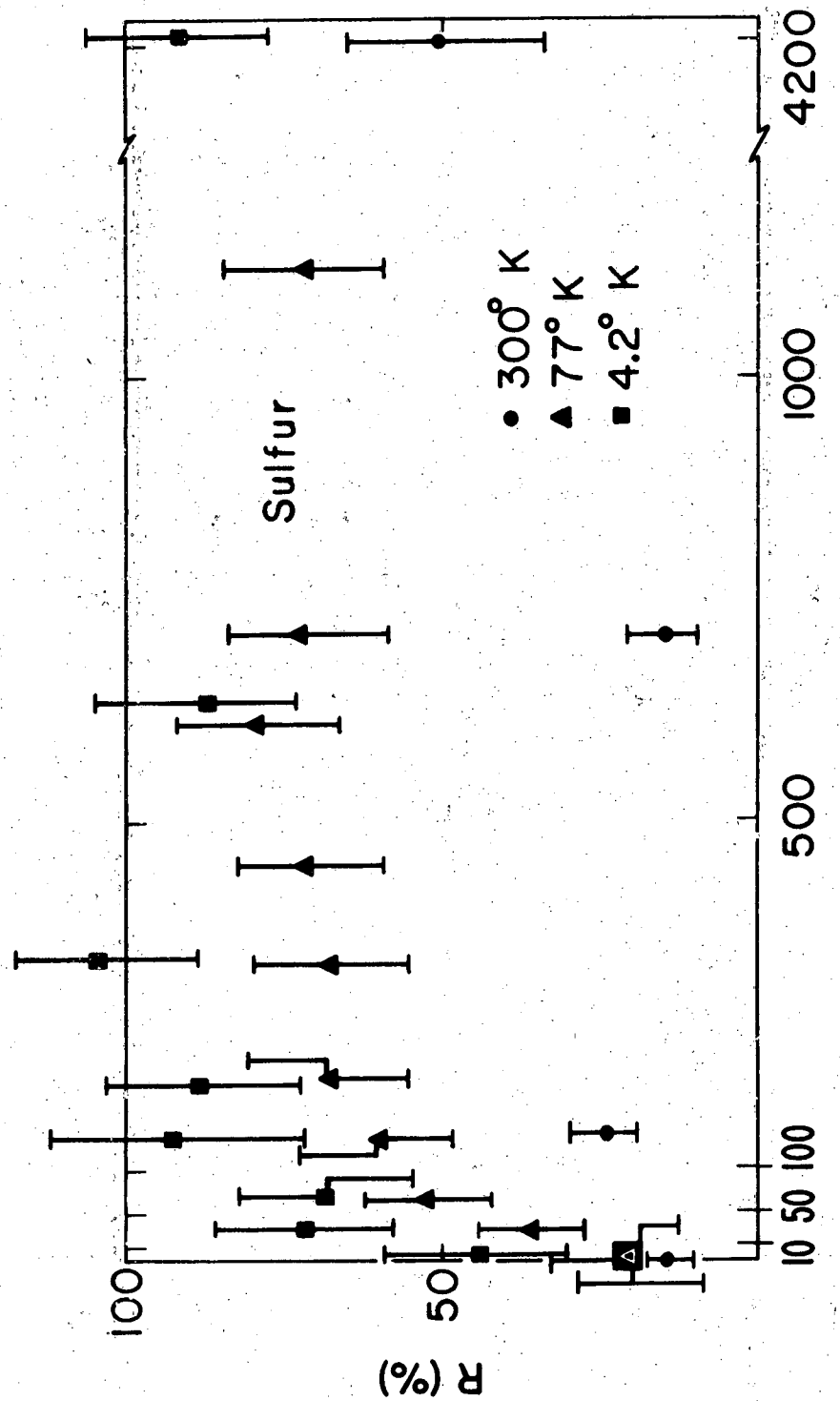
Sulfur
• 300° K
▲ 77° K
■ 4.2° K
Magnetic field (gauss)
10 50 100 500 1000 4200
R (%)
100
50
XBL7310-4193

Fig. 9.

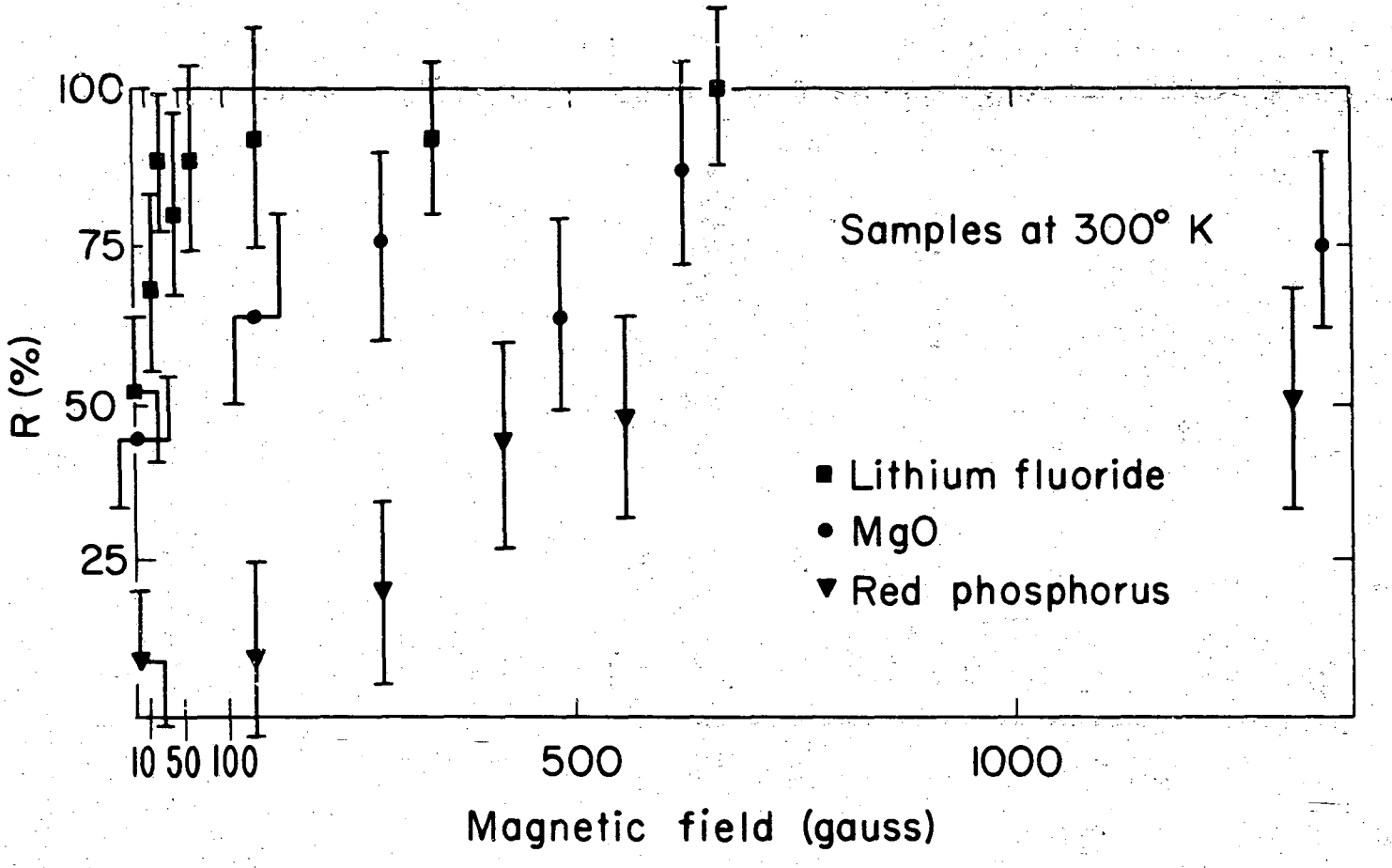

Fig. 10.

XBL7310-4194

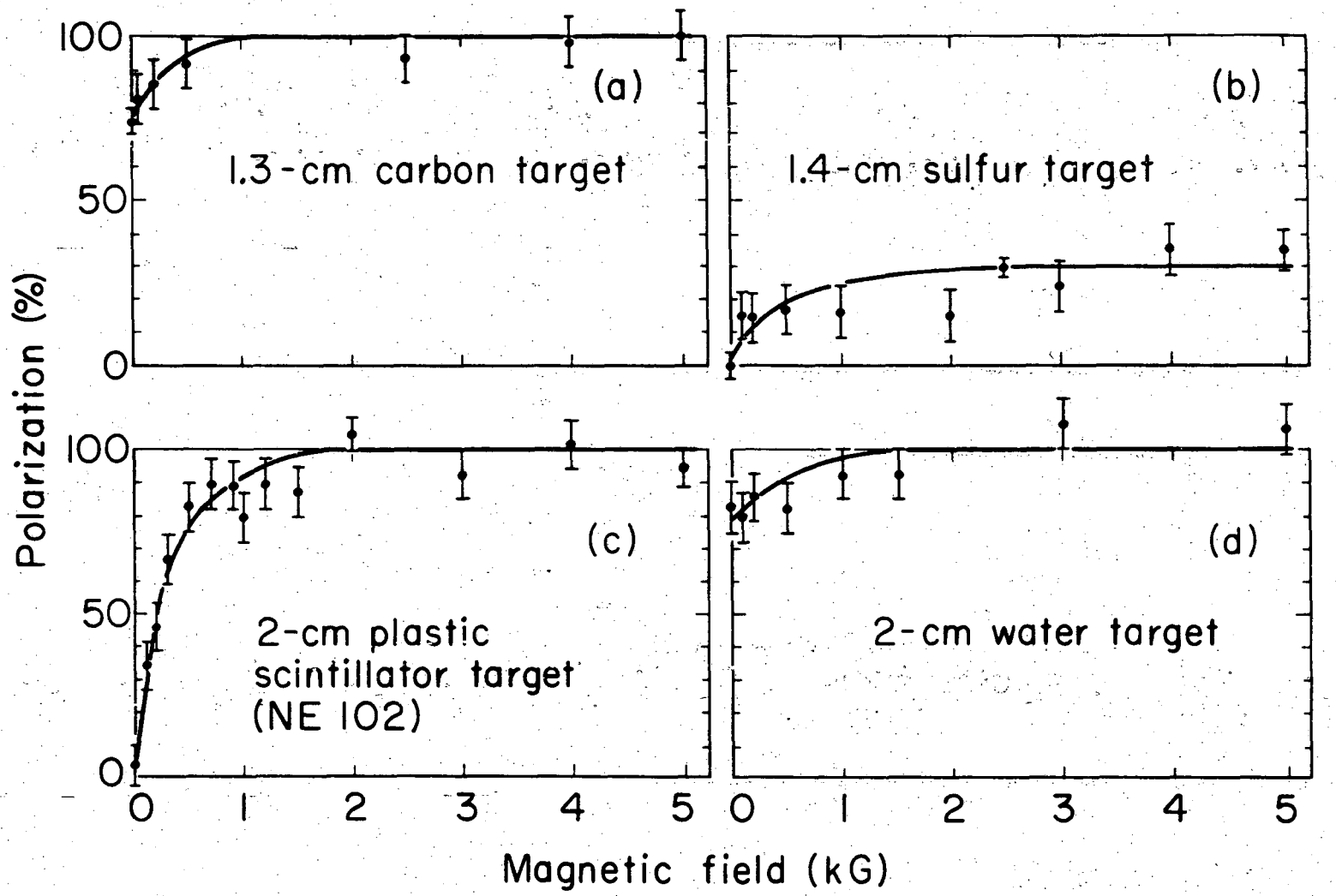

Fig. 11.

XBL7310-4192

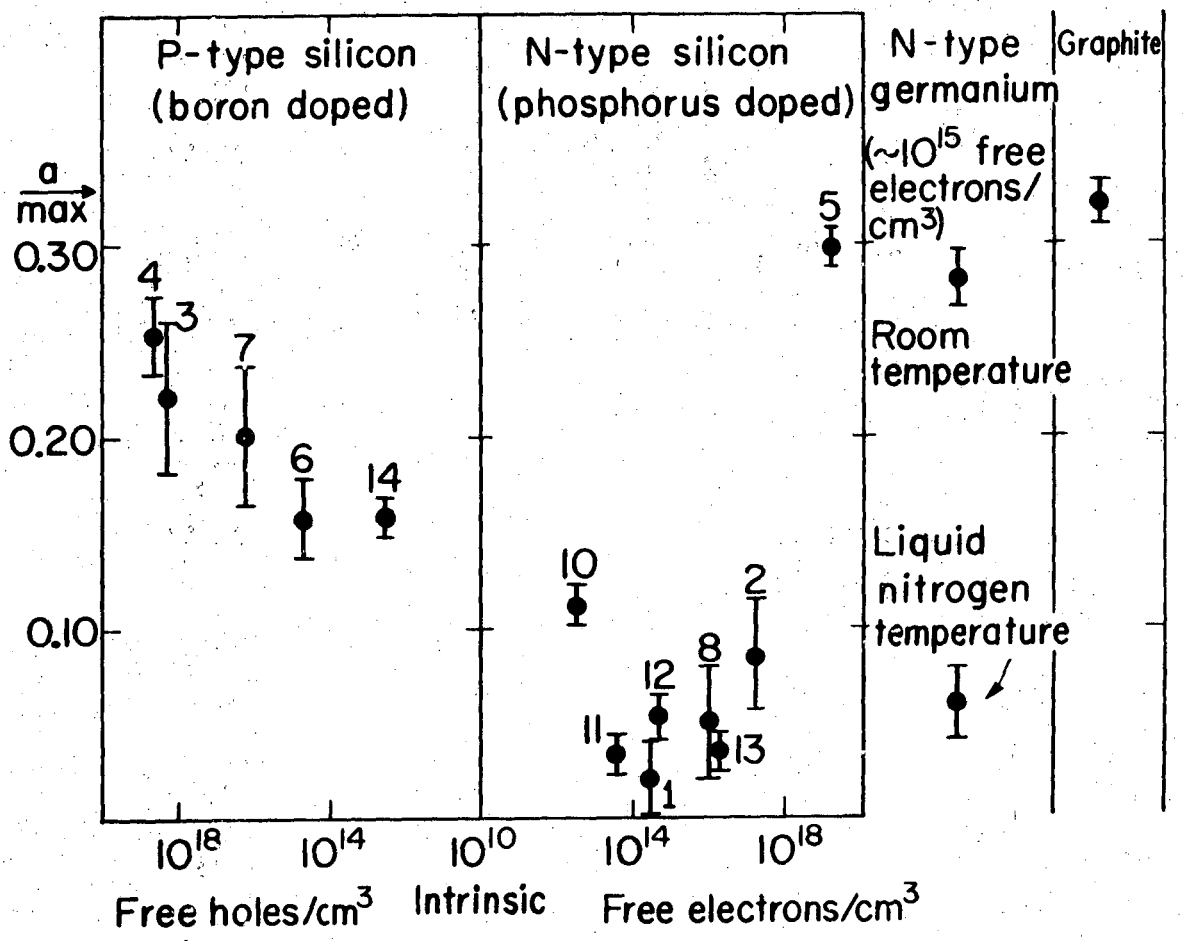

Fig. 12.

XBL7310-4196

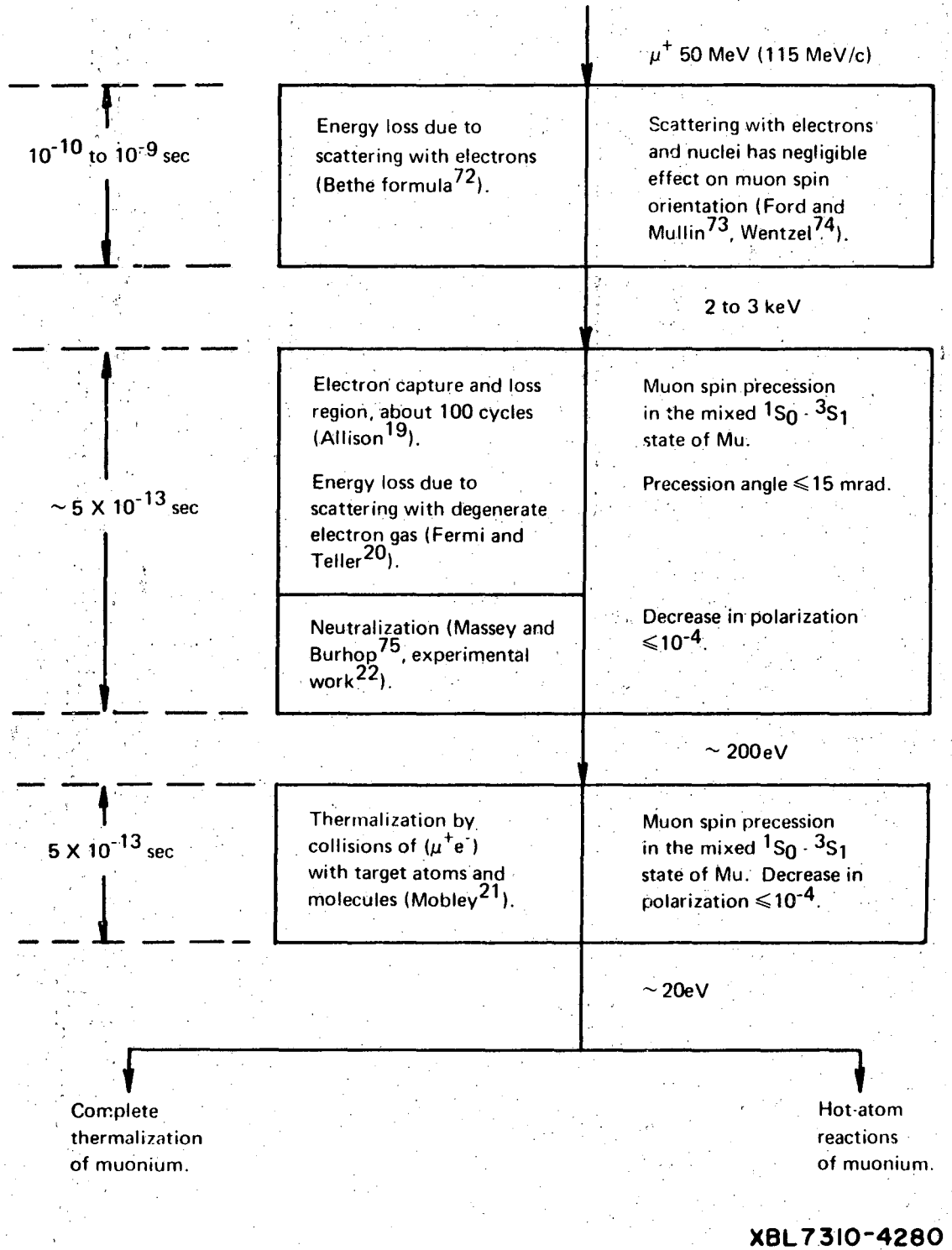
μ^+ 50 MeV (115 MeV/c)
10^{-10} to 10^{-9} sec
Energy loss due to scattering with electrons (Bethe formula[72]).
Scattering with electrons and nuclei has negligible effect on muon spin orientation (Ford and Mullin[73], Wentzel[74]).
2 to 3 keV
~ 5 X 10^{-13} sec
Electron capture and loss region, about 100 cycles (Allison[19]).
Energy loss due to scattering with degenerate electron gas (Fermi and Teller[20]).
Muon spin precession in the mixed $^1S_0$ - $^3S_1$ state of Mu.
Precession angle ⩽15 mrad.
Neutralization (Massey and Burhop[75], experimental work[22]).
Decrease in polarization ⩽10^{-4}.
~ 200eV
5 X 10^{-13} sec
Thermalization by collisions of (μ^+e^-) with target atoms and molecules (Mobley[21]).
Muon spin precession in the mixed $^1S_0$ - $^3S_1$ state of Mu. Decrease in polarization ⩽10^{-4}.
~ 20eV
Complete thermalization of muonium.
Hot-atom reactions of muonium.
XBL7310-4280

Fig. 13.

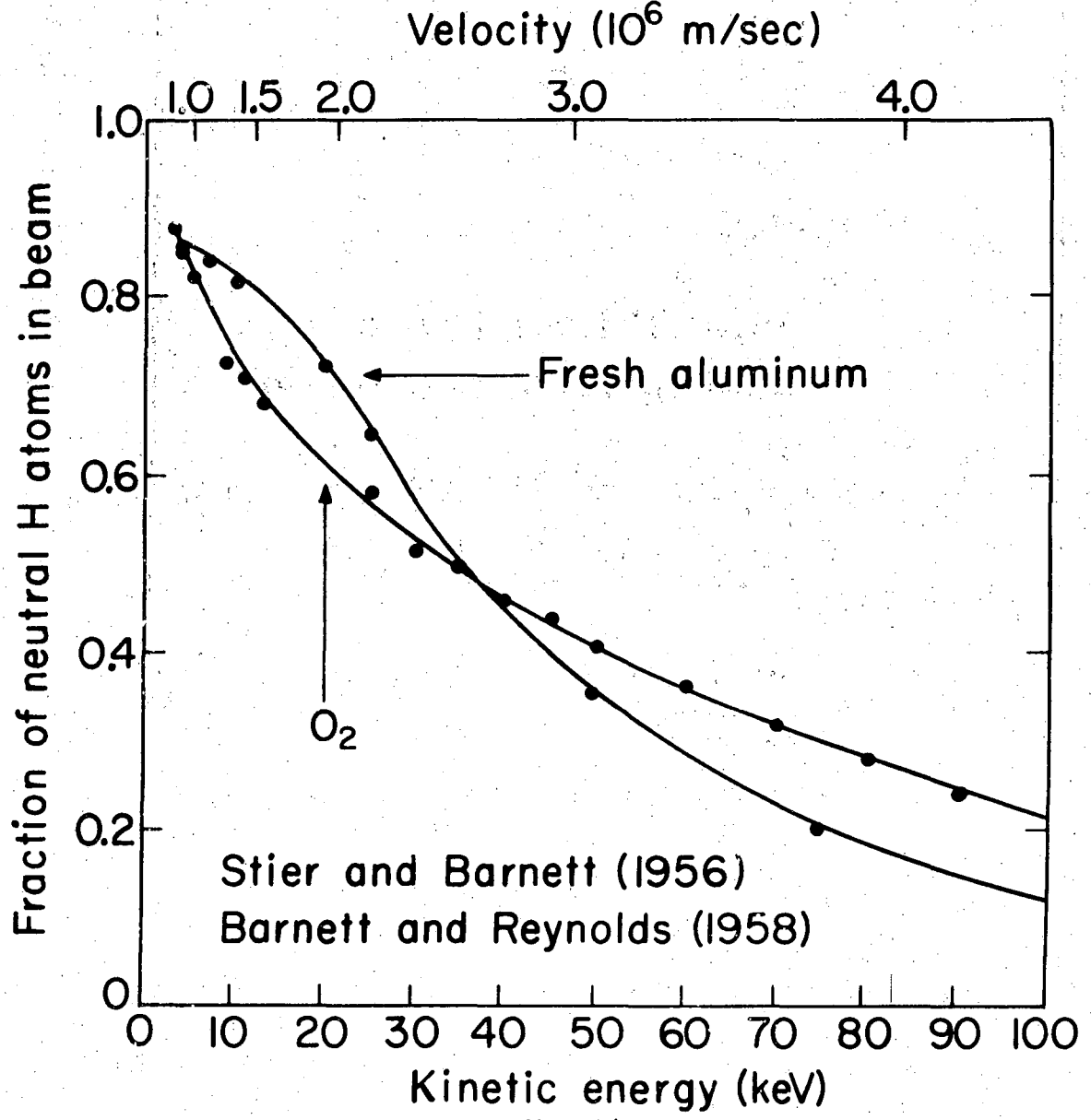

Fig. 14.

XBL7310-4197

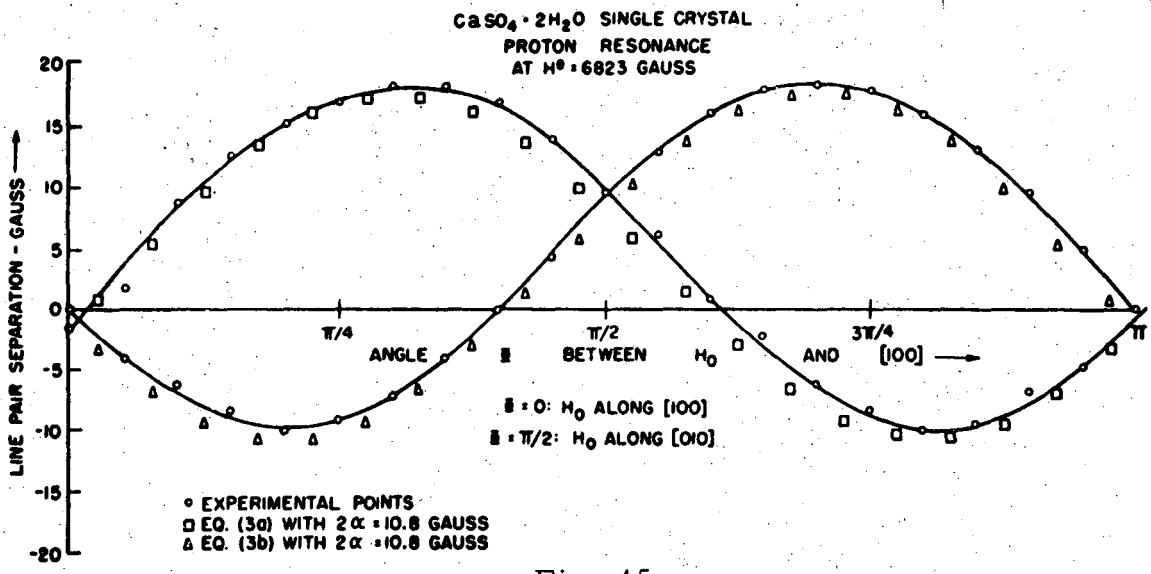

Fig. 15.

XBL 708-1701

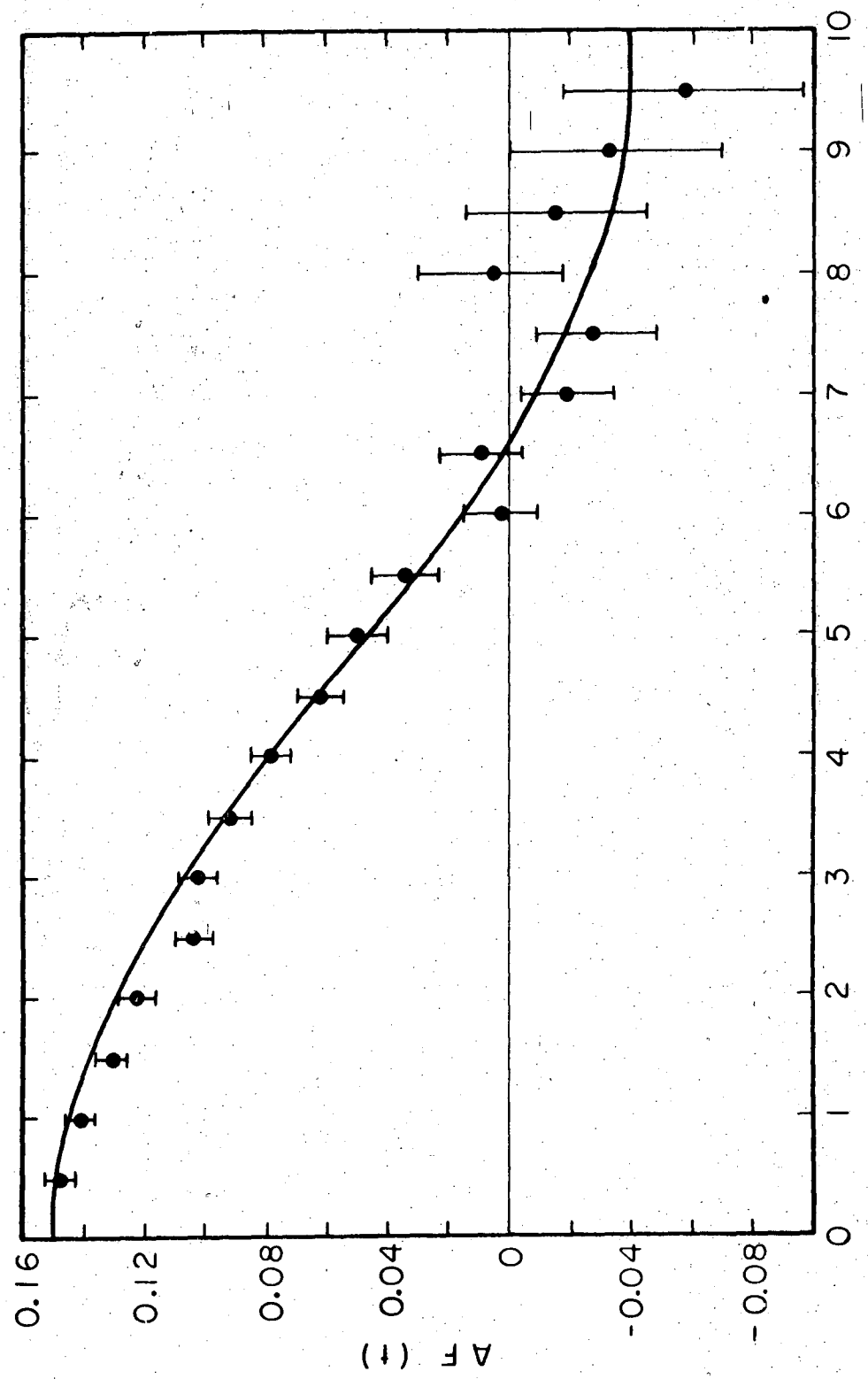

XBL7011-4115

Fig. 16a.

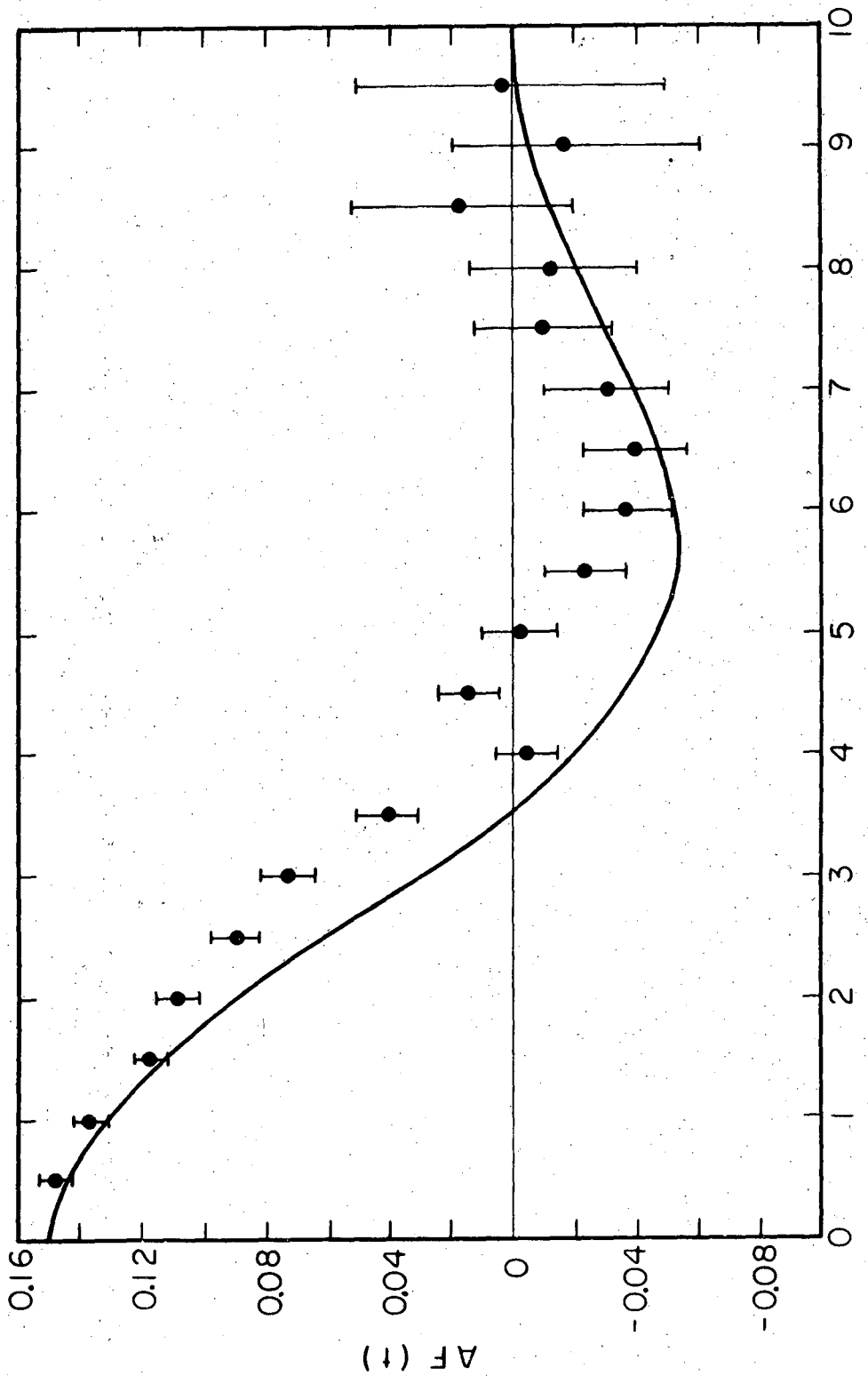

XBL 7011-4114

Fig. 16b.

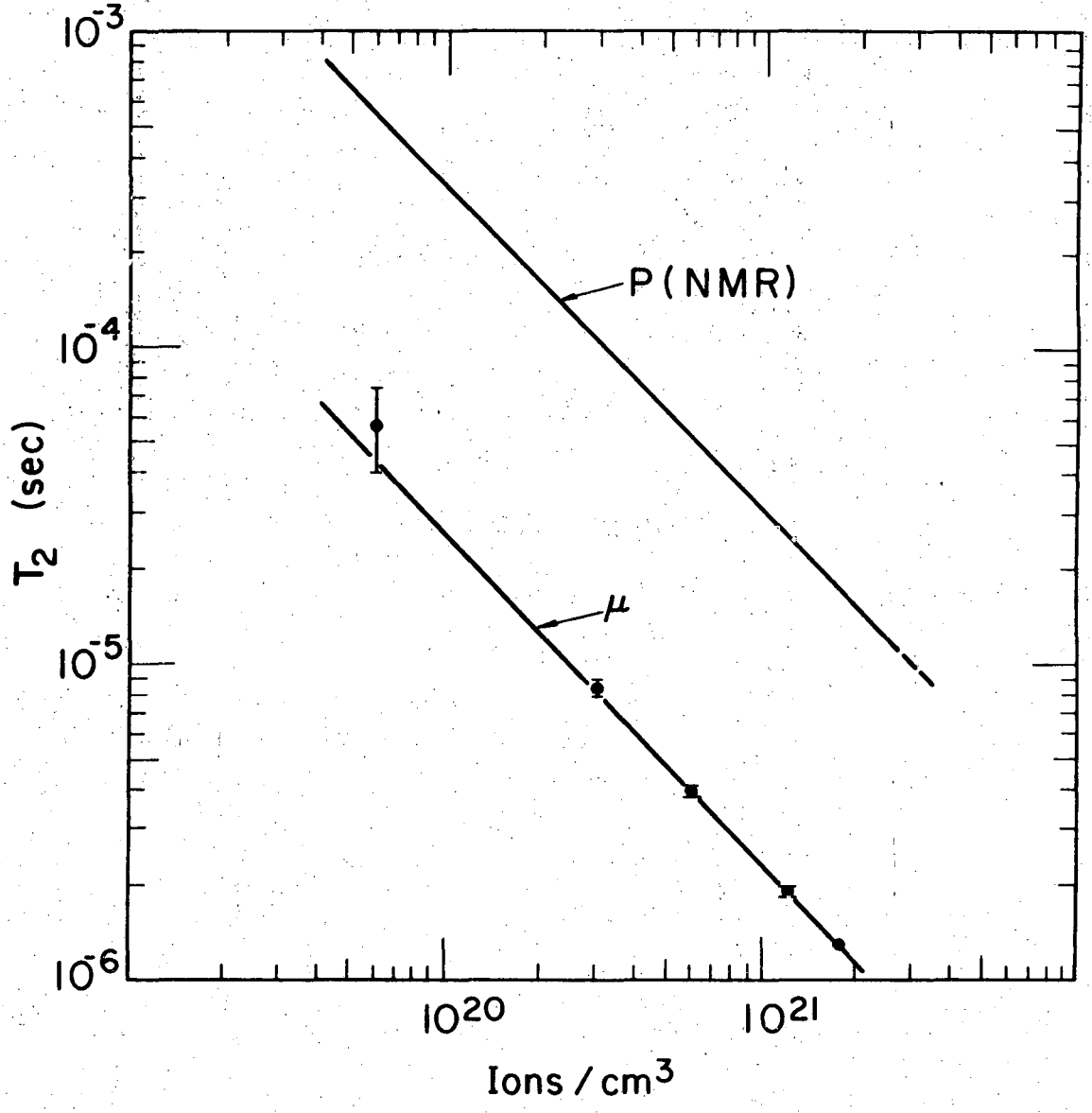

Fig. 17. XBL7310-4303

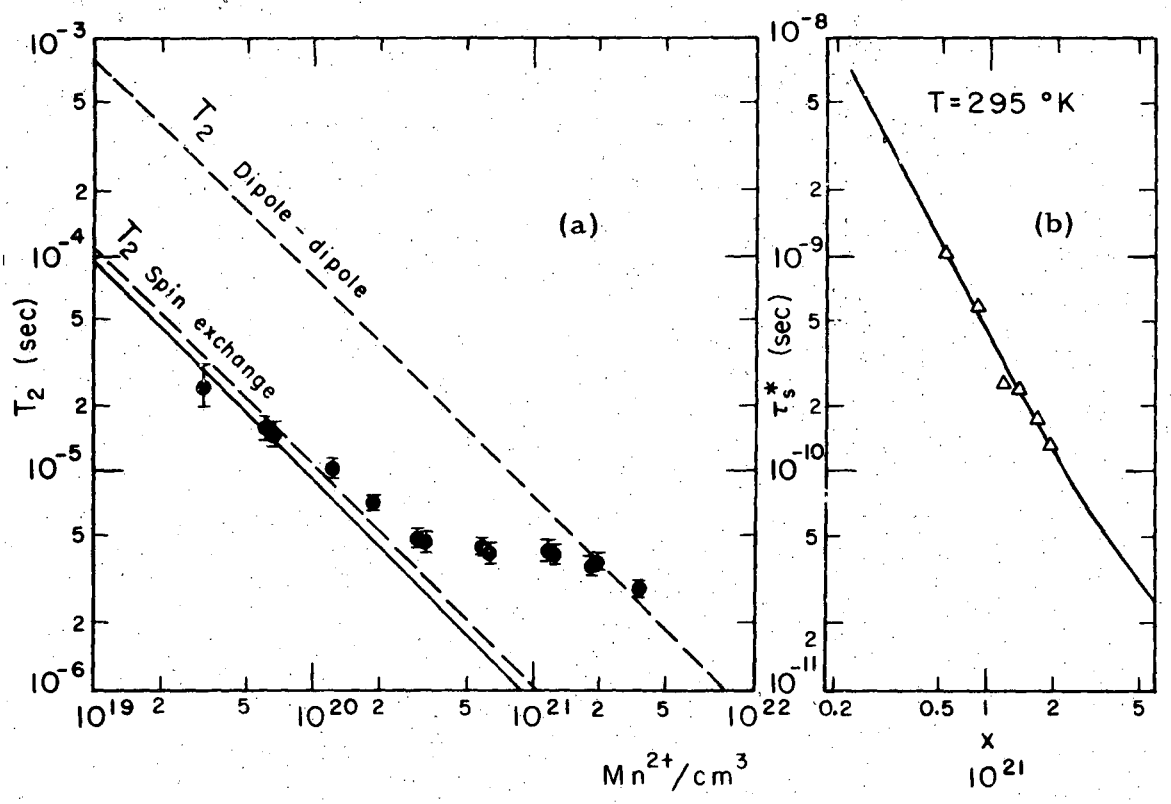

Fig. 18.

XBL718-4008

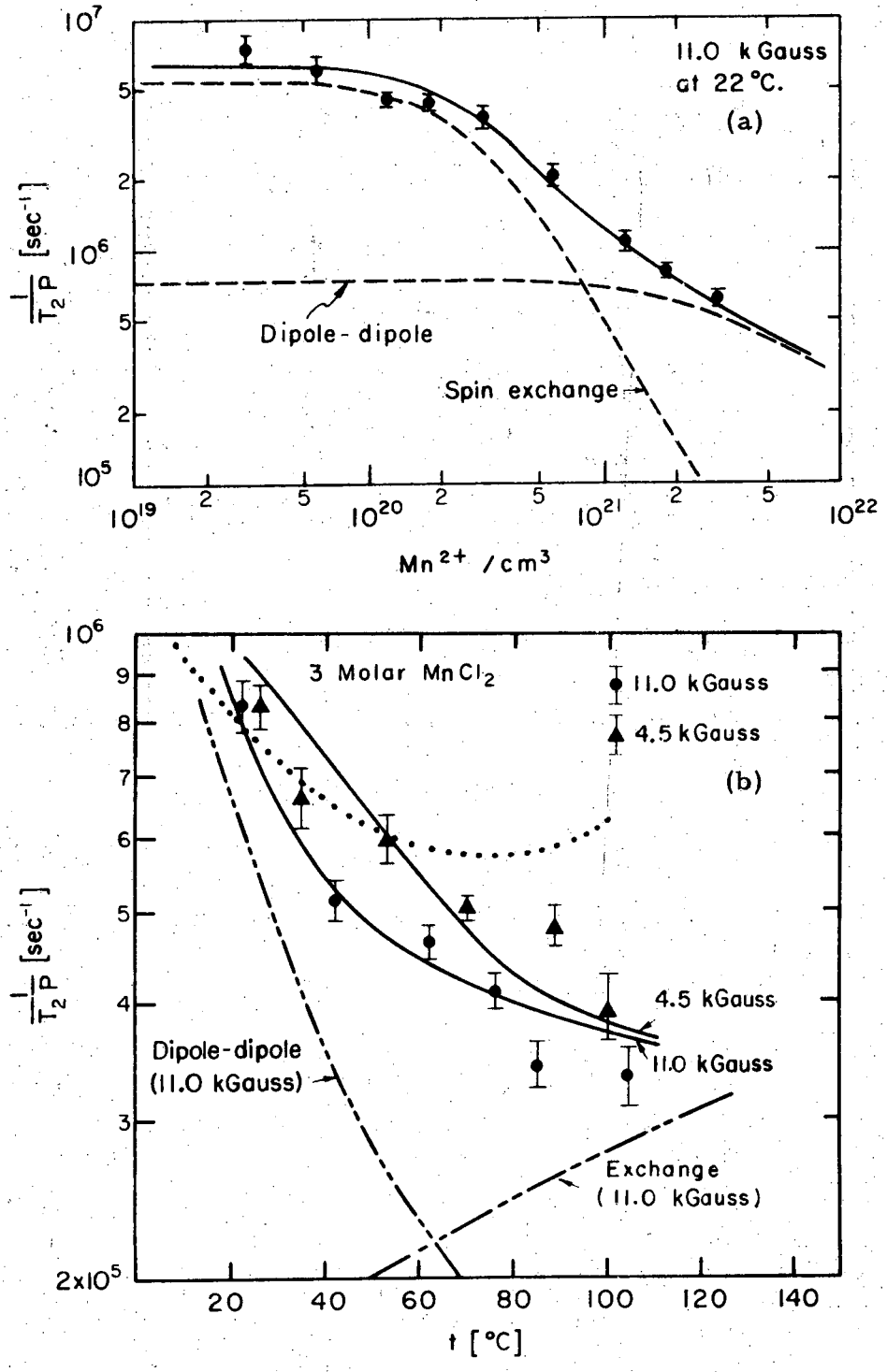

Fig. 19. XBL718 - 4007

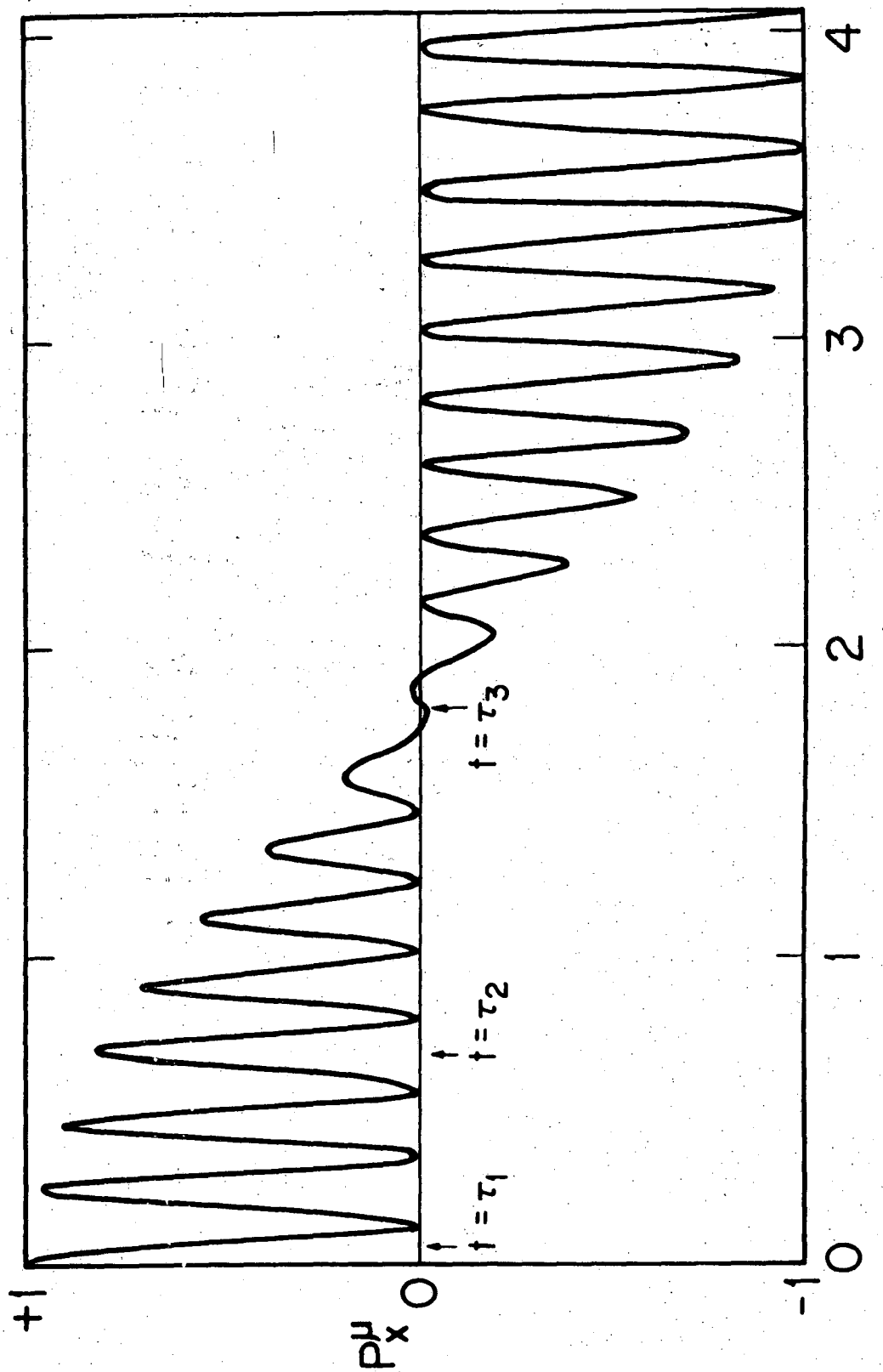

XBL7210-4190

Fig. 20.

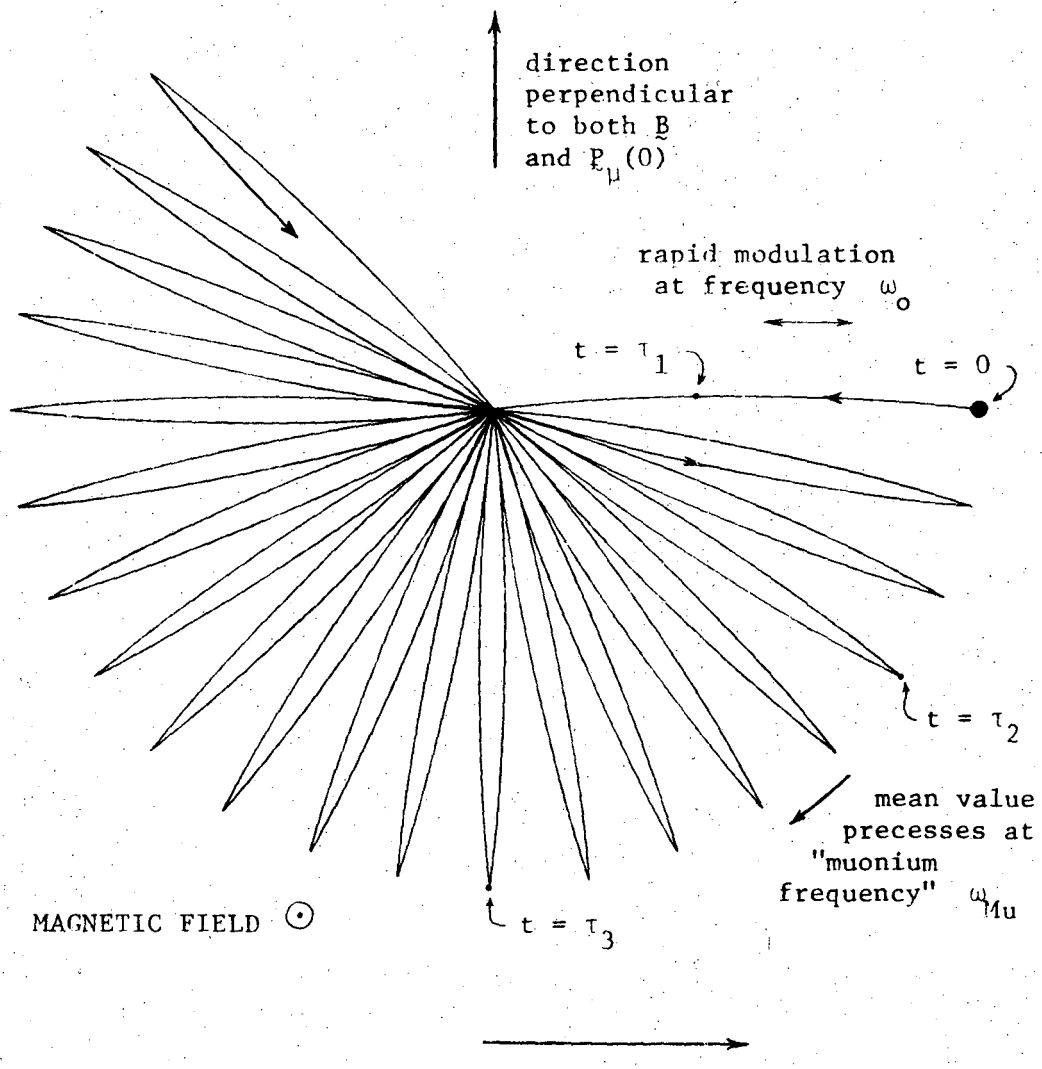

XBL 726-1093

Fig. 21.

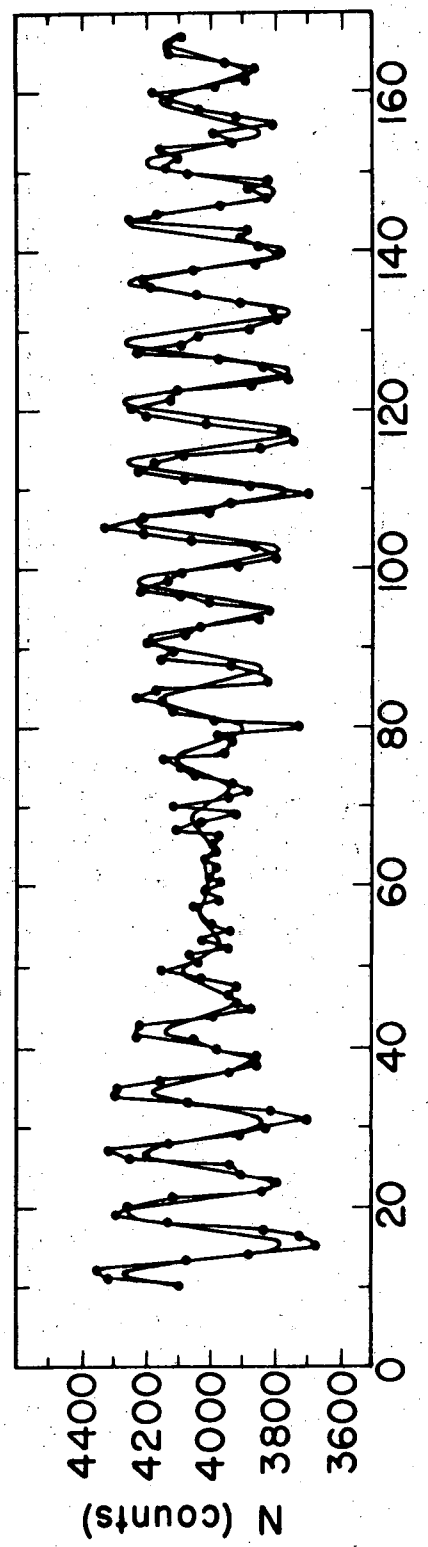

XBL7310-4195

Fig. 22.

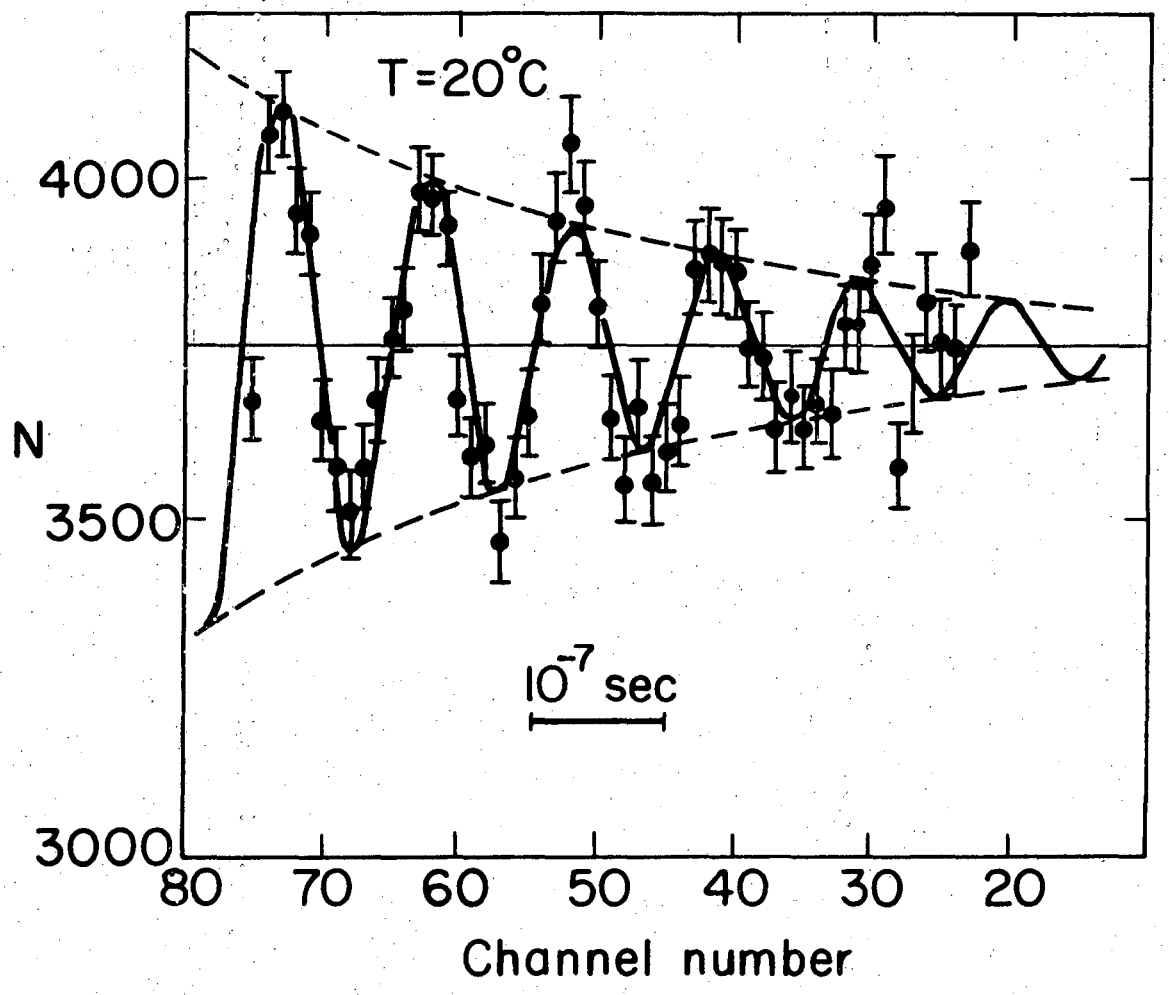

Fig. 23. XBL7310-4198

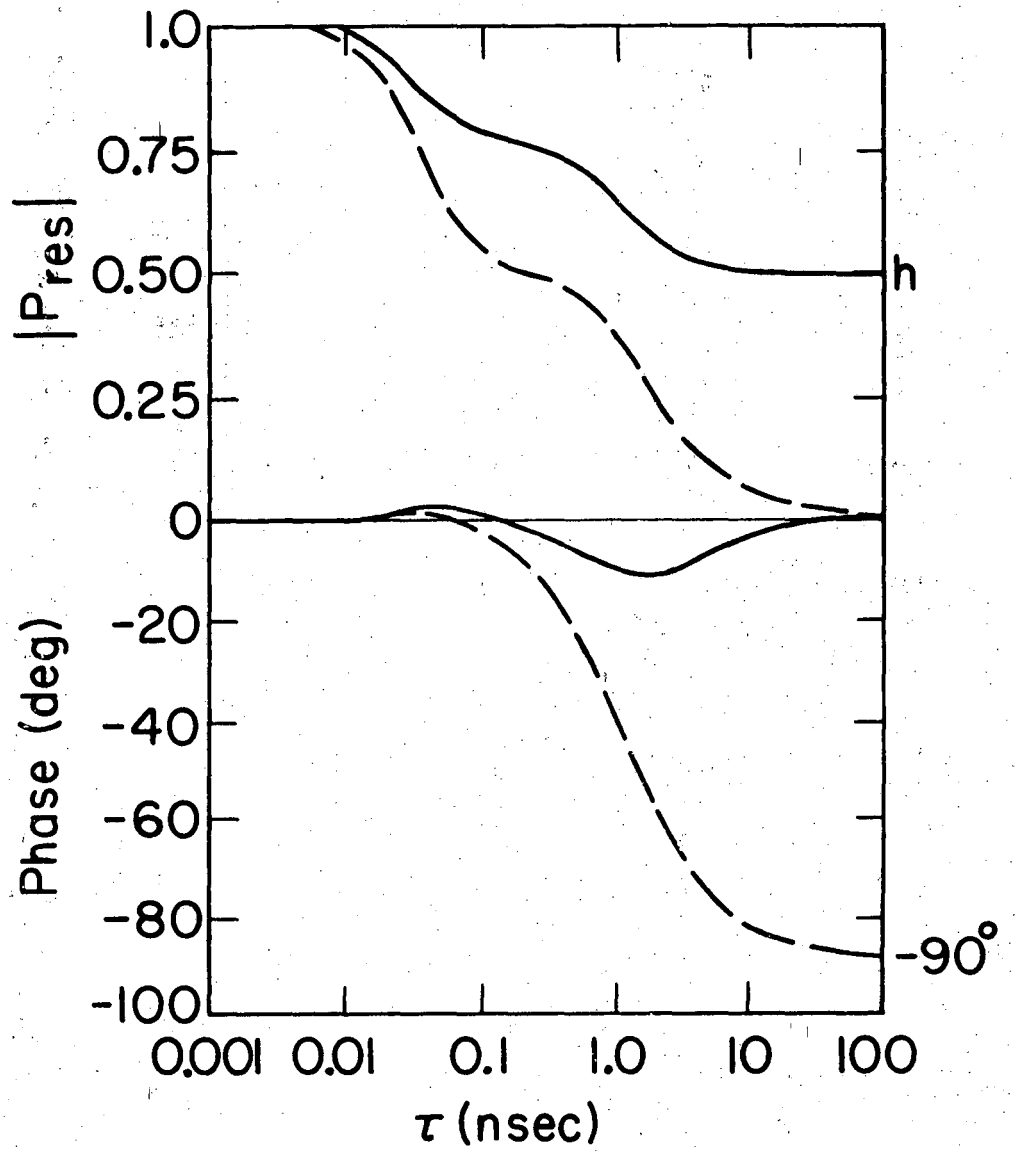

Fig. 24. XBL7310-4190

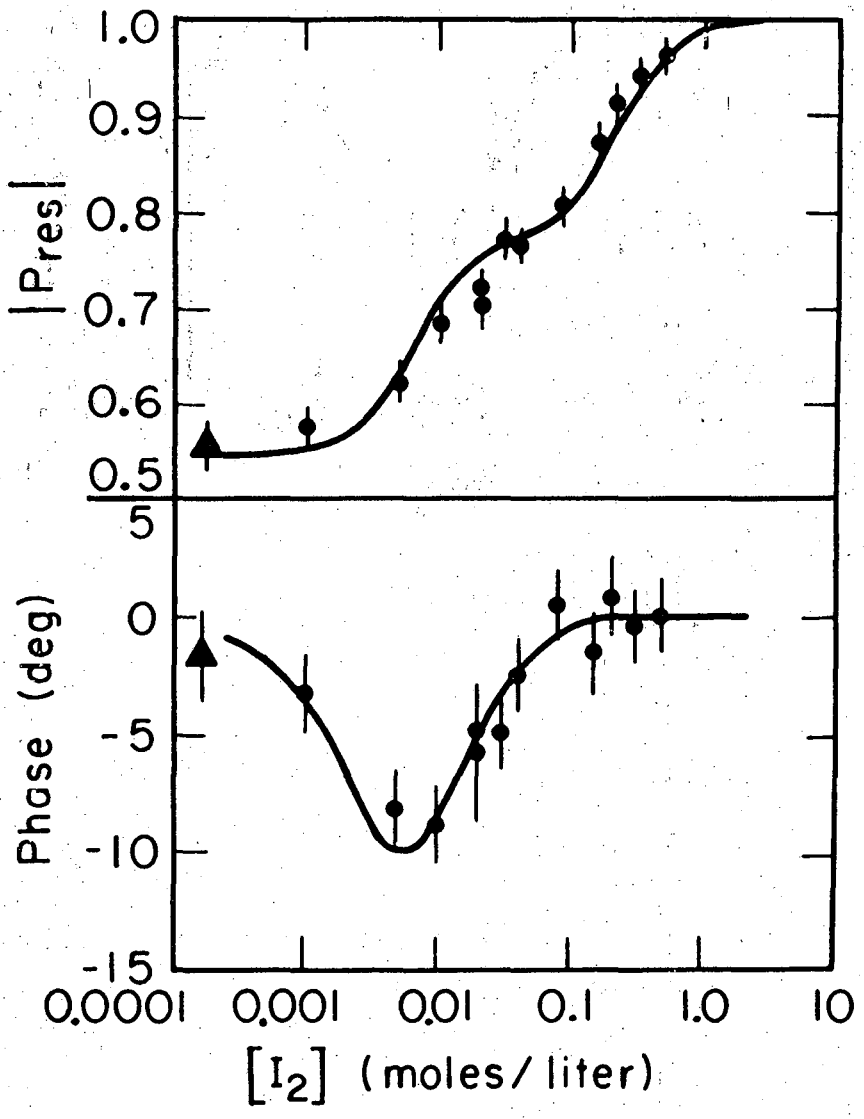

Fig. 25. XBL734-2763

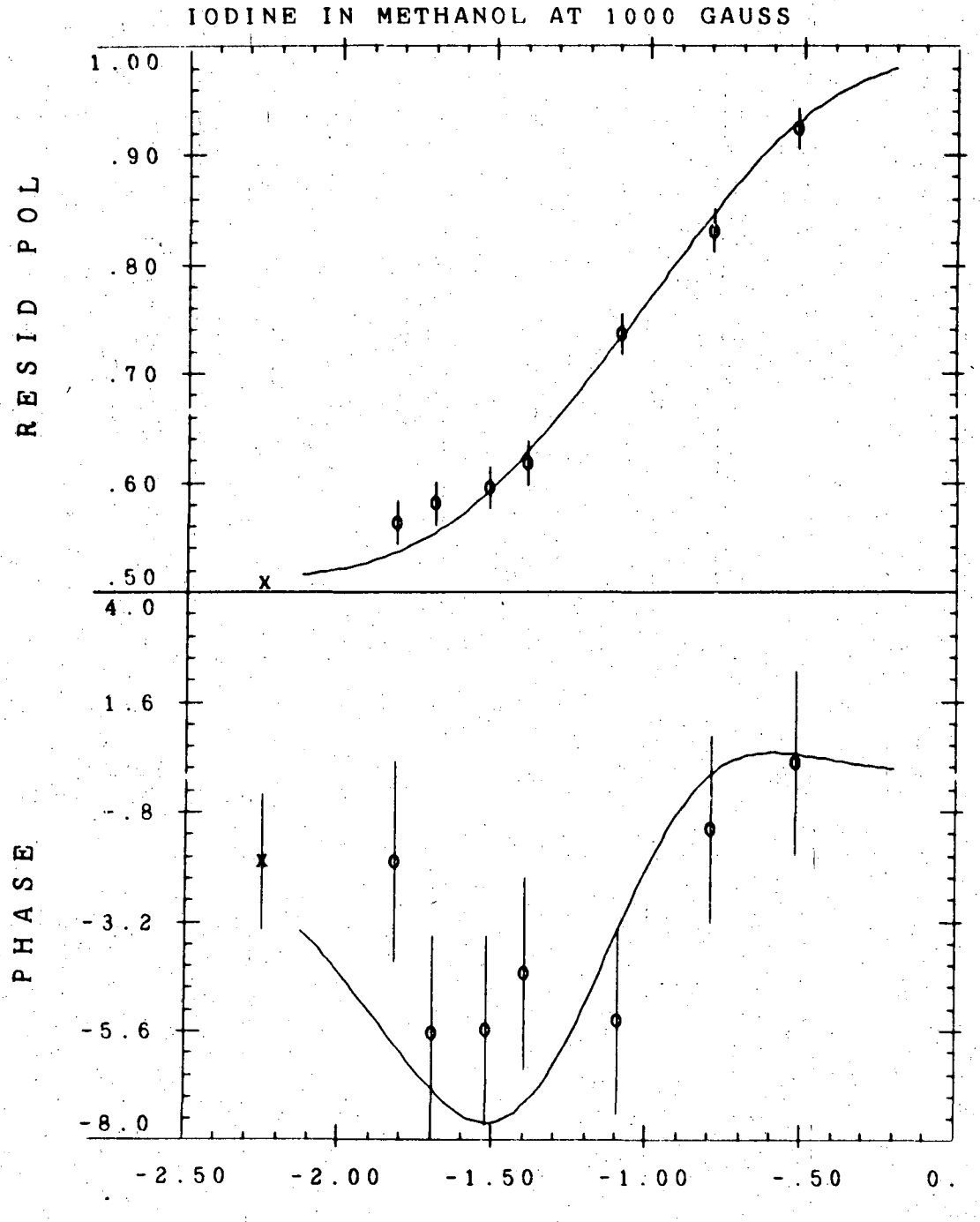

Fig. 26.

XBL 726-1122

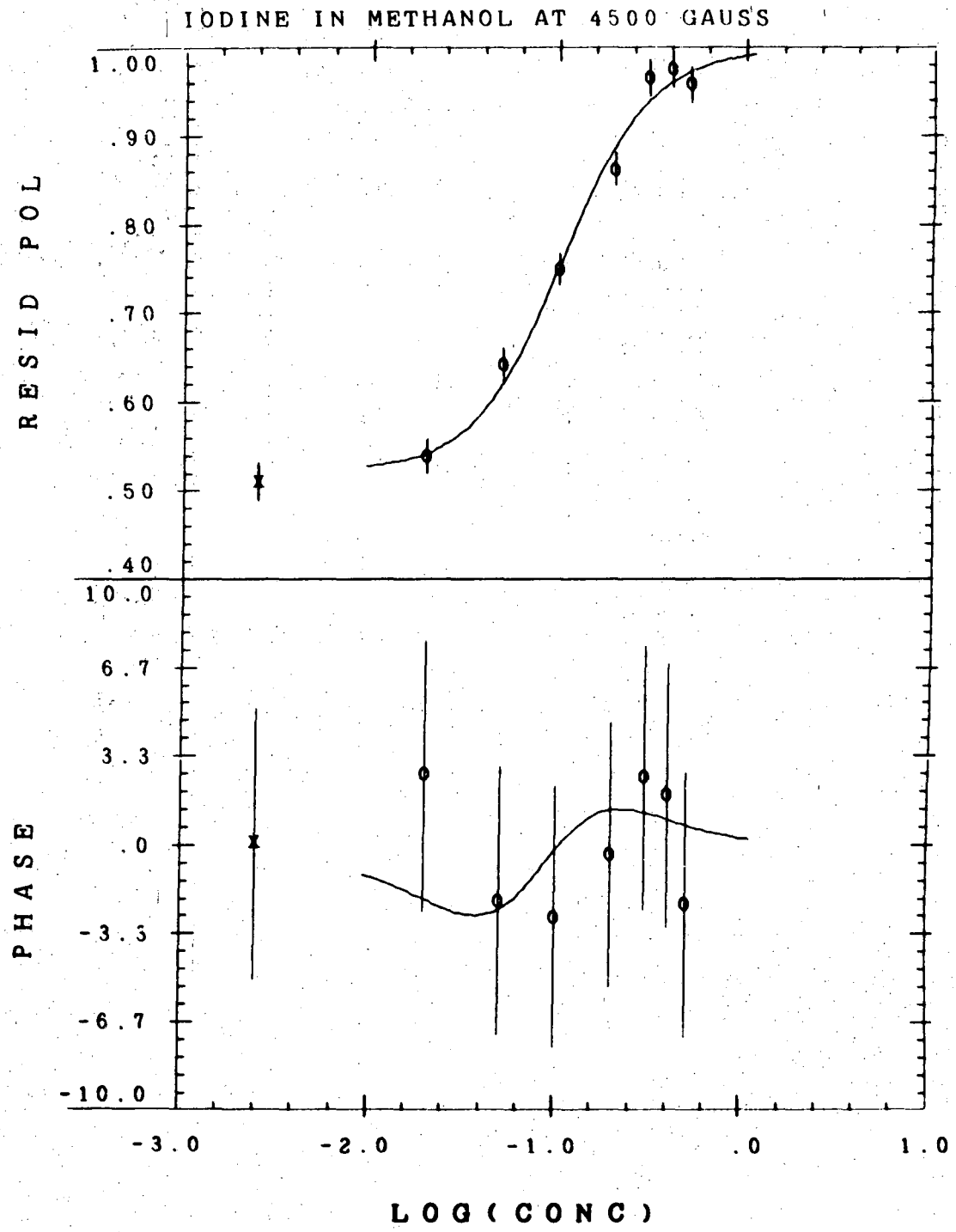

Fig. 27.

XBL 726-1106

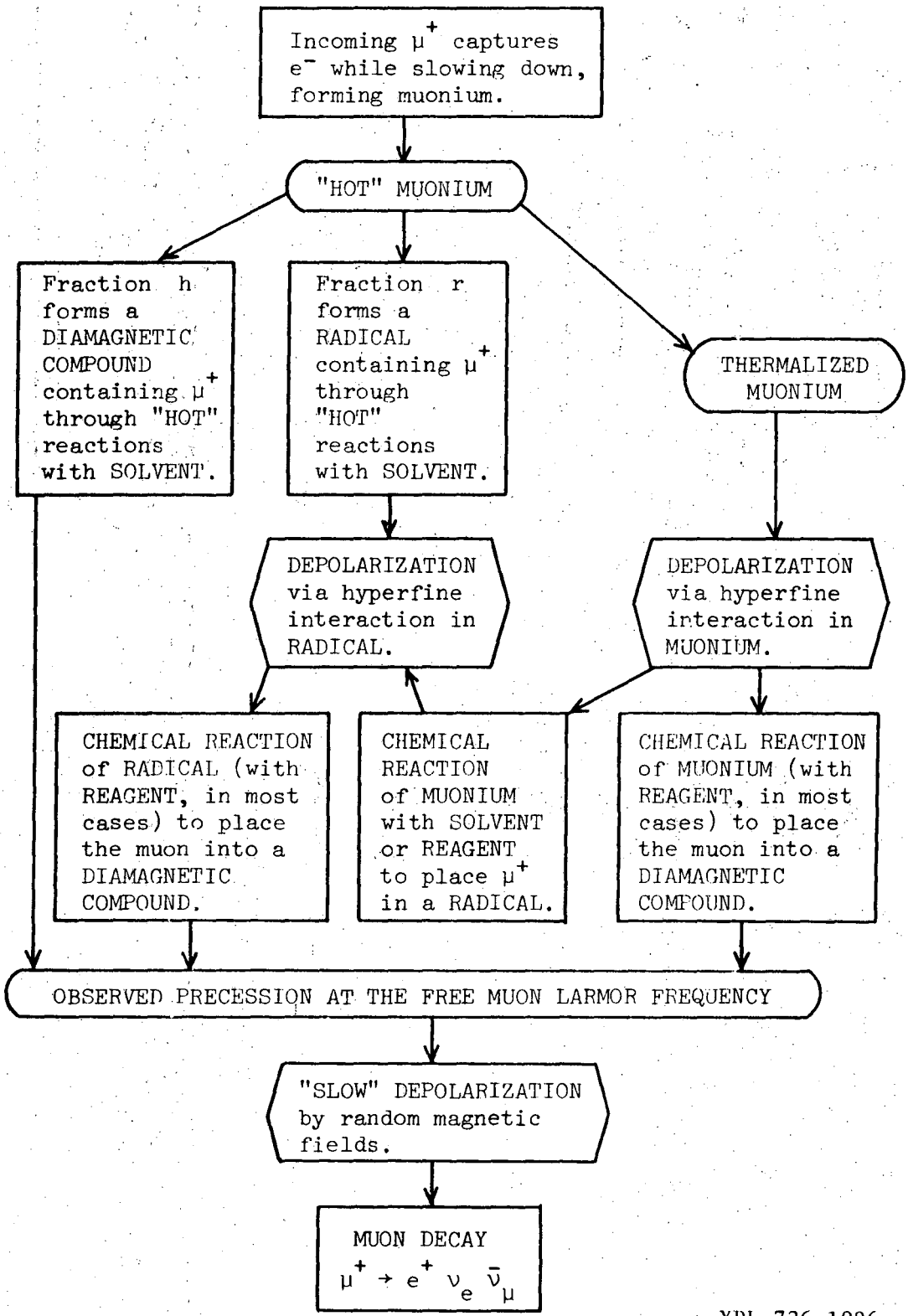

XBL 726-1086

Fig. 28.

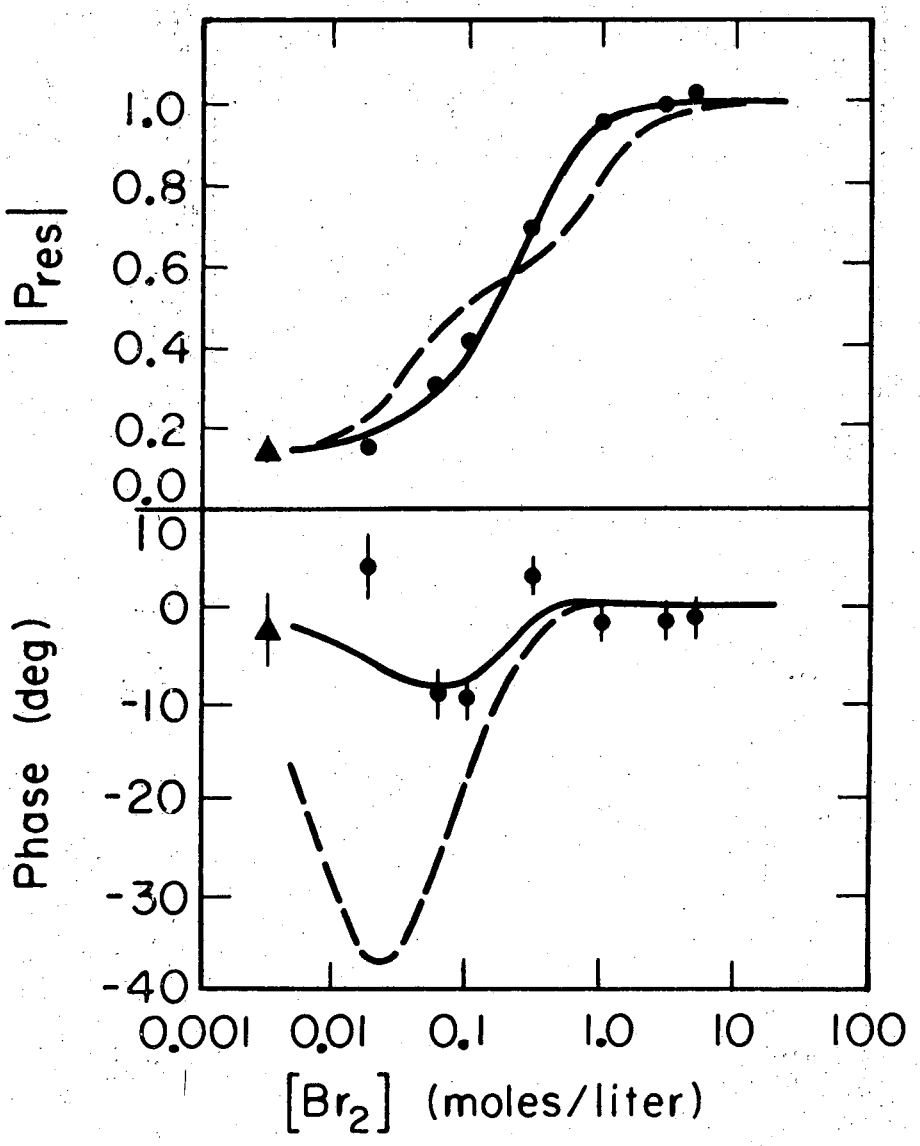

Fig. 29. XBL7210-4167

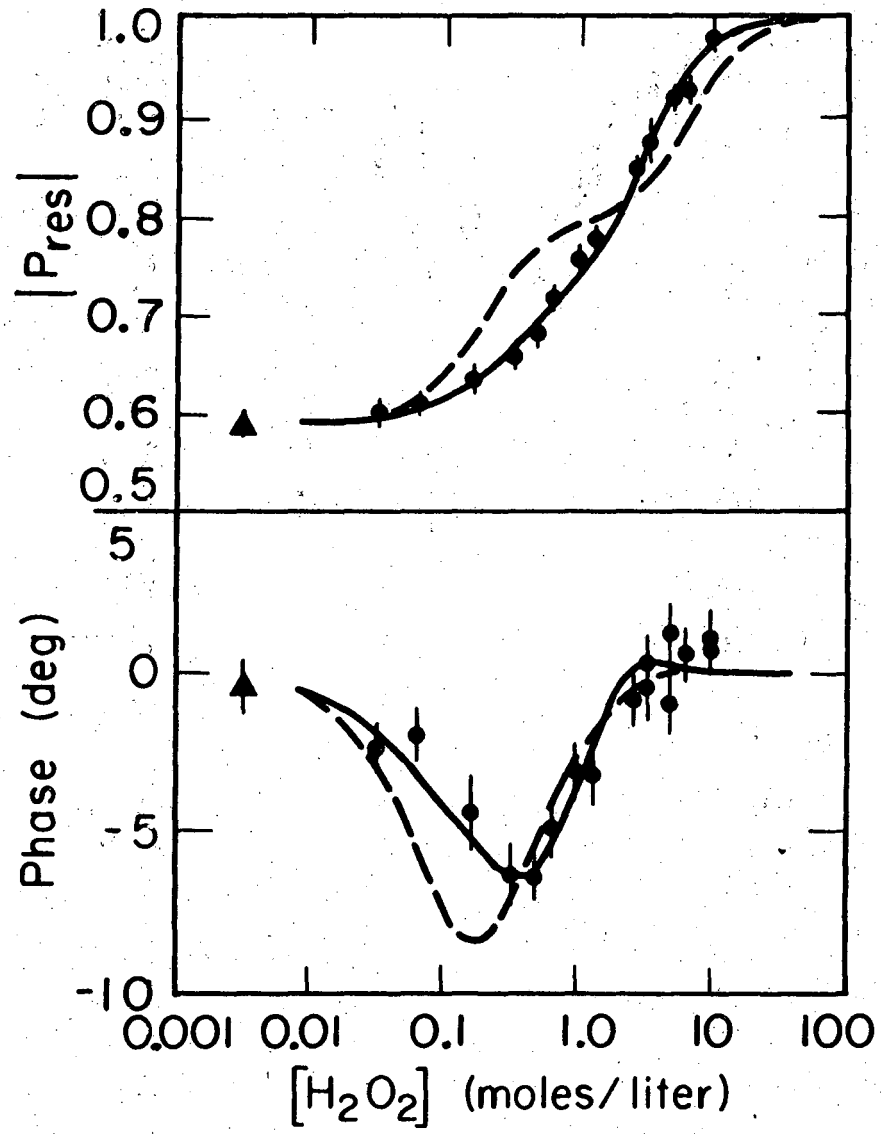
1.0
0.9
0.8
0.7
0.6
0.5
|Pres|
5
0
-5
-10
Phase (deg)
0.001
0.01
0.1
1.0
10
100
[H2O2] (moles/liter)
XBL7210-4166

Fig. 30.

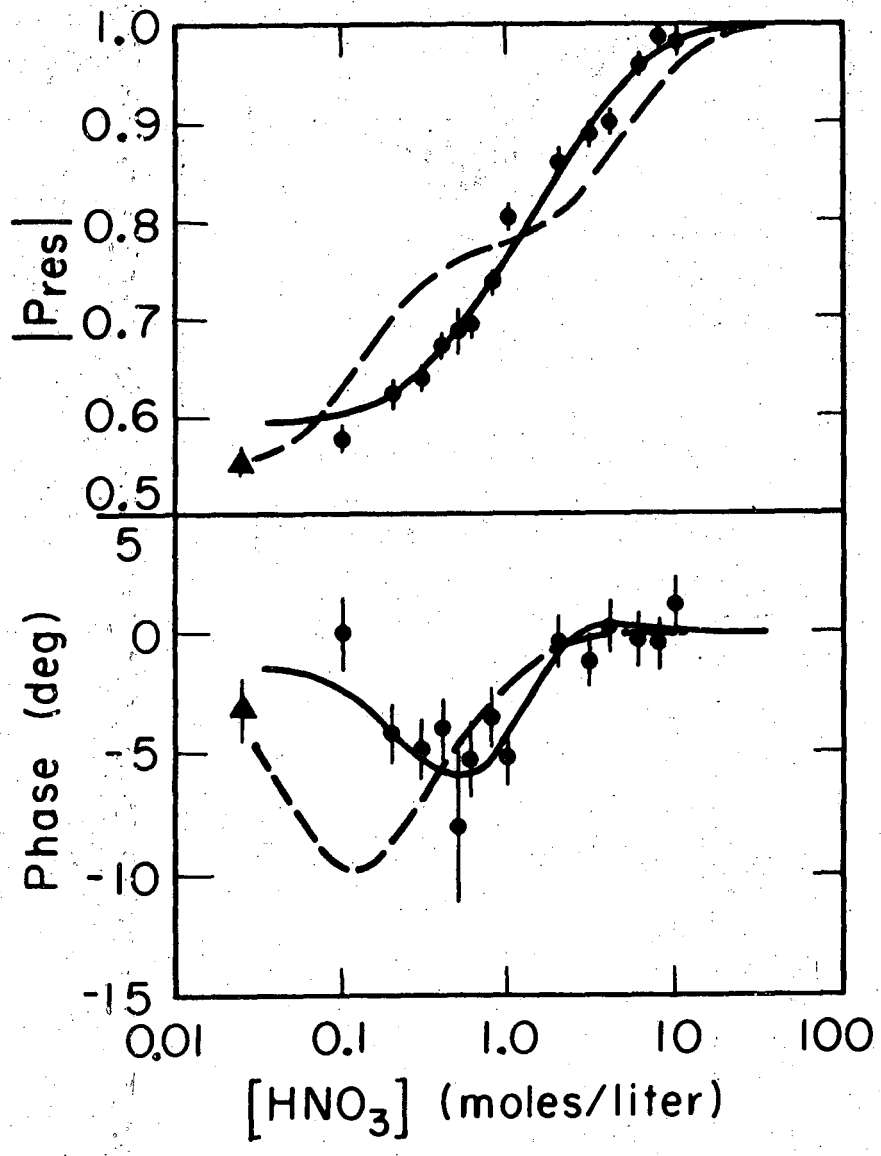

XBL7210-4165

Fig. 31.

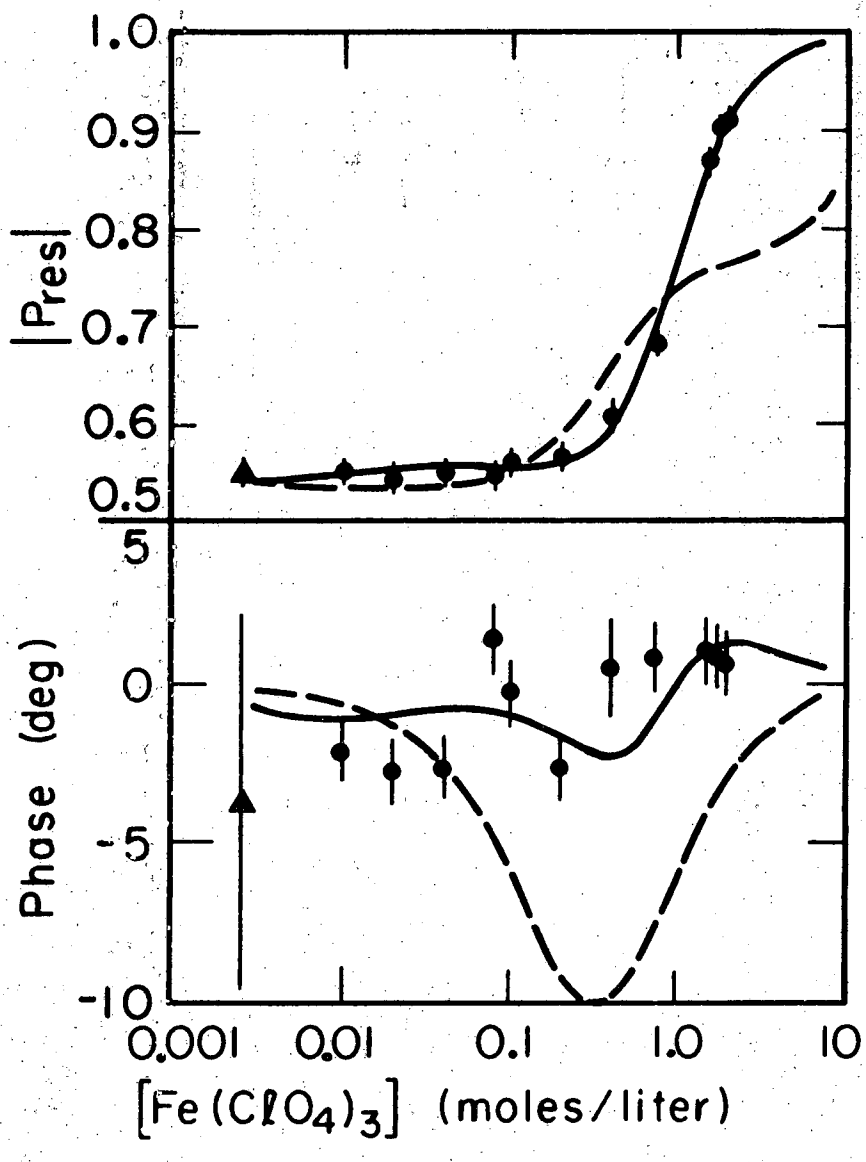

XBL 7210-4164

Fig. 32.

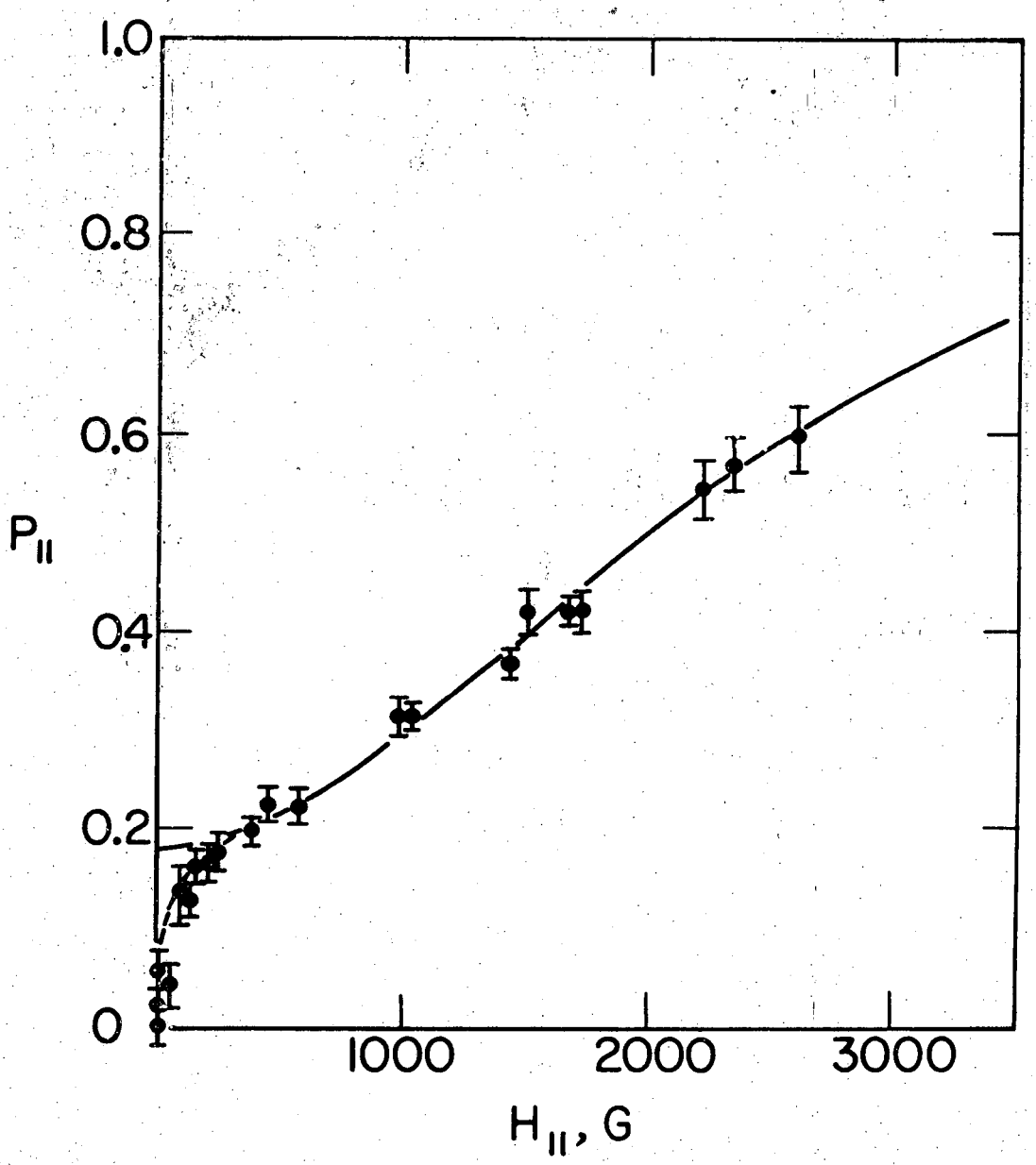

Fig. 33.

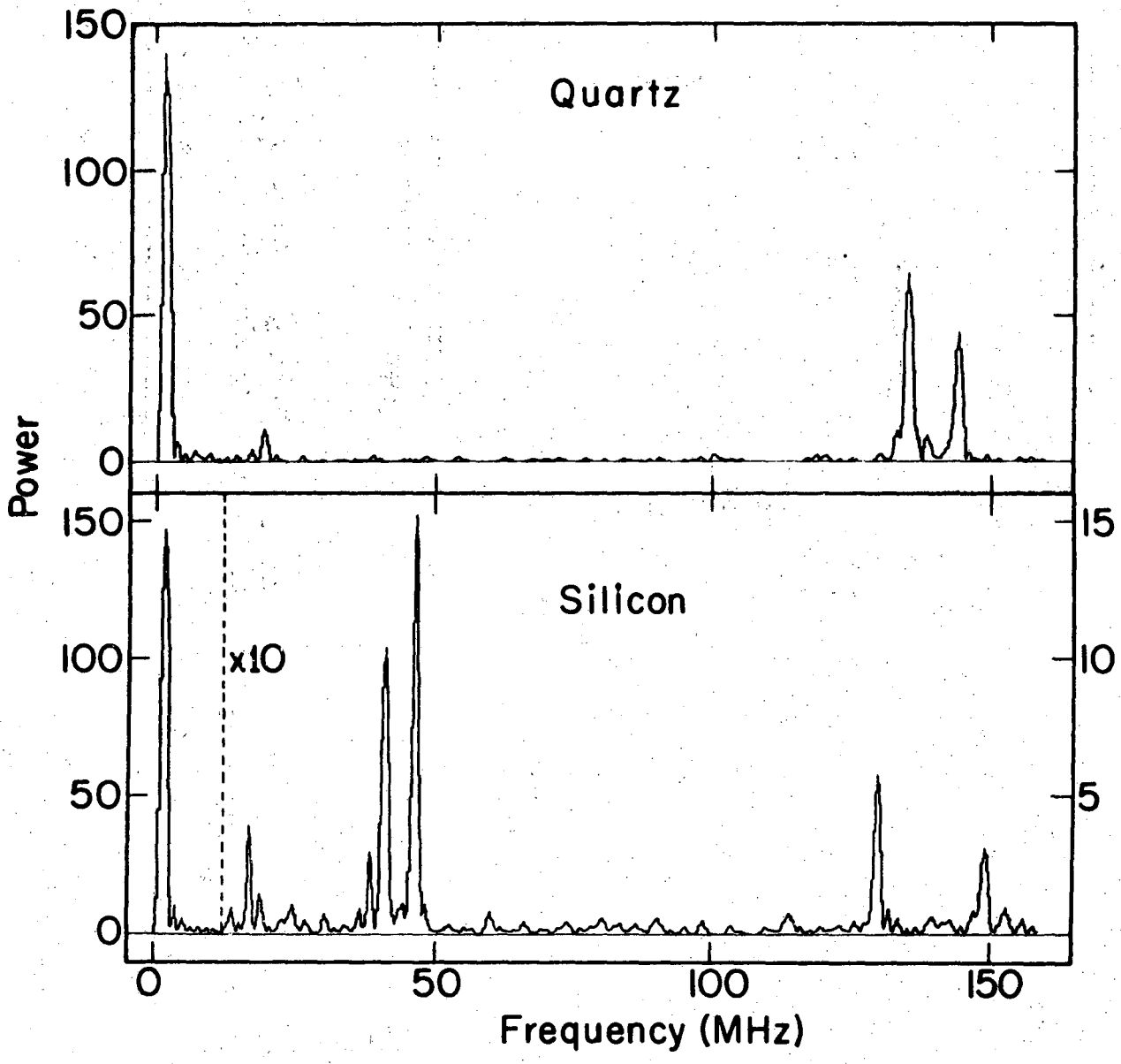
Quartz
Silicon
x10
Power
Frequency (MHz)
150
100
50
0
15
10
5
XBL734-2593

Fig. 34.

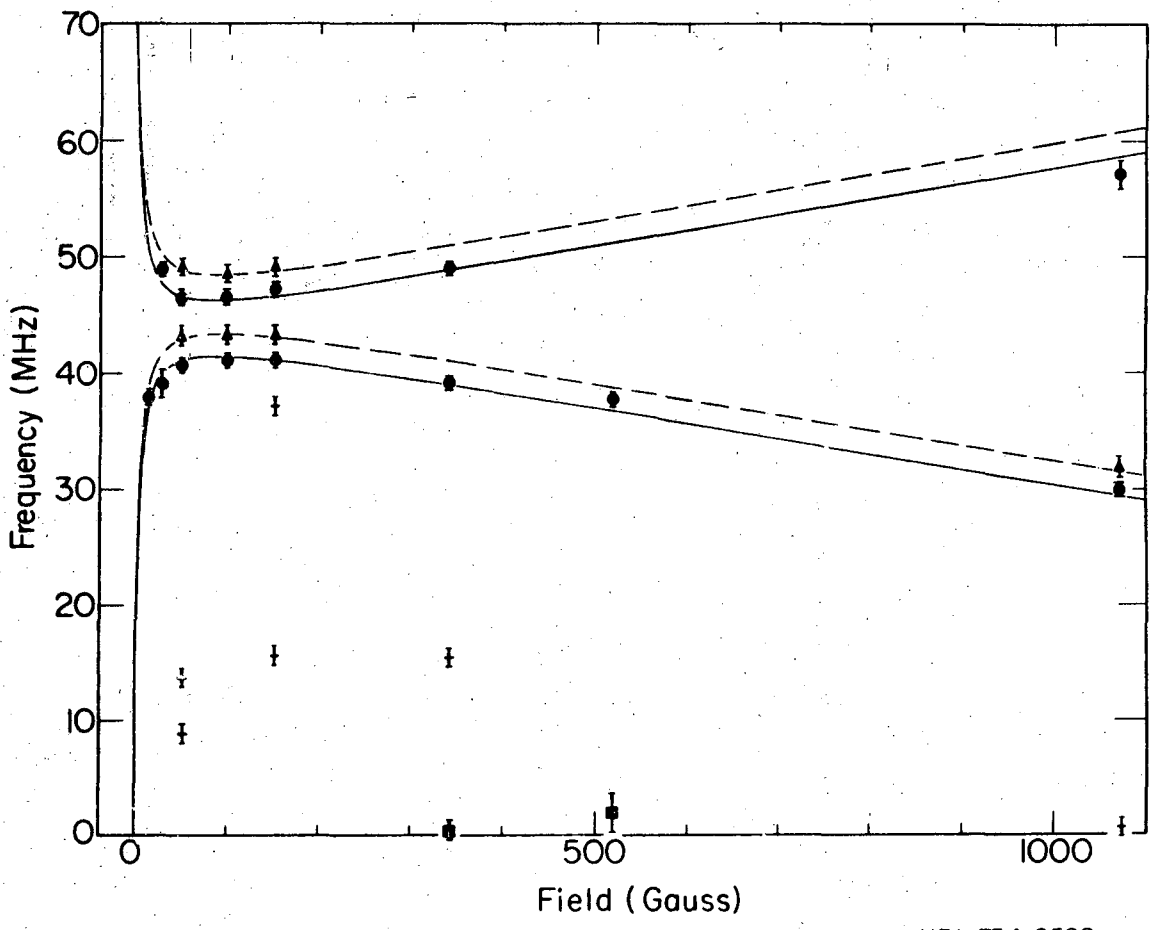
70
60
50
40
30
20
10
0
Frequency (MHz)
0
500
1000
Field (Gauss)
XBL 734-2592

Fig. 35.

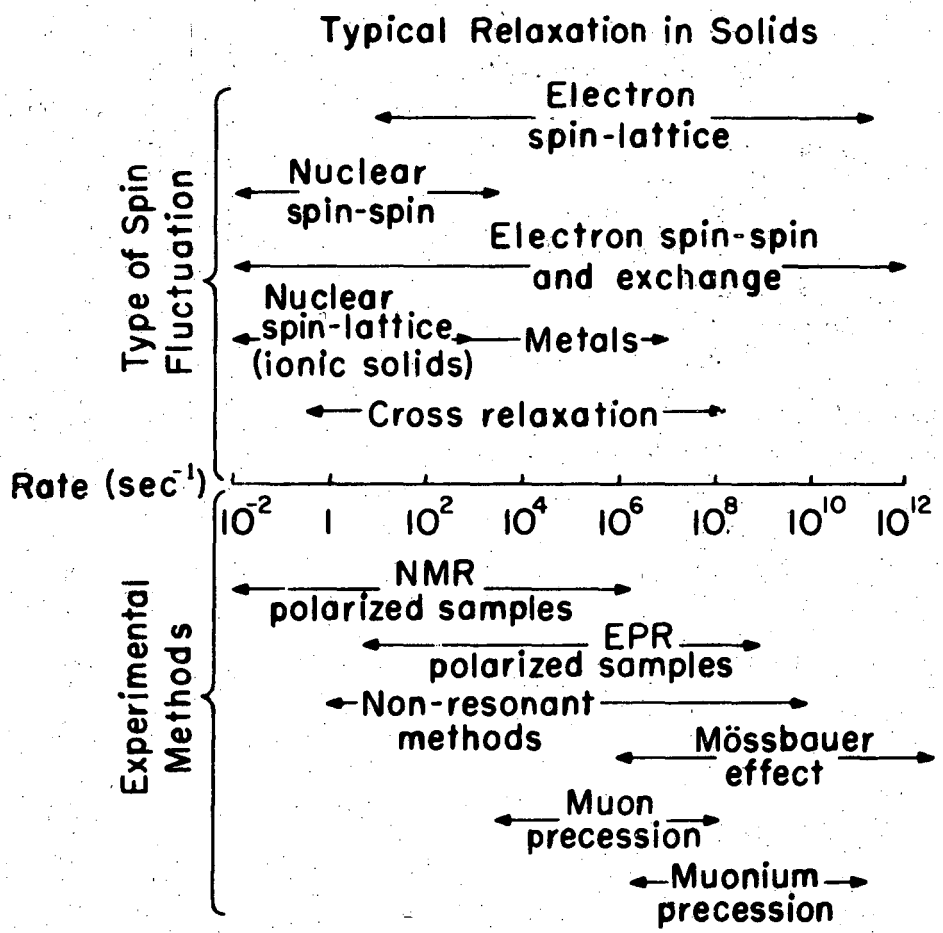
Typical Relaxation in Solids
Type of Spin Fluctuation
Electron spin-lattice
Nuclear spin-spin
Electron spin-spin and exchange
Nuclear spin-lattice (ionic solids)
Metals
Cross relaxation
Rate (sec⁻¹)
10⁻² 1 10² 10⁴ 10⁶ 10⁸ 10¹⁰ 10¹²
Experimental Methods
NMR polarized samples
EPR polarized samples
Non-resonant methods
Mössbauer effect
Muon precession
Muonium precession
XBL7310-4241

Fig. 36.

TECHNICAL INFORMATION DIVISION
LAWRENCE BERKELEY LABORATORY
UNIVERSITY OF CALIFORNIA
BERKELEY, CALIFORNIA 94720